UNIVERSITY OF GENOA, ITALY

DITEN - Department of Electrical, Electronics and
Telecommunication Engineering and Naval Architecture

Ph.D. in Science and Technology for Electronic and
Telecommunication Engineering – Cycle XXXIII (2017-2020)

Embedded Electronic Systems for Electronic Skin Applications

PhD Thesis

PhD Candidate: Moustafa Saleh

Tutor: Prof. Yasser Mohanna – Lebanese University

Tutor: Prof. Maurizio Valle – University of Genova

Coordinator of the PhD Course: Prof. Mario Marchese

Acknowledgements

First and foremost, praises and thanks to the Almighty God for His blessings throughout my research work to complete the research successfully.

I would like to express my sincere gratitude to my research supervisor Prof. Maurizio Valle head of COSMIC lab at the University of Genova for providing me invaluable guidance throughout this research. It was a great privilege and honor to work and study under his guidance. Also, I would like to thank Prof. Yasser Mohanna my supervisor at the Lebanese university for what he has offered me during my journey.

I am extremely grateful to my colleague Dr. Ali Ibrahim for his support, friendship, empathy and great guidance until the last moment. He influenced me to work hard and persist in my determination.

I am extremely grateful to my parents for their love, prayers, caring and sacrifices for educating and preparing me for my future. Special thanks go to my friends and lab mates at the COSMIC lab for the lively discussion and unforgettable adventures.

Abstract

The advances in sensor devices are potentially providing new solutions to many applications including prosthetics and robotics. Endowing upper limb prosthesis with tactile sensors (electronic/sensitive skin) can be used to provide tactile sensory feedback to the amputees. In this regard, the prosthetic device is meant to be equipped with tactile sensing system allowing the user limb to receive tactile feedback about objects and contact surfaces. Thus, embedding tactile sensing system is required for wearable sensors that should cover wide areas of the prosthetics. However, embedding sensing system involves set of challenges in terms of power consumption, data processing, real-time response and design scalability (e-skin may include large number of tactile sensors). The tactile sensing system is constituted of: (i) a tactile sensor array, (ii) an interface electronic circuit, (iii) an embedded processing unit, and (iv) a communication interface to transmit tactile data. The objective of the thesis is to develop an efficient embedded tactile sensing system targeting e-skin application (e.g. prosthetic) by: 1) developing a low power and miniaturized interface electronics circuit, operating in real-time; 2) proposing an efficient algorithm for embedded tactile data processing, affecting the system time latency and power consumption; 3) implementing an efficient communication channel/interface, suitable for large amount of data generated from large number of sensors.

Most of the interface electronics for tactile sensing system proposed in the **literature** are composed of signal conditioning and commercial data acquisition devices (i.e. DAQ). However, these devices are bulky (PC-based) and thus not suitable for portable prosthetics from the size, power consumption and scalability point of view. Regarding the tactile data processing, some works have exploited machine learning methods for extracting meaningful information from tactile data. However, embedding these algorithms poses some challenges because of 1) the high amount of data to be processed significantly affecting the real time functionality, and 2) the complex processing tasks imposing burden in terms of power consumption. On the other hand, the literature shows lack in studies addressing data transfer in tactile sensing system. Thus, dealing with large number of sensors will pose challenges on the communication bandwidth and reliability. Therefore, this thesis exploits three approaches:

1) **Developing a low power and miniaturized Interface Electronics (IE),** capable of interfacing and acquiring signals from large number of tactile sensors in real-time. We developed a portable IE system based on a low power arm microcontroller and a DDC232 A/D converter, that handles an array of 32 tactile sensors. Upon touch applied to the sensors, the IE acquires and pre-process the sensor signals at low power consumption achieving a battery lifetime of about 22 hours. Then we assessed the functionality of the IE by carrying out Electrical and electromechanical characterization experiments to monitor the response of the interface electronics with PVDF-based piezoelectric sensors. The results of electrical and

electromechanical tests validate the correct functionality of the proposed system. In addition, we implemented filtering methods on the IE that reduced the effect of noise in the system. Furthermore, we evaluated our proposed IE by integrating it in tactile sensory feedback system, showing effective deliver of tactile data to the user. The proposed system overcomes similar state of art solutions dealing with higher number of input channels and maintaining real time functionality.

2) **Optimizing and implementing** a tensorial-based machine learning algorithm for touch modality classification on embedded Zynq System-on-chip (SoC). The algorithm is based on Support Vector Machine classifier to discriminate between three input touch modality classes “brushing”, “rolling” and “sliding”. We introduced an efficient algorithm minimizing the hardware implementation complexity in terms of number of operations and memory storage which directly affect time latency and power consumption. With respect to the original algorithm, the proposed approach – implemented on Zynq SoC – achieved reduction in the number of operations per inference from 545 M-ops to 18 M-ops and the memory storage from 52.2 KB to 1.7 KB. Moreover, the proposed method speeds up the inference time by a factor of 43× at a cost of only 2% loss in accuracy, enabling the algorithm to run on embedded processing unit and to extract tactile information in real-time.

3) **Implementing** a robust and efficient data transfer channel to transfer aggregated data at high transmission data rate and low power consumption. In this approach, we proposed and demonstrated a tactile sensory feedback system based on an optical communication link for prosthetic applications. The optical link features a low power and wide transmission bandwidth, which makes the feedback system suitable for large number of tactile sensors. The low power transmission is due to the employed UWB-based optical modulation. We implemented a system prototype, consisting of digital transmitter and receiver boards and acquisition circuits to interface 32 piezoelectric sensors. Then we evaluated the system performance by measuring, processing and transmitting data of the 32 piezoelectric sensors at 100 Mbps data rate through the optical link, at 50 pJ/bit communication energy consumption. Experimental results have validated the functionality and demonstrated the real time operation of the proposed sensory feedback system.

Table of Contents

List of Figures

List of Tables

Chapter 1 Introduction

1.1 Tactile Sensing System and E-skin

1.1.1 Background

Tactile sensing in humans is one of the fundamental sensory modalities (visual, auditory etc.) that plays an important role in conveying information to the brain about objects they touch (e.g. contact surface, roughness, shape, grasp stability, slip detection and temperature [1] etc.). This information is also crucial for allowing prosthetic and robotics to carry-out human-like movements such as manipulation and exploration tasks [2]. To perform such tasks successfully, an electronic/artificial skin carrying tactile sensors should be equipped in prosthetic and robotic systems [3]. There is wide spectrum/variety of tactile sensors [4], [5], however, there usage in practical applications is still limited due to some difficulties including sensor performance, signal conditioning, data acquisition, data communication and data processing. Addressing these issues is recommended to effectively utilize tactile sensor in tactile sensing system for prosthetic and robotics [6].

The tactile sensing system is constituted of: (i) a tactile sensor array, (ii) an interface electronic circuit (signal conditioning with data acquisition), (iii) a processing unit, and (iv) a communication interface to transfer sensor data. Fig. 1.1 presents the general block diagram of the tactile sensing system. Applied input touch is detected by the sensor, which is then measured and sampled by the interface electronics (IE). The output of the IE is then sent to the processing unit for data decoding e.g., touch modality classifications.

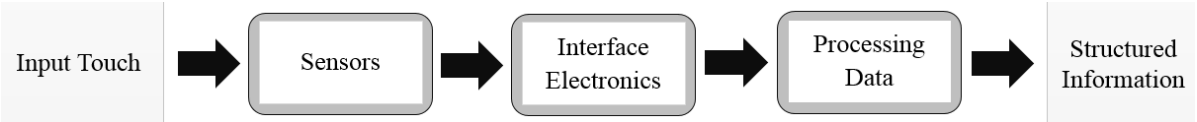

Fig. 1.1 Block diagram for the tactile sensing system

On the other hand, the tactile sensors should be distributed on the prosthetic/robotic hand/surface which requires the physical presence of the sensors with the sensing system components on the same surface. However, embedding tactile sensing system poses several challenges: 1) hardware issues related to the design complexity, scalability and size; 2) processing strategies that can deal with large amount of data and run on embedded hardware with acceptable hardware computational resources; 3) system power consumption and real-time operational requirements that are acceptable for wearable system. More about system requirements are discussed and introduced in the next section.

1.1.2 Requirements and expectations

Signal conditioning and data acquisition

The specifications of the front-end/electronic circuits of the tactile sensing system is merely dependent on the general application requirements and specifically on the type and the number of the tactile sensor. However, the front-end electronics generally comprises specific components despite what would be the type of the sensors. Almost, most electronic circuits that should interface tactile sensors include three main components/circuits: signal conditioning, data acquisition and processor/microcontroller. Together, these three components form what is called “interface electronics (IE)”.

The signal conditioning circuit handles directly the tactile sensors and it includes signal amplification and in some cases filtering. The output of the conditioning circuit is the input of data acquisition circuit which usually includes the analog-to-digital converter (A/D). Designing both circuits is affected by some issues related to the acquisition mode and some parameters such as sampling rate, data resolution etc. For sequential acquisition where set of sensors are connected to a single signal conditioning or data acquisition channel through a switching multiplexer. This mode will cause delay in acquiring data from large number of sensors, while minimum delay is recommended in delivering tactile data to the prosthetic user or robotic controller. Reducing the acquisition time is possible by adopting parallel/simultaneous acquisition. However, in parallel/simultaneous acquisition mode, each sensor needs a dedicated signal conditioning and data acquisition A/D converter channel. This will lead to a complex IE design posing challenges in terms of sensor wiring and power

consumption. Moreover, the IE design complexity will increase as for handling specific type of tactile sensors that generate bipolar signals/charges when they are exposed to contact touch. Thus, this requires including some additional circuits in the signal conditioning circuit. All these challenges and requirements should be considered and addressed when designing an IE (signal conditioning and data acquisition circuit) for tactile sensing system. Table 1.1 lists some of the embedded IE features.

Table 1.1 GENERAL EMBEDDED INTERFACE ELECTRONICS SYSTEM FEATURES FOR TACTILE SENSOR

Analog-to-digital converter	Simultaneous sampling
Signal conditioning circuit	Handle current-output sensors
Controller	Retrieve and pre-process sensor data
Offset circuit	Handle bipolar sensor signals
Sampling rate	Wide frequency range
Time latency	Real-time operation
Number of sensors	Large number
Power consumption	Battery powered system
Power supply	Single

Tactile data processing

Data processing methods and algorithms (machine/deep learning) are important to extract meaningful information from tactile sensor data [7], [8]. For example, extracting some features (force, temperature), slippage detection, object texture recognition and touch modalities classification. Machine learning has emerged in different scientific fields and everyday tasks in today's electronic systems and smartphones. ML and deep learning paradigms have been effectively used to address standard regression and classification problems.

The complexity of such paradigms ranges according to number of computations and the structure of the algorithm itself. For wearable prosthetic and robotic applications, these algorithms are recommended to run locally on embedded hardware. Thus, imposing several challenges on the hardware performance in terms of power consumption and latency. In addition to some other hardware constraints such as memory storage and number of operational units to perform the necessary computations. The structure of the algorithm depends, first, on the type of the tactile data, and second, on the information required to be

extract from these data (features, textures, touch modalities). For touch modality classification, time is an important dimension for predicting the touch modal in addition to the position and number of the tactile sensors on the prosthetic/robotic surface. However, employing such algorithms for embedded platforms imposes challenges in terms of time latency, energy consumption, and storage. Therefore, designing and employing a tactile processing algorithm should address and consider some of the aforementioned challenges and requirements. Table 1.2 reports some of the main specifications of embedded processing unit for tactile data processing.

Table 1.2 GENERAL EMBEDDED PROCESSING UNIT SYSTEM FEATURES AND SPECIFICATIONS FOR TACTILE DATA PROCESSING

Data processing paradigm	Sophisticated algorithms to extract meaningful information from raw data (slip detection, touch modality, force estimation etc.)
Local computation on hardware	Low number of operations
Processing Algorithm complexity	No burden on the hardware resources
Energy consumption	Low power
Response time	Fast prediction/classification response
Processing algorithm output results	reliable data with high accuracy

Tactile data transmission

Sensor data propagate in the tactile sensing system to the user/controller through communication channels. Various communication channels could exist at different levels in the sensing system. This is according to the number of sensors and the IE design. In addition to some power and transmission bandwidth issues. For example, some systems may include wiring buses connections (I2C, SPI, CAN) for acquiring sensors signals with wireless connection (Bluetooth, Zigbee [9]) for transferring the acquired data to the next levels in the sensing system. Increasing the number of sensors should be associated with high transfer rates to avoid large delays in the system. Moreover, data loss and reliability are another important factor that may affects the type for the required communication channel. Therefore, achieving an efficient communication channel for tactile sensing system is possible by fulfilling some of the mentioned constraints and requirements.

1.2 Thesis Contribution

The thesis contributions summarized as follows:

1.2.1 Low power interface electronics with PVDF-based sensors

Developing a portable electronic system for tactile sensory feedback for prosthetics. The electronic system is based on real-time and low power IE design. The IE comprises three main blocks: sensor offset circuit, DDC232 current-input analog-to-digital converter and Arm microcontroller. The proposed design is capable of handling 32 input piezoelectric (PVDF) sensors with performing simultaneous sampling at high rates i.e. 2 kHz; relative to the application requirements. This has reduced the delay in the system. The IE design has been implemented and tested with a sensing array for measuring their charges that have been generated upon applying forces. Results show that range of charges have been acquired and measured by the design with 56 dB signal-to-noise ratio and 14 bits of effective number of bits (ENOB). Moreover, the power consumption and time latency of the IE have been measured when it has been integrated in sensory feedback system for providing tactile information to the user. Results demonstrated very small and acceptable delay with 32 ms and power consumption around 300 mW, providing about 22h of battery lifetime. The proposed electronic system overcomes similar state-of-the-art solutions by featuring higher number of input channels with low power and real time operation.

1.2.2 Embedded data processing unit based on optimized machine learning algorithm

Optimizing and implementing a tensorial-based machine learning algorithm for touch modality classification on embedded Zynq System-on-chip (SoC). The algorithm [10] is based on Support Vector Machine classifier to discriminate between three input touch modality classes “brushing”, “rolling” and “sliding”. Implementing such complex algorithm on embedded hardware requires enough memory to store data and will consume large number of operations to perform classification. In this regard, the aim was to introduce an efficient algorithm minimizing the system complexity in terms of number of operations and memory storage which directly affect time latency and power consumption. The proposed approach has been implemented on the Zynq-Arm processer where the algorithm has been executed and its performance has been analyzed. Results demonstrated that the proposed approach have reduced the computational complexity with respect to the original algorithm presented in the state of the art. And, the required number of operations has significantly decreased leading to a classification speedup of 43×. Moreover, the needed amount of memory storage has been minimized from 52.2 KB to 1.7 KB; These results have been reached at a 2% of accuracy loss with respect to the literature. This approach enables

embedding tactile data processing algorithm in a sensory feedback system where the embedded algorithm could receive sensor data and extract tactile information in real-time.

1.2.3 Wide bandwidth and low power transmission bus interface for tactile data based on optical communication channel

Implementing an optical fiber communication channel in tactile sensory feedback system for the prosthetic application. The purpose is to provide an efficient communication channel for tactile data transfer. The channel is based on UWB pulsed data coding technique that allows high data transfer rate with low power consumption. The assembled system is composed of both digital transmitter and receiver block, and an acquisition circuit which interfaces 32 piezoelectric sensors. The transmitter acquires, encodes and sends sensor data via the optical channel. Whereas, the receiver decodes, recovers and translate the sensor data into commands. These commands control an electrotactile stimulator, conveying the tactile information to the user as electrotactile stimulations. The system performance has been evaluated where results showed correct functionality of the proposed system and validated that it can transfer large number of data at 100 Mbps with low power consumption, 50 pJ/bit. This means that this approach could enable employing large number of tactile sensors for the sensory feedback system while maintaining real-time operation.

1.3 Thesis Outline

The thesis is organized as follows:

Chapter 2 reviews the development of the tactile sensing system mainly for prosthetics and robotics. This chapter divides the literature into three sections, each related to a specific block of the tactile sensing system. First section reports several studies that have used some electronic circuits for interfacing sensors for the purpose of evaluating their response and behavior. Also, this section covers some dedicated interface electronics for several tactile sensors (capacitive, piezoelectric) showing their performance and highlighting their limitations. The second section presents some tactile data processing methods and demonstrates some implementations of such methods on embedded hardware. While the third section reviews and highlights on the most used communication channels in the tactile sensing system to transfer the tactile data to the user/controller in prosthetic/robotics.

Chapter 3 introduces and describes the whole process of designing, implementing, assessing and enhancing the interface electronics for tactile sensing system. The chapter includes the description of tactile sensor structure/model. Also, it presents the experimental tests that has been carried out to analyze the performance of the interface electronics design in terms of power consumption and signal-to-noise ratio. Finally, the chapter introduces and

discuss the effect of implementing in the interface electronics some signal processing methods for the purpose of improving its behavior.

Chapter 4 demonstrates the behavior of the proposed interface electronics in a sensory feedback system. The architecture of the feedback system has been introduced including the interface electronics. Then the system was evaluated by conducting experiments on three healthy subjects. The behavior of the system is assessed by measuring the subject recognition rate and the system delay from touch to stimulation applied on the subject.

Chapter 5 demonstrates an optimized tensorial-based machine learning algorithm for touch modality classification. First, an overview of the tensorial-based approach was described. Then an optimization method was proposed to reduce the complexity of the algorithm. Moreover, the hardware implementation of the optimized algorithm has been described and evaluated by passing set of new samples to the algorithm and recording the classification accuracy. Finally, results were discussed and analyzed by measuring the execution time per classification and calculating the reduction in the number of operations and memory storage required after applying the optimization.

Chapter 6 demonstrates the implementation of a novel architecture based on the use of an optical fiber communication link for data transmission in the tactile sensory feedback systems for the prosthetic applications. The chapter includes a description of the sensory system with additional details on each block. In addition, the communication protocol is fully explained, and a prototype that transmits data information measured from real sensors to the electrotactile stimulator has been experimentally validated. The implementation of the communication channels has been presented and the experimental setup used to evaluate the overall system has been described.

Chapter 2 Literature Review

2.1 Introduction

This chapter reviews the development of the tactile sensing system mainly for prosthetics and robotics. The literature has highlighted several studies either focusing on the sensing system as a whole block or by carrying out individual studies related to the system sub-blocks. Several studies have focused on the sensing material that would cover large areas on the robotic or prosthetic surface. Where the purpose was characterizing and evaluating the behavior of multiple sensors after fabrication. This brought attention to the electronic block of the sensing system and motivated several researches to focus on developing specific/dedicated electronics to effectively utilize tactile data. Contributing to the tactile sensing system requires knowing the development status of the system and defining the achievements and the gaps as well in this field. In this regard, it's important to review the literature regarding each block of the tactile sensing system (sensors with electronic circuits, communication channels and tactile data processing).

We divided the literature into three sections, corresponding to the three main blocks of the tactile sensing system: interface electronics (IE), data processing and data communication. Section 2.2 reports several studies that have used electronic circuits for interfacing sensors and evaluating their response and behavior. Also, this section covers some dedicated IE for several tactile sensors (capacitive, piezoelectric) showing their performance and highlighting their limitations. Section 2.3 presents some tactile data processing methods and demonstrates some implementations of such methods on embedded hardware. While section 2.4 reviews and highlights on the most used communication channels in the tactile sensing system to transfer the tactile data to the user in prosthetic or

controller in robotics.

2.2 Review of Interface Electronics

The IE block could be reviewed from several viewpoints. In the first viewpoint, we will start with the studies that focused on developing sensing materials with new structures and demonstrates the electronic circuits that have been used to interface these sensors for further evaluation and characterization. In the second viewpoint, we will present some works that have focused on developing dedicated IE for several tactile sensors (capacitive, resistive and piezoelectric). In the third viewpoints, we will demonstrate some IE performance in terms of power consumption, real-time functionality and the number of attached sensors. Finally, we discuss the gaps and some limitations that should be addressed to achieve powerful sensing system for prosthetic application.

Tactile sensors are capable of measuring various contact parameters and are classified according to their transduction method i.e. capacitive [11], resistive [12] and piezoelectric [13] sensors. The piezoelectric sensors provide high flexibility [14] and sensitivity [15] among other sensors since it is based on PVDF materials (polyvinylidene fluoride). Several tactile sensors have been developed and characterized [16], [17], [18]. Acer et al. [19] developed piezoelectric sensors of ceramic type and performed a study to show the effect of the thickness of the silicon substrate on the sensor sensitivity. They connected a 4x2 sensor array to signal conditioning circuit, composed of TLV2772 operational amplifier, to convert sensor charge into voltage. The output voltage is then sampled through DAQ device (National instrument, USB-6009). Another study has been conducted in [20] to show the flexibility of the tactile sensors under three-axis dynamic forces. 3x2 tactile units (24 sensors) were fabricated and then tested by applying normal forces within the frequency range 4-500 Hz on the sensor surface. Charges generated by sensors were measured by DH5862 charge amplifier and then collected by NI-DAQ device (USB-6343). Drimus et al. [21] developed a robotic fingertip equipped with a PVDF-based piezoelectric. The main idea was to find the best coupling of sensor material with protective layer for the purpose of studying the performance of three learning methods for classifying surfaces textures. A single taxel was connected to a charge amplifier (OPA637) with a 16-bit NI DAQ USB 6341. Figure 2.1 provides a capture of the experimental setup in [19] to evaluate the performance of the designed sensor elements.

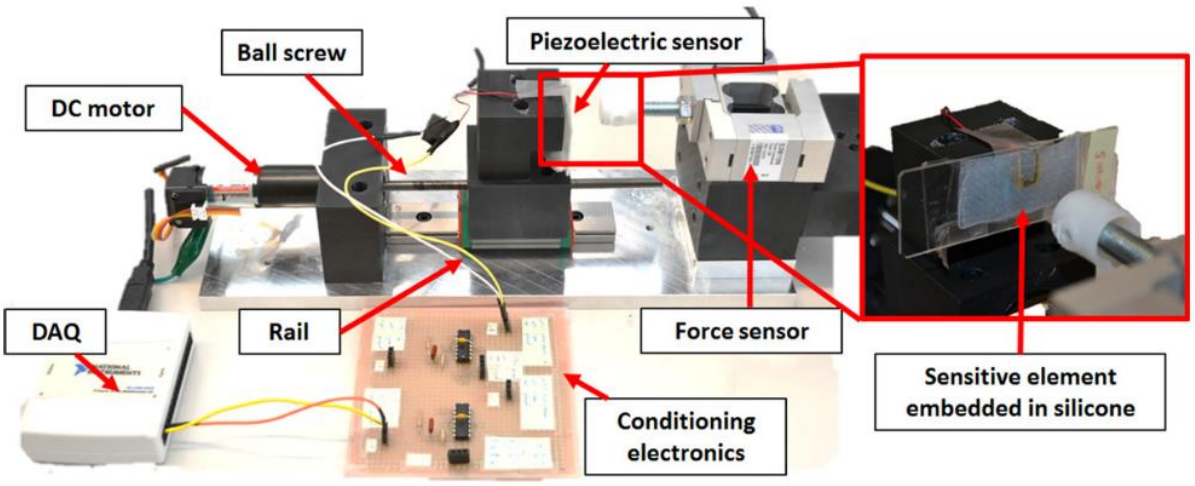

Fig. 2.1 Experimental setup for characterizing the PZT sensors embedded in silicone (adapted from [19]).

Other studies aimed a dedicated IE to read charges from tactile sensors [22], [23]. Pinna et al. [24] have presented a design methodology to define the metrics required for developing an IE prototype. The prototype design depends on the sensor charge value that should be detected. So, tests were performed to check the prototype behavior when coupled to a PVDF sensor. The IE is composed of an op-amp (OPA348) and a low pass filter. Results reported a sensitivity of about 5.7 pC/N after the PVDF sample has been stimulated with a shaker with fixed frequency (i.e., 230 Hz) at variable force amplitude (i.e., 0.2-0.6 N). Moreover, a 2-input sensors IE circuit has been developed in [25]. The design adopts a dual channel analog to digital converter DDC112U [26] and an FPGA Xilinx Spartan®-6. The design was capable of measuring sensor signals with 0.6 pC/kPa average sensitivity in the frequency range from 10Hz to 250 Hz. Furthermore, the functionality of this IE design has been more assessed and was experimentally characterized in [27]. Rossi et al. [28] proposed a design that can be integrated between the prosthetic limb and the patient body. The main idea is to relieve the patient pain by measuring the dynamic and static stimuli that usually occurs during movement. Two sensors of different models (piezoelectric and piezoresistive) have been staked in a single package and interfaced to the proposed design (see fig. 2.2). The design is based on CC3200 Launchpad board Texas Instrument (embeds two ARM cores) and a signal conditioning circuit composed of a charge amplifier. The four input sensors signals were acquired, sampled and then sent through Wi-Fi to the PC in continuous mode at an average 111 mA current consumption.

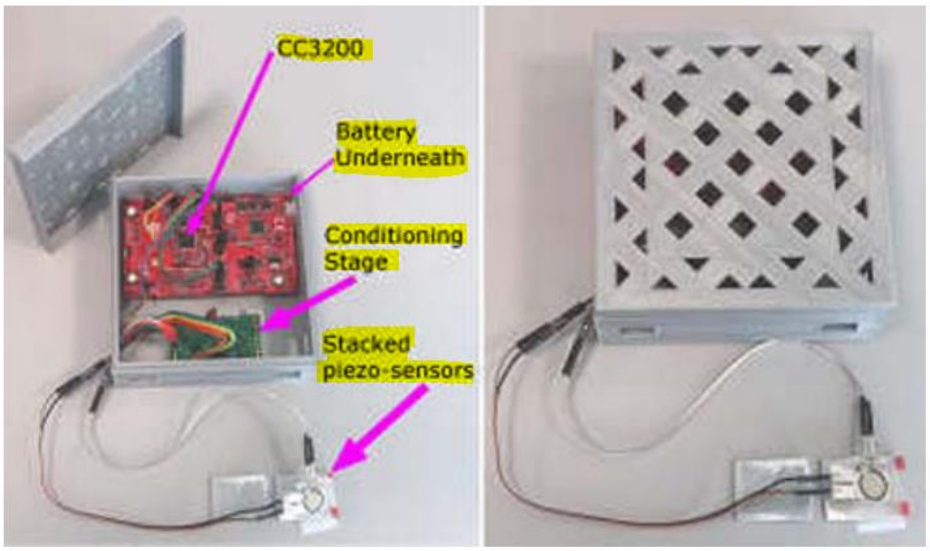

Fig. 2.2 electronic circuit prototype in [28]

Handling a large number of sensors to provide high-resolution tactile information should be taken into consideration when designing the IE [28]. Recently, large number of capacitive sensors were implemented in robotics applications [29]. For instance, a tactile sensor suite in [30] can handle more than 32 taxels in a fingertip as well as in the palm. Each finger pad carries sensors connected directly to FPGA, and all pads are connected through SPI interface (see fig. 2.3). The tactile sensors are scanned, and the data are preprocessed in the palm unit with power consumption around 1175 mW (235 mA at 5V). Another approach in Schmitz et al. [31] proposed a PCB of sensors and charge to voltage converter AD7147. The AD7147 handles up to 13 inputs channeled through a switch matrix and provides I2C serial bus for communication. This allows building a chain of sensor PCBs with I2C connection in between and a microcontroller master board connected just to one of the sensor PCBs for acquiring data.

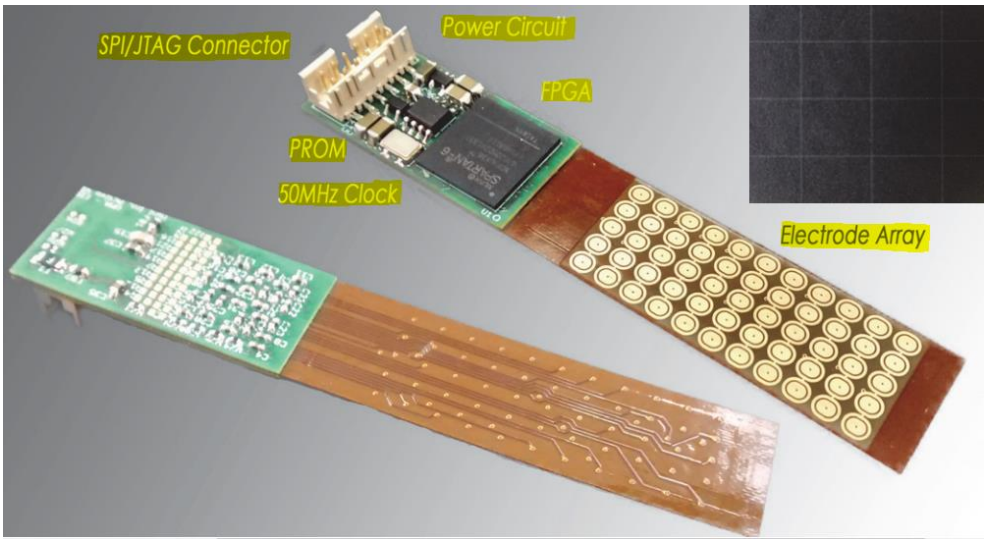

Fig. 2.3 Smart tactile finger sensor: photograph of the device with array of sensors (adapted from [30]).

On the other hand, some IE have been designed to tackle non-tactile sensors that target applications rather than prosthetic and robotics. The ALPHADET board in [32] handles four BJT detectors where FPGA and DDC114 are used to detect the alpha particles that are ejected from the nuclei of unstable atoms. Authors in [33] proposed NI-sbRIO-9632 mainboard connected to DDC112 to provide high-resolution measurements for gas concentration of the two photo detectors inputs.

Despite the developments of tactile sensors and their interface electronic units presented in the aforementioned literature, the interface electronic units were not targeting wearable devices especially from the hardware size and energy consumption point of view [34], [35]. Wearable devices must be capable of performing the requested tasks with minimal budget in terms of energy consumption and time latency powered by a small battery size [36], [37]. Table 2.1 shows some recent implementation of interface electronic circuits indicating their power consumption and design specifications. Most of the recent IE are based on charge amplifier and data acquisition (DAQ) boards. Some approaches [25],[32] proposed analog-to-digital converters with FPGA devices or microcontroller.

Table 2.1 RECENT WORK ABOUT INTERFACE ELECTRONICS

Ref	Signal Conditioning	ADC/ Control	Frequency Bandwidth	Number of channels	Power consumption
[19]	TLV2772	NI USB 6009 DAQ		8	0.4-2.5 W
[20]	DH5862	NI USB-6343 DAQ	5-400 Hz	24	11 W-30 W
[24]	OPA348	NI-DAQ 9174	1 kHz	1	---
[28]	Charge amplifier	With CC3200 Launchpad board TI	1 KSps	4	0.396 W
[30]	---	Raw sensor/FPGA Xilinx Spartan 6		55	0.84-3.3 W
[31]	---	AD7147/Microcontroller	500 Hz	12	---
[32]	---	DDC114 + FPGA	---	4	---
[33]	---	DDC112 + NI-sbRIO-9632	---	2	8 W
[38]	OPA637	NI USB 634 DAQ	1 kHz	1	11 W- 30 W
[39]	---	DDC112 + FPGA	1 kHz	2	1.278 W

Another important viewpoint should be highlighted in the literature is reviewing the IE as a part of the tactile sensing system. Some researchers developed sensing systems [40], while others proposed PC controlled stimulation systems [41]. Few studies in the literature

proposed embedded-real time feedback systems that incorporate the two systems. Pamungkas and Ward. et al [42] developed a sensory feedback system based on sixteen polymer film force sensors fitted to the fingers and palm of a prosthetic hand. Six electrotactile feedback channels were used for force feedback. A host PC was used to monitor the sensor data and to deliver appropriate pulses to the six electrodes. Whereas Franceschi et al. [35] and Hartman et al. [43] investigated the possibilities of communicating tactile information such as touch position from artificial skin (PVDF based sensor array) through a host PC. Information from an array of 64 piezoelectric sensors is translated into electro-cutaneous stimulation patterns and conveyed to the subject through 32 electrodes or concentric electrodes attached to the subject's arm skin.

The speed in communicating sensation information has not been widely reported on when examining the performance of a sensory feedback system. A healthy nervous system can take approximately 14-25 ms to deliver tactile information to the brain [44]. A change in the dynamics of a prosthetic feedback system (e.g., response time constants, pure time delays) affects the overall system behavior, even its stability. One example of this is the integration of advanced haptic intelligence within the feedback loop. Huang et al. [45] examined a multi-modal sensory feedback system with three amputees. Sensory information from five piezoelectric barometric sensors was mapped into stimulations through vibrotactile or mechano-tactile feedback. The developed system can communicate sensory information to the remaining stump of the amputees within 85 ms. Schoepp et al. [46] used a microcontroller (ATmega32u4) to map force level from two SingleTact sensors into one tactor fixed on the upper arm. The system operates with a time delay of 200 ms between touch instant and activation of the tactor.

Therefore, the literature highlights several aspects that should be addressed when designing an IE. First most of the proposed IE are based on commercial data acquisition devices that make the design bulk. In addition, to some designs that carry small number of sensors and sample their signals at low rate in a sequential mode. This leads to a delay in the acquisition process and thus making the design not suitable for real-time operations. Power consumption is another important aspect, that should be addressed to achieve a wearable system. This requires a miniaturized IE design that can be embedded and enable a PC-free sensory system that can deliver tactile information to the user with minimum delay.

2.3 Review of Tactile Data Processing Methods on Embedded Processing Unit

Tactile data processing is required for extracting meaningful tactile information from the raw sensor data. Several works have focused on developing algorithms including, but no

limited to, machine learning and neural networks for either identifying textures or classifying touch modalities [47], [48]. This section will report some of the processing methods that are useful for such task. In addition to few works that demonstrate some hardware implementations and present their performance.

Martinez-Hernandez et al. [49] proposed a novel approach that combines both perception with active exploration methods to allow autonomous robots to explore, perceive and feel what they are touching. The perception method is composed of Bayesian formulation that performs a random selection of object locations. Six objects have been contacted by a three-fingered robot integrated with tactile and strain sensors. The data of object position and orientation have been collected to implement offline object exploration and recognition. The exploration and perception processes make a decision when a predefined belief threshold is exceeded. This approach allowed the robot to achieve better trade-off between accuracy and reaction time. Fishel et al. [50] concentrated on classifying specific textures from signals detected by BioTac pressure sensor. The texture properties (traction, roughness, and fineness) are extracted and processed by Bayesian exploration classifier. Where data for 117 textures have been collected to create the training set for the classifier. This approach yielded to classify these textures with a high accuracy of 95.4%. Madry et al. proposed an unsupervised spatio-temporal feature learning method, named Spatio-Temporal Hierarchical Matching Pursuit (ST-HMP) [51]. The main idea is to extract features from the raw consecutive frames and then pool them over the time dimension. They further demonstrated the effectiveness of the proposed method on two tactile-based robotics applications, including the grasping stability assessment and object instance recognition. Aimed to recognize objects from four mechanical categories (Rigid-Fixed, Rigid-Movable, Soft-Fixed, and Soft-Movable.) during the interactions with tactile sensor array, Bhattacharjee et al. [52] developed a classification and recognition algorithm. They first extracted features such as maximum force, contact area and contact motion from the object and then they used the k-nearest neighbor algorithm K-NN classifier. Another object recognition approach proposed in [53]. The purpose is to classify eight objects: finger, hand, arm, pen, scissors, pliers, sticky tape, and Allen key, using a 28 × 50 high-resolution tactile sensors. They proposed two classification approaches. Both approaches include feature extraction followed by supervised vector machine (SVM). However, in the first approach the speeded-up Robust Features descriptor has been used for feature extraction, while Deep convolutional Neural network DCNN used in the second approach.

Aiming to build a smart tactile sensing system, Alameh et al. [54] has presented several implementations of convolutional neural networks (CNNs) to classify objects from tactile dataset e.g. they proposed a CNN model based on decreasing the trainable parameters to

minimize the hardware complexity. The model has been tested on different hardware platforms achieving inference time of 1.2 ms and consuming around 900 uJ. Osta et al. [55] has proposed an energy efficient hardware platform for tactile sensing system. The approach is based on an ultra-low power processor with multi-core architecture. This allowed to achieve an energy efficient implementation of touch modality classification problem based on Support Vector Machine (SVM). The proposed platform consumes 81 mJ per classification and the inference time is 3.3 s. Ibrahim et al. [56] has presented the hardware architectures and implementation of ML based on tensorial kernel approach. The proposed implementation deals with tensorial structure of the tactile data and provides parallel architecture to achieve real-time touch modality classification. The system has achieved a peak performance of 302 G-ops for the Virtex-7 FPGA and achieved 350 ms inference time with 945 mJ energy for three class classification.

Most of the tactile processing methods are complex requiring powerful computational processors to perform their tasks. This become highly recommended when the target is to run these algorithms on embedded hardware to achieve wearable tactile sensing system. Unfraternally, this usually comes at the cost of power consumption and time delay. Thus, trade-off between algorithm complexity and hardware performance should be considered when implementing tactile processing methods.

2.4 Review of Tactile Data Communication Channels

Most of the sensing system research has focused on developing sensing elements with their electronics and with some methods for data processing. However, to the best of our knowledge, there is no study which addressed the data transmission channel of a sensory feedback system either in prosthetic or in robotic applications. This section reviews the recent developments in sensory feedback systems where we highlight the communication protocols used to transmit tactile sensors data.

Aiming the reconstruction of hand posture and tactile information, Bianchi et al. [57] has proposed a multi-modal sensing glove composed of piezoresistive fabric for measuring normal forces with more than 50 taxels spread over the palm surface. During manipulation, force was recorded through a data acquisition board: each single sensor is connected to a voltage divider and an analog-to-digital converter (ADC). A PIC18-microcontroller is used on the acquisition board to collect sensors data and to transmit them via USB to the host PC. The sensory system of a robotic arm in [58] includes large patches based on commercial force sensors to cover large areas of the robotic arm. Each patch has 16×9 force sensors, sampled at 78 frames per second through an acquisition board. They used PIC18F4680 for 1) scanning the array of sensors, 2) sorting data and 3) transmitting them via a CAN bus

communication to a central processing unit. In Schmitz et al. [31] the tactile sensory system for robotic hands provides distributed pressure measurements and information about the contact location, obtained during interaction with the environment. Each sensing unit carrying 12 taxels, shares an I2C bus with a master unit in order to receive the sensor data and then transmit them to the PC through CAN bus.

Delivering tactile information from sensors to the user remains a challenge. Researchers are investigating methods that provide useful tactile information in both prosthetics [59], [45] and robotic hands [60] , such as force, object texture and slippage. The sensing feedback system in [59] enables the prosthetic user to feel various objects touched by means of electrotactile stimulations. The system is composed of 16 resistive film force sensors connected to a control board. The microprocessor on the control board collects the sensor data at 20 samples per second and sends them to a PC via USB. The data in the PC are processed and then sent through a USB wireless transmitter to the user as Electrotactile-stimulation feedback. Similar approach with different stimulation modality has been proposed in [45] to improve the recognition rate and to reduce mental workload when identifying different stimulation patterns. The system incorporates vibro-tactile and mechano-tactile modalities. The system consists of five piezoelectric tactile sensors, which are multiplexed to a low energy communication module (CC2640R2F). The sensory data are combined into packet and then sent via Bluetooth to the customized-design multi-modal stimulator. Regarding robotic hands, Choi et al. [60] have introduced sensing system based on robotic fingertip containing 4 force and 2 PVDF sensors. The system can detect normal contact and slip forces applied on the surface of the robotic fingertip. The signals coming from different PVDF sensors are received by six ADC converters on a microcontroller-based board (C8051F311) and then transmitted to the PC via RS232 or SMBus. Thus, integrating multiple fingertips will make collecting large numbers of data a complex task and consequently will require a wide transmission bandwidth.

For robotics applications, a POSFET sensor arrays has been proposed in [61] to recover the contact forces of frequency contents up to 1 KHz. Authors defined the main parameters for the data acquisition system for 16 taxels to be 1.6 Mbps. So, the employment of a larger number of taxels will result in the need of a wider bandwidth in order to transfer the increased amount of data. Moreover, Schmitz et al. [62] have addressed dedicated IE aiming a wearable sensing system. The design is based on a single chip containing digital microcontroller and 13 charge sensitive analog front ends. The chip measures and processes locally the information generated by the taxels and then sent them to the PC through a USB to UART converter chip.

Data transfer is crucial in the tactile sensing system, where data reliability, transfer

bandwidth and power requirements could affect the behavior of the system leading to safety issues in prosthetic and robotic systems. Thus, implementing an efficient and wide-bandwidth channel enables the system to handle large number of tactile sensor and thus providing high-resolution tactile data. This paves the way toward having more human-like functionality provided by prosthetic and robotic systems.

Chapter 3 Real Time Interface Electronics for PVDF-based Piezoelectric Tactile Sensing Array

3.1 Introduction

Developing the interface electronics (IE) for a prosthetic tactile sensing system needs a thorough understanding of the sensing system and hardware related requirements. Most of these requirements stem out from the "human-like" behavior conception, where initially from the mechanical aspect, the system should be wearable and user friendly. In addition to that, the system should be capable of performing several sensing tasks (e.g. restoring sense of touch, slippage detection, touch force/pressures) which thus requires a specific type of set of sensors [63]. Several tactile sensors have been used to detect tactile stimuli when covered on the robot body and prosthetic hand, such as capacitive [4], piezo-resistive [60] and piezoelectric [64] sensors. Among these sensors, the piezoelectric sensors based on polyvinylidene fluoride material (PVDF) provide a high sensitivity, flexibility and a wide range of touches [65] (i.e. 1 kHz frequency bandwidth). They generate bipolar charges when are get exposed to contact touches on their surfaces. Acquiring such type of signals become challenging especially when large number of tactile sensors are used to cover large areas of the prosthetic hand for providing high spatial resolution [66]. Considering all these requirements leads to the general requirements of the IE in the sensing system. Therefore, the IE should be miniaturized, battery powered (low power); and it should be suitable for carrying large number of tactile sensors (PVDF-based) of specific features and

characteristics – that enables performing the system sensing tasks.

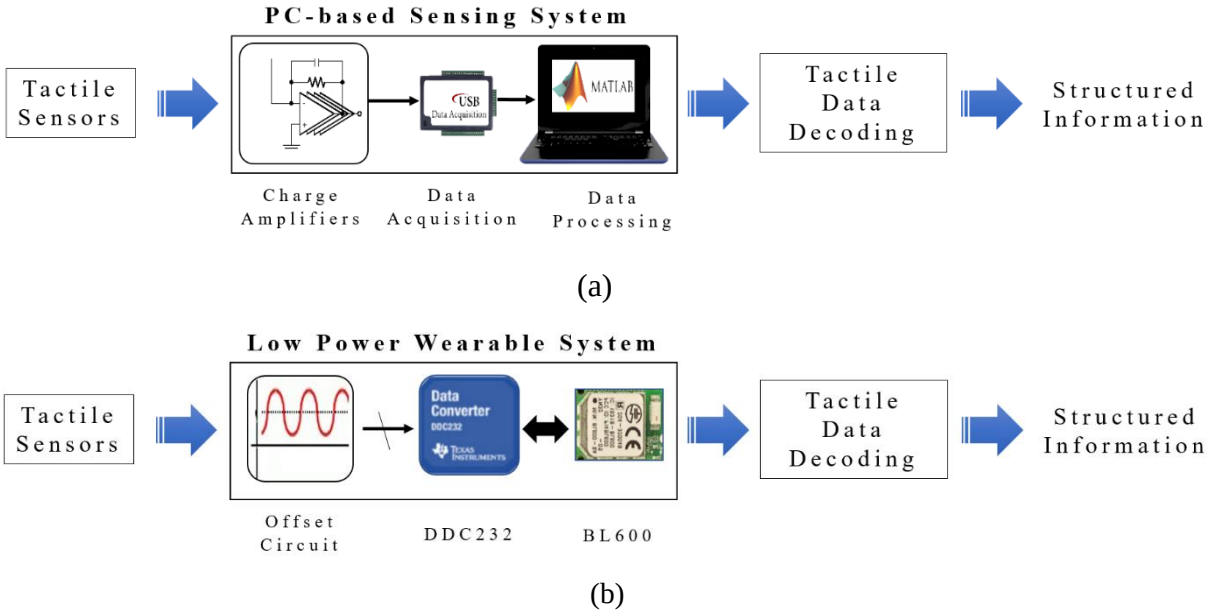

Fig. 3.1 Tactile sensing system (a) using PC-based system and (b) proposed low power wearable sensing system

The recent works as reviewed in the literature (see chapter 2) have focused on designing IE, most are based on data acquisition devices (DAQ) and some are based on power hungry processors (i.e. FPGA) with limited number of sensors (i.e. two sensors). Most of these systems have been developed for the purpose of characterizing sensors, by acquiring their signals and recording the data on PC for further processing and analysis.

In this chapter, we introduce the development of a low power real time miniaturized IE system, capable of providing tactile sensory feedback for prosthetics. The system provides the possibility to interface 32 piezoelectric PVDF-based sensors with low power budget maintaining real time operation. This work provides the first portable version of the electronic skin-electrotactile stimulation system moving from the system depicted by Fig. 3.1 (a) [35] to a wearable system shown in figure 1 (b).

Moreover, the chapter demonstrates the functionality of the proposed system describing the experimental setup carried out to this aim and it validates the suitability of the system for the target prosthetic application when power consumption and time latency are analyzed.

The chapter is outlined and divided into four main parts: design implementation, design characterization, design enhancement and design integration in a feedback system. In the implementation part, the sensing system is introduced, and the IE design implementation is demonstrated, as in sections 3.2 and 3.3, respectively. Section 3.2 deals with the sensor structure/model and the IE circuit design and its specifications. Whereas, section 3.3 presents the experimental tests carried out to analyze the behavior of the IE circuit design. The second part - design characterization - is covered in sections 3.4 and 3.5 where the experimental results are discussed and analyzed. Section 3.6, as the design enhancement

part, introduces some signal processing methods for the purpose of improving the behavior of the IE in reconstructing sensors signals. The conclusion is drawn in section 3.7.

3.2 Sensing System

This section introduces the sensing system blocks including piezoelectric sensor array and IE. The model of the sensor with the fabrication process are presented and the IE circuit design is demonstrated.

3.2.1 Piezoelectric tactile sensor

Piezoelectric materials such as PVDF have been used to make tactile devices/sensors. These materials deform and thus generate charges when they are touched. Typically, the piezoelectric sensors consist of two electrodes of area A separated by the piezoelectric material with thickness t, see fig. 3.2. When contact force F is applied on the piezoelectric sensor, it generates charges +Q and -Q, leading to a potential voltage across the sensor electrodes. Whereas, when the contact force is maintained, the sensor output degrades to zero. This enables the piezoelectric PVDF-based sensors to detect dynamic forces and to operate without the need of a power supply. Thus, PVDF-based sensors are good choice for tactile sensing because they are reliable and efficient in terms of power consumption.

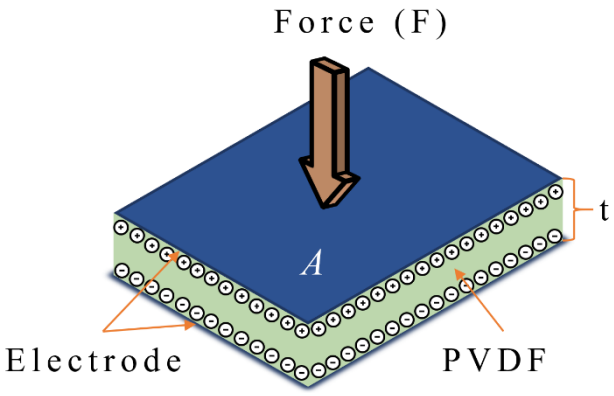

Fig. 3.2 The scheme of piezoelectric PVDF-based sensor

Sensor structure

Fully screen-printed flexible sensor arrays based on P(VDF-TrFE) piezoelectric polymer sensors have been fabricated by JOANNEUM RESEARCH (in the following, JNR) [67]. They patented a low-temperature sol-gel based synthesis for P(VDF-TrFE) inks [68]. Fig. 3.3 shows the structure of a sensing patch built on a sensory array. The fabrication of these sensor arrays is done by screen-printing at a Thieme LAB 1000 [67]. First, a circular bottom electrode is screen-printed on a transparent and flexible (175 µm thick) DIN A4 plastic foil (Melinex® ST 725) substrate. The ferroelectric polymer P(VDF-TrFE) is then screen-

printed onto the bottom electrodes, followed by screen printing the top electrodes (Either PEDOT: PSS or carbon have been used as top electrodes [67]). A final UV-curable lacquer layer is deposited on top for overall sensor protection. As a final step, a pooling procedure is then needed to align in the thickness direction randomly oriented dipoles contained in P(VDF-TrFE) crystallites.

The very thin thickness of the electrode layer (0.4µm) with respect to the thicker PVDF-

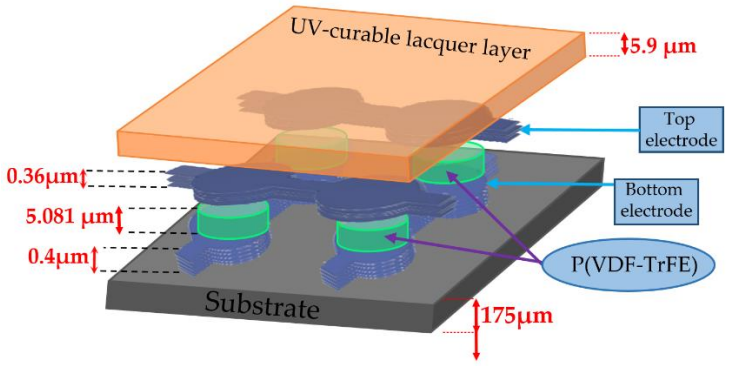

Fig. 3.3 Cross sectional view of a single sensor unit, sketch with indicative thicknesses of the various layers.

TrFE layer (5µm) allows considering its mechanical action negligible for the sensor electromechanical modeling [24], which will be described in the next section.

Sensor model

The behavior of the piezoelectric sensor is a function of the reaction of piezoelectric transducer layers under an applied contact stress, see fig. 3.4. Accordingly, the amount of the generated charges from the sensor are function of the amplitude of the applied force. Thus, to estimate such amount, it is important to have an electromechanical model that shows a relation between the sensor charge and the contact stress. For that, the mathematical mechanical model described in [25] has been adopted. The derived model finds the relationship between the applied mechanical stimulus and the corresponding charge that will be measured by the IE. Equation (1) represents the open circuit voltage generated by the piezoelectric sensor when a constant vertical stress T3 is applied:

$$V_{oc} = -\frac{Q_{sensor}}{C_p} = -\frac{d_{33}A_{piezo}}{C_p}T_3 \quad (1)$$

Where d33 is the longitudinal piezoelectric charge coefficient, T3 is the mechanical stress, Cp is the equivalent capacitance between the electrodes of the piezoelectric film and A_{piezo} is the loaded piezoelectric area. Since the sensor is covered with a protective layer of thickness h, the direct applied stress is not T3.

According to equation (1), author in [25] defined an electrical circuit consisting of

voltage source (Voc) connected in series with a capacitor (Cp). This represents an equivalent electrical model of the piezoelectric sensor. Thus, the output charge (Qsensor) of the electrical model – equivalent to the output of the real sensors – is calculated in equation 2. Further, equation 2 will be used to calculate the charge generated from the model at the input of the analog-to-digital converter of the IE. Where (w) is the signal frequency and (TINT) is the integration time of the internal integrators in the analog to digital converter.

$$q_{sensor\_int} = C_p V_p \sin(wT_{INT}) \quad (2)$$

Equation (2) will be used as a reference point for electrical validation of the IE in section 3.4.

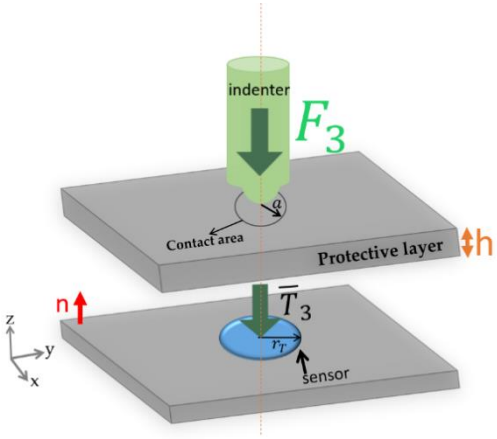

Fig. 3.4 Sketch of the general working mechanism of P(VDF-TrFE) sensors.

3.2.2 Interface Electronics

Requirements and specifications

The development of an interface electronic system necessitates possessing quantitative information about the application requirements such as defining the contact stress/force range and the electrical response of the piezoelectric sensor. These dynamics has been quantified in [69] and can be used as reference point for defining the electronic design specifications. Based on their estimations, the application range goes from 50 Pa to 5 MPa (over 5 orders of magnitude) resulting a charge response ranging from 0.01 pC to 1 nC. However, the range of interest according to [70] is to cover stresses of the order 10-100 kPa for normal manipulation tasks and lower than 10 kPa correspond to gentle touches.

Given the above considerations and based on the frequency range of interest for electronic skin application mentioned in [65], the IE should be able to measure an input charge up to hundreds of pC with large frequency bandwidth up to 1 kHz. Thus, the sampling rate must satisfy the Nyquist condition (above or equal 2 kSps). Moreover, the design must take into consideration many input sensors that will be integrated into the

prosthetic glove attached to the amputee forearm. Thus, this requires an acquisition strategy based on simultaneous sampling in order to reduce the delay in the system.

Block diagram and circuit design

The IE comprises four main components: sensor offset circuit, signal conditioning, analog-to-digital converter and microcontroller. Fig. 3.5 shows the general block diagram of the IE. The tactile sensor array contains set of sensors where each sensor is connected to an offset circuit. The offset circuit is followed by a signal conditioning channel including integrators. The output of the integrators is connected to analog-to-digital converters which are controlled by a microcontroller to acquire the sampled data. Each component is explained in the following subsections.

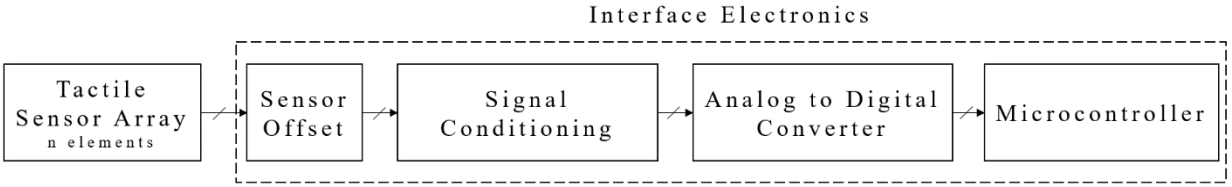

Fig. 3.5 General block diagram of interface electronics for sensing system

1. Sensor Offset Circuit

The tactile sensors can be classified into two categories: sensors that detect dynamic contacts and sensors that detect static contacts. When applying a dynamic contact, the piezoelectric sensor becomes electrically polarized generating potential voltage across the electrodes of the sensor. The voltage polarity changes according to the contact force direction (press or release), applied on the sensor surface. In this case, a sensor offset circuit is needed to handle both voltage polarities (positive/negative). The offset circuit implementation depends on a passive component (resistor) with a voltage reference (Vref) connected in parallel with sensor output, see fig. 3.6. In this way, the sensor output will be shifted up to (Vref/2) level. The offset level value depends on the signal conditioning parameters – the integrator feedback capacitance (Cf) and the integration time (Tint) [39].

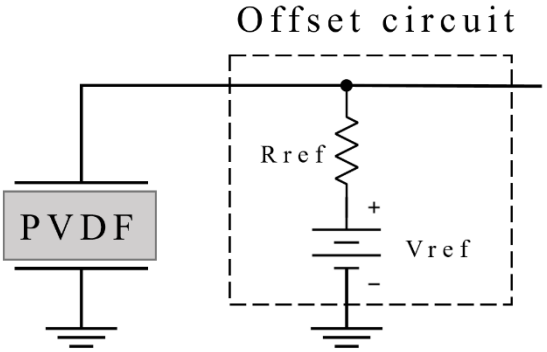

Fig. 3.6 Single piezoelectric sensor connected to a current offset circuit

2. Signal conditioning and analog-to-digital converter

The signal conditioning block implements set of integrators that converts current input to voltage. The output of the integrator is the input of the analog to digital (A/D) converter. Each piezoelectric sensor element in the array requires a dedicated integrator and A/D. For a big sensor array (up to 32 sensing element), the signal conditioning with A/D circuit design becomes complex. To avoid design complexity, a component-off-the-shelf DDC232 has been used. The DDC232 is a current-input analog-to-digital converter which provides simultaneous sampling for 32 input channels. It combines both current-to-voltage integrator and A/D converter. Each input has two integrators so that the current-to-voltage integration can be continuous in time and the output of the 64 integrators are switched to 16 delta-sigma A/D converters via multiplexers. The output of the first 32 integrators are digitized while the other 32 are in the integration mode. The A/D features a synchronous serial interface used to configure the conversion rate and to read the valid converted data [71]. The conversion process is controlled by a CLK pin (configured at frequency 10 MHz) connected to the system clock of the microcontroller. The results of each conversion are stored in an output shift register. The output signal (DVALID) goes low to indicate data are valid and trigger the controller to start the retrieving process.

The retrieved data format can be configured to be either 20 bits or 16 bits. This is done by writing to the 12-bit on DDC232 configuration register the corresponding format value. Three pins DIN_CFG, CLK_CFG, and RESET pins of the ADC are used to write to this register and set the feedback capacitance of the integrators.

3. Microcontroller for data acquisition

Since the DDC232 supports a serial connectivity, a microcontroller is required – first, to control the DDC232 conversion process; second, to acquire and process the converted data. The Laird BL600 module has been used for this purpose. The module contains a Nordic nRF51822 microcontroller which is based on 32-bit ARM Cortex M0 processor. It is an ultra-low power chip integrating the nRF51 series 2.4 GHz transceiver and supporting Bluetooth low energy (BLE). BL600 is a BLE single mode device operating as a slave. Hence, enabling wireless connectivity option which is high recommended in wearable systems.

Implementation

The block diagram and the printed board circuit of the proposed IE are presented in fig. 3.7. The SPI serial peripheral of the microcontroller has been enabled for controlling the conversion and data retrieval process using Keil-ARM IDE. The microcontroller was programed to run three main processes: configuration process, control process and data

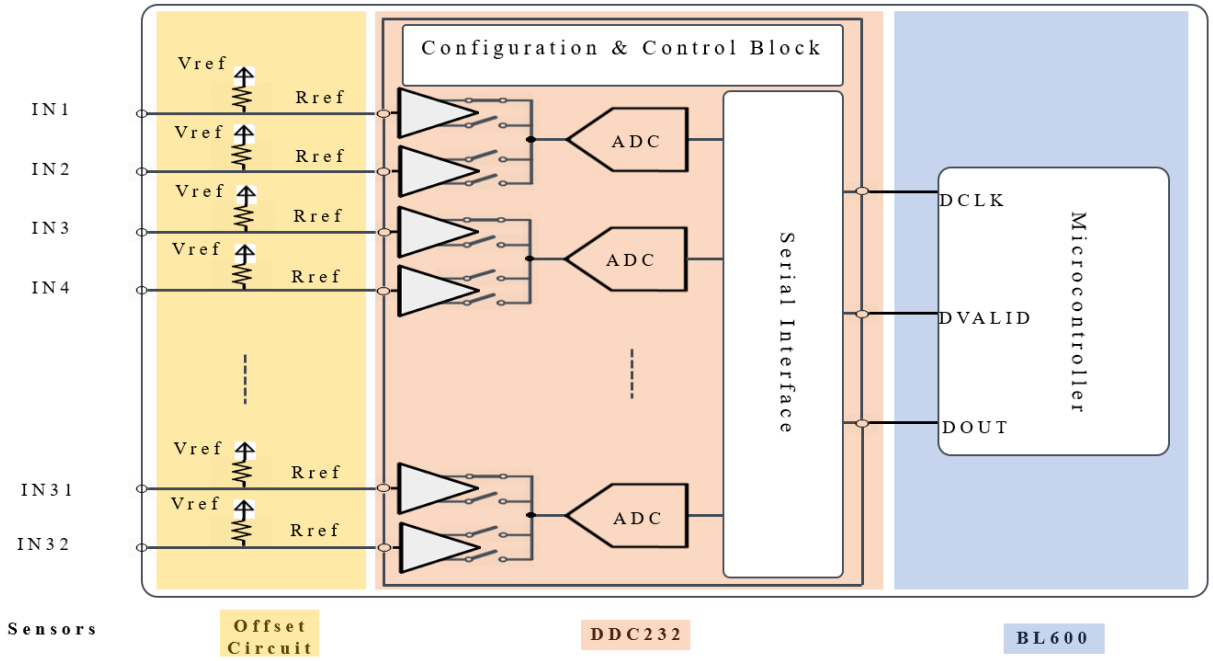

(a)

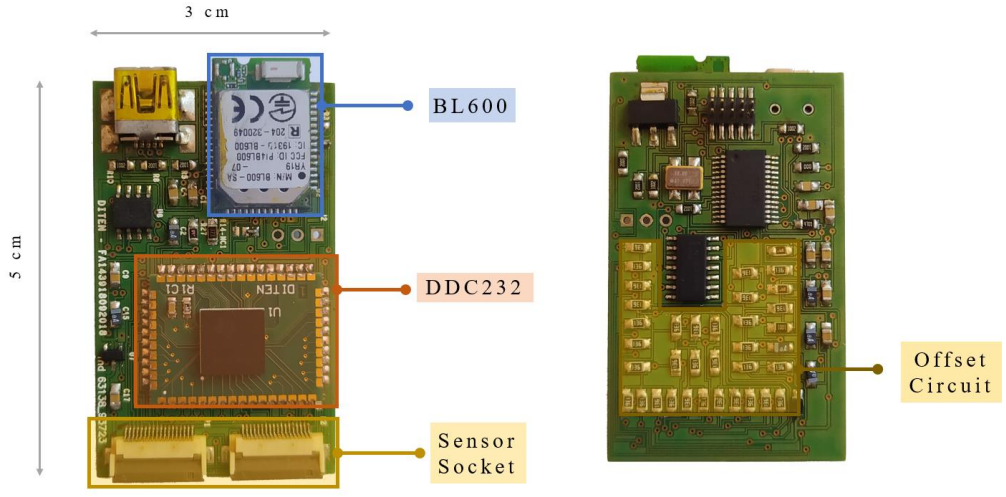

(b)

Fig. 3.7 Interface electronics: (a) block diagram of the design; (b) printed board circuit.

retrieval process. First, in the *configuration process* two main parameters (data format/resolution and the integrator feedback capacitance) of the A/D are configured. Where the A/D is initialized to retrieve data with 16-bit resolution and the feedback capacitance was set to its maximum value (Cf = 87.5 pF) to achieve a high input range of

charges. The configuration process is performed as the microcontroller runs two sequential steps: 1) hold the CONV signal and set the RESET signal hi to control the switching between integrators, then 2) shift 12-bit data (containing the parameters) to the A/D configuration register over DIN_CFG pin (data input pin) at the falling edge of CLK_CFG (the configuration register clock input). At the instant the configuration is done, the *control process* starts generating a clock signal CLK at 10 MHz frequency which activates the A/D. in parallel, the CONV square signal runs at 1 kHz frequency, allowing the A/D to convert sensor signals (32 sensors) at sampling rate 2 kSps. This is because the A/D stores new samples during the high and low states of the CONV square signal. When the A/D is done with sampling the 32 input sensors and stored their data in a register, its DVALID pin goes low to trigger the *data retrieval process*. Where on the falling edge of DCLK pin (serial data clock) the data are shifted out and retrieved by the microcontroller at 4 MHz frequency. Finally, data are sent via UART-to-USB port at a baud rate of 115200 bits per second (bps), to be collected in MATLAB tool and further analyzed.

3.3 Experimental Setup and Methods

After design implementation, first we aimed to verify the correct functionality of the design (experiment one) and second to characterize the response/behavior of the IE with piezoelectric sensors (experiment two). For experiment one, we conducted an electrical test, where the IE was tested with a source generate in series with a capacitor connected at its input, as shown in fig. 3.8. The purpose is to inject sinusoidal signals with defined frequencies and amplitudes and then measure the charges of these signals. The measured charges are then compared to the results which has been estimated through the equation (2) derived for the equivalent sensor model mentioned in section 3.1.2. The test details are discussed next in section 3.4.1.

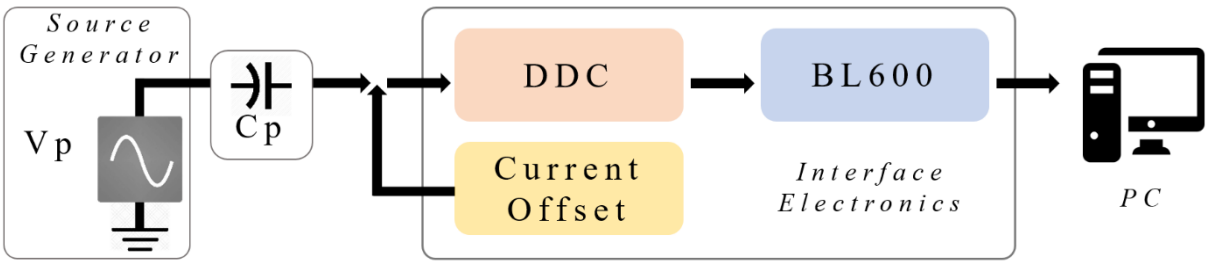

Fig. 3.8 Block diagram of the Electrical setup; Equivalent circuit of sensor (left) connected to interface electronics; Generated signals are reconstructed by the IE and sent to the PC.

For experiment two, we prepared an electromechanical setup in order to perform consistent tests on the IE when connected to real piezoelectric sensors. The setup provides a controlled mechanical indentation on the sensors with the recording of several measurements – obtained by the IE and force sensor. The mechanical chain used for

measurements is shown in fig. 3.9 and it follows the order (up-down). The sensing patch was integrated on a rigid circular substrate and covered by an elastic protected layer (PDMS elastomer layer with thickness 2.5mm) using double-sided adhesive tape (Model 3M300L, 3M) around the sensor array. The skin patch (sensing patch + PDMS+ circular substrate) was then mounted on a fixed support and faced downside. The aim of this coupling is building a skin structure that mimics as close as possible real application conditions. A rigid spherical indenter (R = 4mm) and a piezoelectric force transducer (Model 208C01, PCB Piezotronics) were coupled on the moving head of an electromechanical shaker (Brüel&Kjaer, Minishaker Type 4810). All these elements have been accurately aligned before any test. A sinusoidal signal (force) was then provided by a source generator (3390 Arbitrary Waveform Generator) and conveyed to the electromechanical shaker using a Power Amplifier Type 2706. The single taxel was then excited by applying a mechanical stimulus (sinusoidal force) directly on the PDMS patch covering the sensing patch using the shaker. Before running each test, a preload was applied to guarantee indenter-PDMS contact during the whole test. Two tests were done on the same sensors and under the same conditions (same coupling and indenter positioning). In the first test, charge generated by the sensor was conditioned and acquired by PCB Sensor Signal Conditioner (482C54), while in the second test the generated charge was acquired by the IE. In the two tests, the electromechanical stimulus measured by the piezoelectric force transducer was conditioned and processed by PCB Sensor Signal Conditioner (482C54). A graphical user interface (GUI) developed with NI LabVIEW on a host PC and NI DAQ data acquisition board was used to collect and visualize both the force transducer (stimulus) and the generated charge.

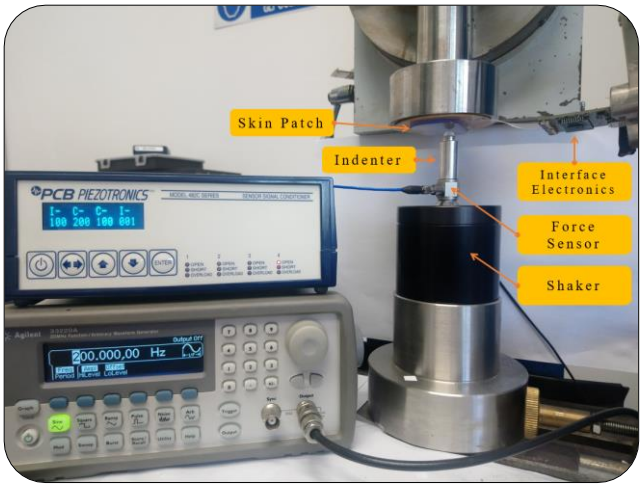

Fig. 3.9 Experimental Setup

3.4 Experimental Results

This section presents the experimental results obtained from both electrical and electromechanical tests.

3.4.1 Electrical measurement results

In the electrical test, several sine signals generated by the source generated have been measured by the IE. The signals frequencies have been varied within the targeted bandwidth (i.e. 1 Hz-1 kHz) with an amplitude range from 100 mV up to 9 V. The IE sends the data to the PC where it has been analyzed in MATLAB tool. Fig. 3.10 (a) shows the charge measured by the IE corresponding to a sine signal of frequency 100 Hz, compared to the charges estimated by equation (2) (Qtheoratical = CpVp sin(wTINT)) – by substituting all its variables (Cp=22 pF; Vp= [100mV-9V]; w=100 Hz; TINT= ½ kSps). The same test was performed for several frequencies. Results illustrated in Fig. 3.10 (b) signifies that the amount of charges become larger as the input frequency increases. Therefore, this validates the correct functionality of IE in measuring charges, matching the theoretical ones estimated by equation (2).

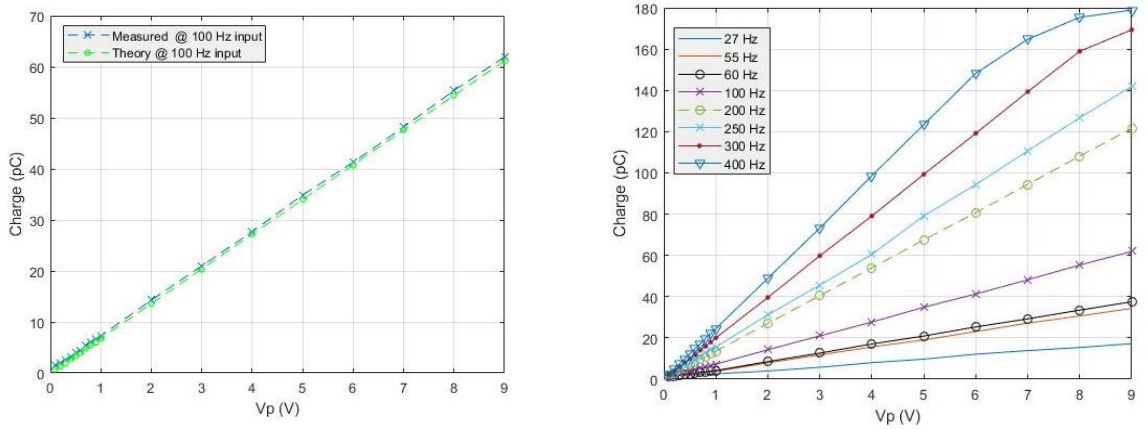

(**a**) (**b**)

Fig. 3.10 (a) The theoretical fit line is calculated from Qtheoratical = CpVp sin(wTINT) derived from the equations presented in [25]; (b) output of IE relative to input signals generated from source generator.

3.4.2 Electromechanical measurement results

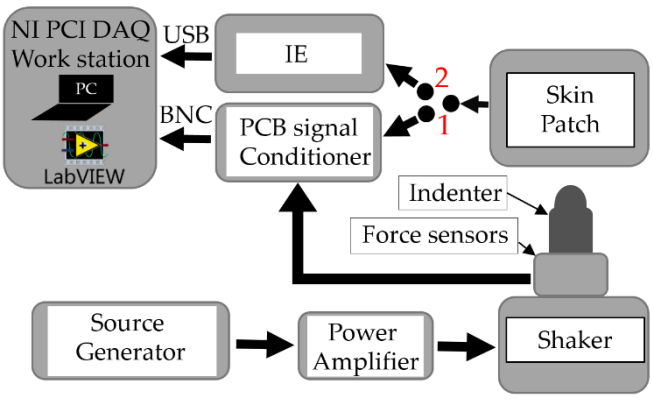

Fig. 3.11 Experimental setup block diagram.

In the electromechanical test, the shaker in the system has been controlled by a source generator to apply stimulus/indentation on the sensor surface, see fig. 3.11. The frequency of indentation has been varied from 20 to 350 Hz and at every frequency value six force levels within 0.2-1.2 N have been applied on the sensor. Note that there were some limitations in the experimental setup that prevented us from reaching frequencies and forces above 350 Hz and 1.2 N, respectively. Two types of data have been recorded during sensor indentation and then sent to the PC-LabVIEW software: the charges measured by the IE; the indentation forces measured by the PCB Piezotronics conditioner. The relation between the indentation force and sensor charges measured by the IE is illustrated in fig. 3.12 (a). It shows the behavior of the IE in detecting a range of charges and provides linear measurements that match with the theoretical estimations presented in the previous section.

To verify more the IE results, the conditioner was included in the test to be a reference point. In this case the IE was disconnected and replaced by the conditioner, which measures both the sensor charges and the indention forces. By repeating the same test conditions done with the IE and with keeping the same parameters (frequency range and force levels), the conditioner demonstrated almost similar results as that obtained by the IE. As it is noticed from fig. 3.12 (b), that the amount of charges increased as the force levels increased, proving the correct results obtained by the IE with just a slight difference in charge values. This difference is also observed from the sensitivity curve reported in fig. 3.13 (a). Although the IE and conditioner curves diverge a little bit, however, it shows similar change over the frequency range which also confirms the correct functionality of the IE. The sensitivities have been estimated from the slopes of the measured charge versus force within the frequency range 20-400 Hz.

In a final test, we aimed to demonstrate the ability of the IE in detecting charges that occurred due to a small indentation force. The test was done by fixing the shaker frequency at 400 Hz and adjusting its amplitude to reach the minimum force value. Results presented in fig. 3.13 (b) show that the IE as the conditioner was capable of measuring charges obtained at 0.01 N force. Also, the difference in results between IE and conditioner is constant, thus, making it is possible to apply setup calibration and find the empirical difference value.

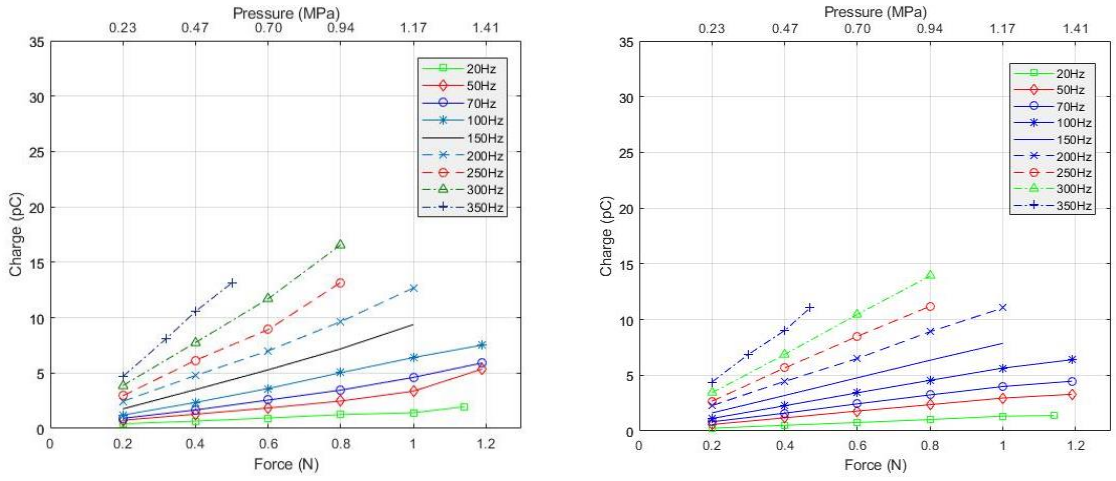

(**a**) (**b**)

Fig. 3.12 (a) IE output measurements with real sensors; (b) Conditioner output measurements with real sensors.

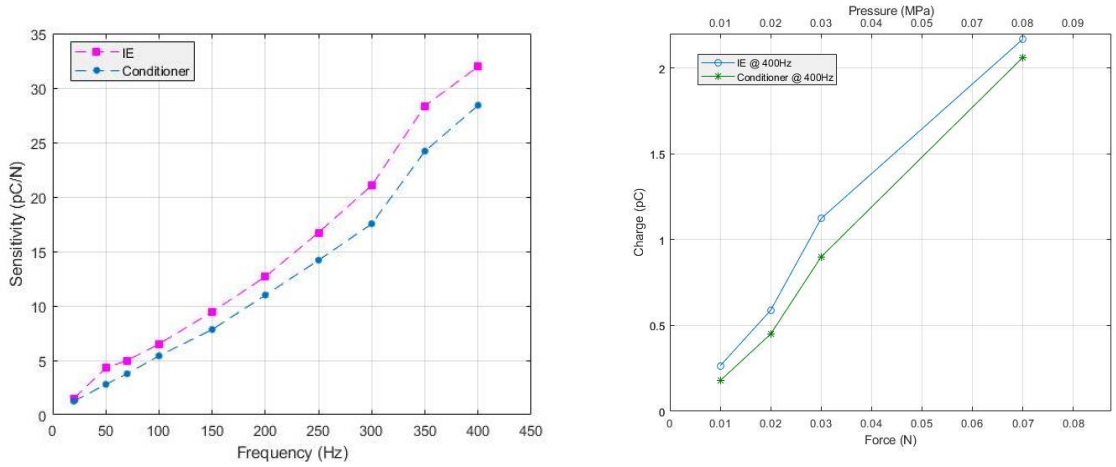

(a) (b)

Fig. 3.13 (a) Sensitivity as a function of frequency; (b) measured charges at minimum detectable force (0.01 N).

3.5 Assessment of results

Two aspects of the design have been analyzed: the IE measurements precision by expressing the signal to noise ratio and the design power consumption.

3.5.1 Signal to noise ratio

Measuring the signal to noise ratio of the achieved results is important to compare the measured charges power to a level of noise power that may exist in the design. Harmonic distortions are one of these noises that would add to the input signal or it may occur at the output of the IE. Such noise contributes directly to the signal-to-noise ratio of the design. According to IEEE [72], SINAD (signal to noise and distortion ratio) and ENOB (effective number of bits) are useful methods for noise analysis. SINAD measures the degradation of

the signal due to unwanted signals in noise and distortion. Also, it provides the basis for calculating the ENOB that specifies the number of bits of the signal which are above the noise floor. The formula for calculating the SINAD expressed below:

$$\text{SINAD} = 20\log\frac{\text{rms(As)}}{\text{rms(n + k)}} \tag{4}$$

It is computed by finding the ratio of the root-mean-square (rms) of the fundamental signal (As) to the root-mean-square of noise and distortion (n + k). After normalizing the input data to scale between 0-4.09 V (A/D reference voltage), FFT has been applied to distinguish the fundamental signal from other harmonics and noise existing in the spectrum. Finally, the amplitude of the signals in the spectrum have been measured and substituted in the equation.

Whereas ENOB has been computed using the equation (5), derived in [73], after applying fast Fourier transform (FFT) to the data. Fig. 3.14 shows the process of applying FFT to compute both SINAD and ENOB. It demonstrates an example for an input signal of 100 Hz; a) original signal in time domain, b) reconstructed signal after A/D conversion, and c) the FFT of the signal demonstrating the fundamental signal at the 100 Hz of frequency.

$$\text{ENOB} = \frac{SINAD - 1.76\,dB + 20\log\left(\frac{Full\ scale\ amplitude}{Input\ Amplitude}\right)}{6.02} \tag{5}$$

Fig. 3.15 illustrates the results of SINAD and ENOB curves versus frequency. It shows a consistent behavior of the IE over frequency where 14 bits out of 16 bits of the digitized signals are above the noise floor. So, this will be an advantage to retain more accurate data and thus acquiring tactile data with high resolution.

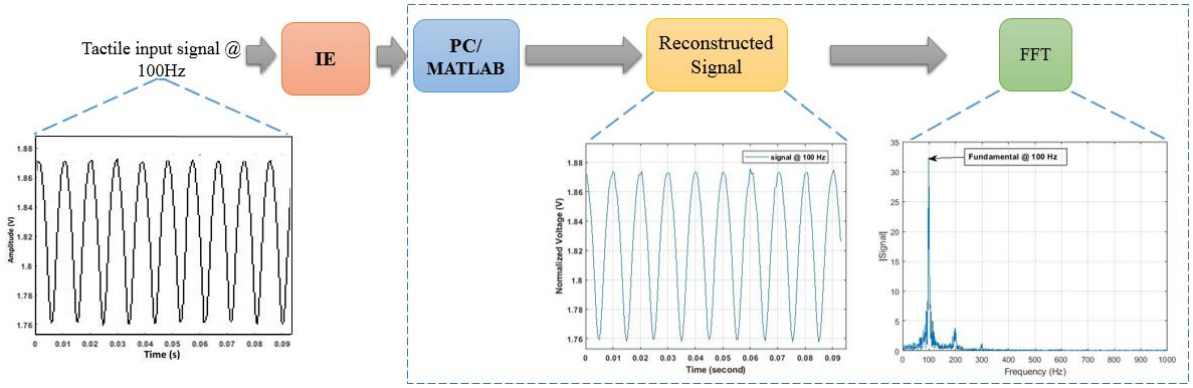

Fig. 3.14 Example of an input signal at 100 Hz of frequency in time and frequency domains.

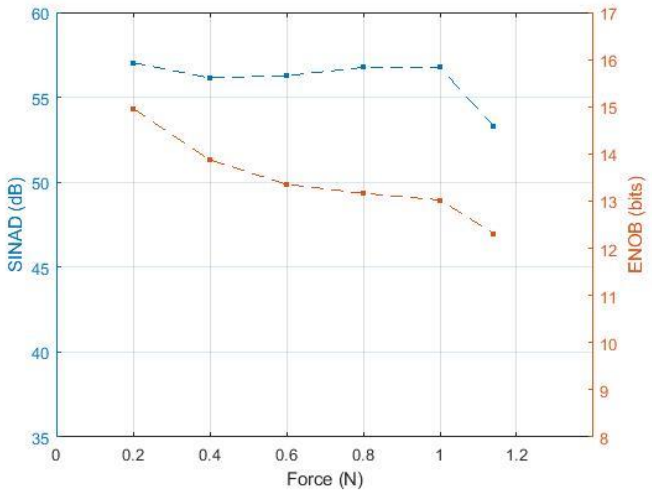

Fig. 3.15 SINAD and ENOB variation with respect to the applied forces.

3.5.2 Power consumption

The current consumption of the whole system has been measured using a DC power supply that provides a current limiter. The current consumed by the system is first measured, then the power consumption is calculated using the equation Power = Voltage × Current with 5V power supply. The power consumption for the different blocks is shown by the bar plot in fig. 3.16 where the total power consumption is equal to 300mW.

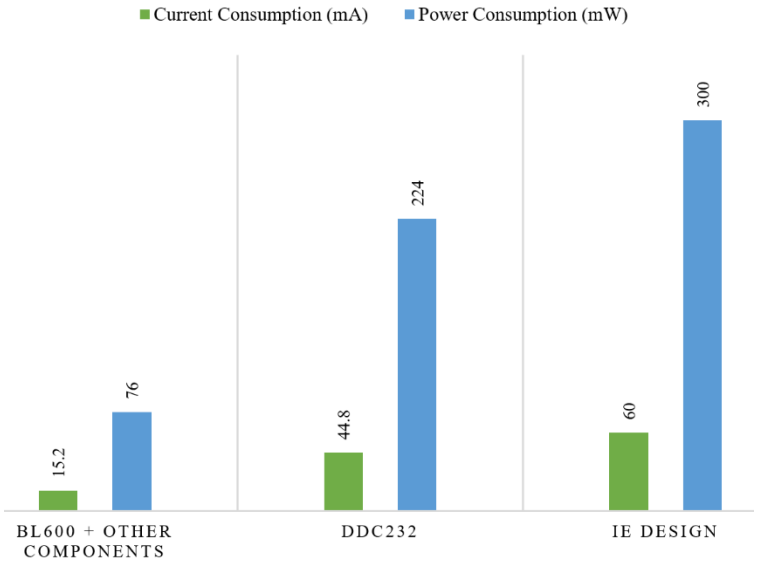

Fig. 3.16 Measured power consumption of the system

To supply the system with a single 2Ah Lithium polymer battery with a voltage of 3.7V, the available energy in joule is:

$$E\,[J] = 2000mAh \times 3.7V \times 3600s = 26640J \quad (6)$$

With 10% efficiency loss to supply the platform with the correct voltages, the usable

energy is then 23976J. Ec [J] the total energy consumed by the prototype is 1080J (300mW*3600s). To find the lifetime of the battery we use the following formula:

$$\text{Lifetime [h]} = E\text{ [J]}/Ec\text{ [J]} = 22.2\text{h} \quad (7)$$

This lifetime of the battery is acceptable for the target application. Moreover, the presented results are promising towards achieving a wearable sensing system that can be powered by a small battery.

3.6 Interface Electronics with signal pre-processing

3.6.1 Motivation

The results demonstrated in the previous sections represent the outcome of a quasi-ideal experimental setup where testing parameters have been pre-defined (i.e. touch alignments, pre-programmed force, and frequency levels for the touch). Although the results verify and validate the good response of the IE in acquiring sensor charges, however, the IE should further be experimented and tested in a more realistic scenario. For this purpose, we have arranged a different experimental setup including the IE with a senor patch (12 sensors) and a load-cell (for measuring force) with a PCB Sensor Signal Conditioner (48C54). The aim is study the correlation between stimuli applied at the surface of the skin patch and the response detected by the IE. The plan was to touch the sensor with a finger and adjust force level.

The setups shown in Figure 3 are composed of a load cell and the skin patch connected to the conditioner (Fig. 3.17, a) or the IE (Fig. 3.18, b). The skin patch was attached to a rigid substrate and the final structure was placed on the top of the load cell. The tactile sensor and the load cell will detect the force stimuli applied on the surface of the skin patch at the same time. Both the output of the load cell and the output from the conditioner are digitized by a National Instrument DAQ and visualized on LabVIEW while the output of the Interface Electronics was connected directly to the PC through USB. The sensing patch in this setup has been sandwiched between two conductive tapes which are connected to a ground reference. This is to avoid any external source of charges (i.e. human hand) and thus limiting the induced charges to the effect of the PVDF piezoelectric material under a contact touch.

Two similar tests have been conducted with the aforementioned setup installation. We have planned a testing scenario composed of applying two types of touches: continuous touch (Cont-Touch) and tapping touch (Tap-Touch). In case of Cont-Touch, we pressed the sensor by finger and changed the force level without releasing the touch. While in case of Tap-Touch the sensor was pressed and released very fast without changing the force level.

The two types of touches were repeated many times with different contact areas and force levels. These types of touches are expected to occur during manipulation as in grasping and rolling objects. On the PC side, a LabVIEW software that receives the sensor data and load cell force measurements.

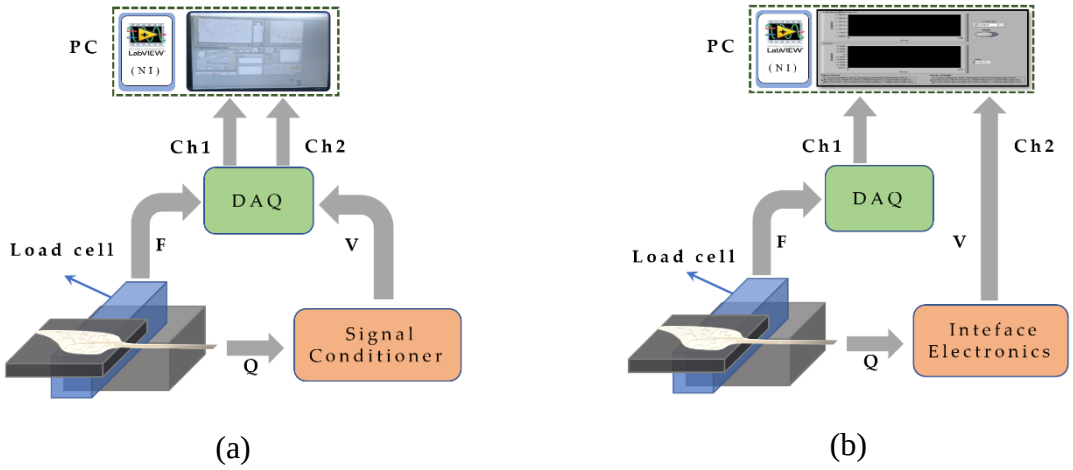

(a) (b)

Fig. 3.17 Experimental setup

Fig. 3.18 shows the IE and conditioner responses for touches with their corresponding forces. The time-domain signal of both IE compared to the conditioner does not present consistent results, signifying a kind of noise included in the IE output. It is difficult to discriminate the touch signals from the no-touch level (0<t< 5s). Thus, a time-frequency analysis has been carried out to identify the frequency contents of the touch's signals. Fig. 3.19 shows the frequency spectrum of both IE and conditioner measurements, presenting two major issues: 1) very low frequency (< 30 Hz) content corresponds to the touches has been detected by the conditioner whereas not detected by the IE and 2) harmonics are spread in the IE spectrum.

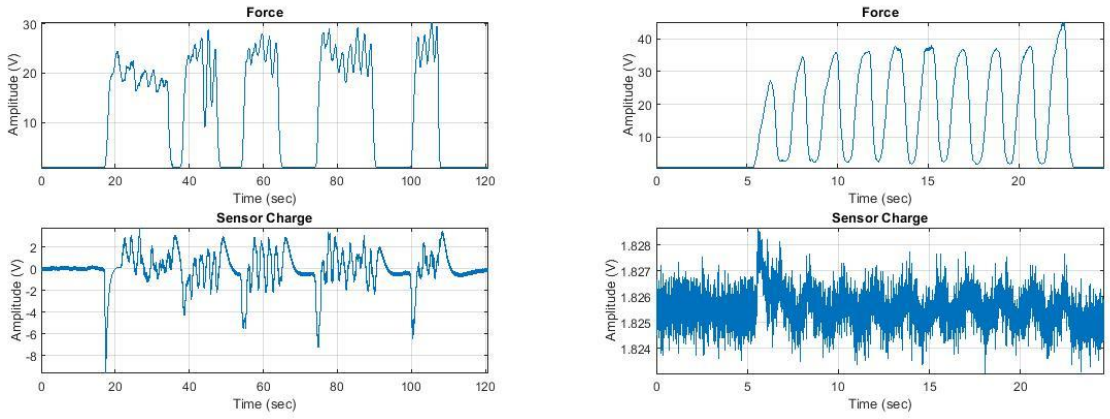

Fig. 3.18 Conditioner measurments (left); Inteface Electronics measurments (right)

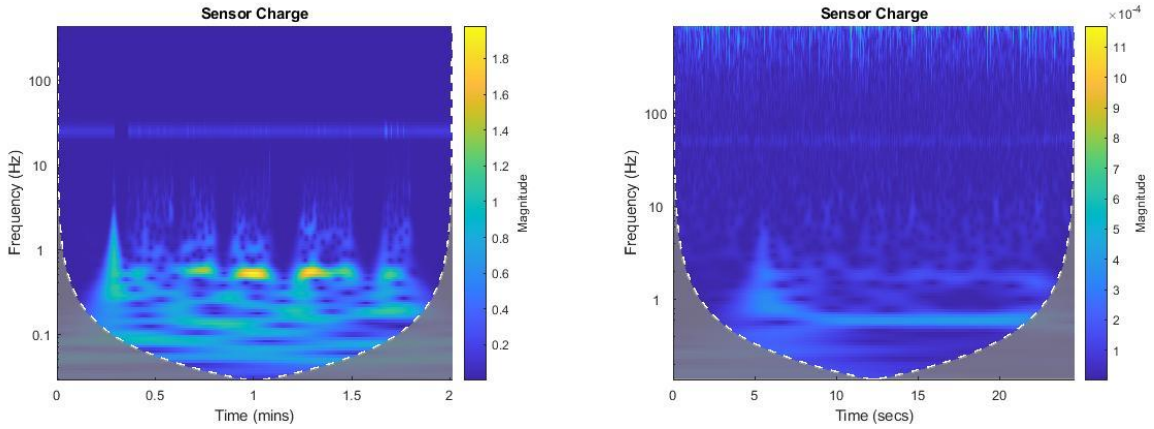

Fig. 3.19 Conditioner measurments Spectrum (left); Inteface Electronics measurments Spectrum (right)

Therefore, signal processing strategy is required to improve the response of the IE at very low frequency touches and to reduce the effect of noise (harmonics). For this purpose, we developed and implemented in the IE three filtering methods: decimation filter, finite impulse response filter (FIR) and moving average filter (MAF). The implementation process are introduced and the results of the three filter are discussed in the subsequent sections.

3.6.2 Implementation of tactile signal processing

Filtering by Decimation method

The issues presented in the previous section concludes that the highest frequency component of interest is within tens of hertz (fm < 30 Hz). This implies that it is feasible to reduce the original sampling rate to a new rate that satisfy the requirements of Nyquist theorem for the new fm. Thus, this process of converting a given high rate F to lower F' is called decimation. It utilizes oversampling and averaging to increase measurement resolution and improve signal-to-noise-ratio, see fig. 3.20. During oversampling, set of samples are accumulated to output a value within the new sampling period. The number of the accumulated samples (N) is defined by the decimation factor M which is the ratio of F to F'. The average process properly scales the result back to 16-bits format.

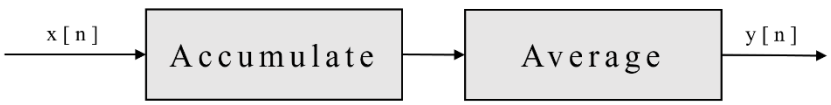

$$y(n) = \frac{1}{m}\sum_{k=0}^{N-1} x(k)$$

Fig. 3.20 Decimation block diagram and equation

Decimation filter has been implemented in the IE. The target is to reduce the sampling

rate from 2 kHz to 64 Hz – the required sampling rate according to the Nyquist frequency (fs = 2fm; fm=32 Hz). Thus, the decimation factor is 31.25, the decimator outputs a value after accumulating and averaging 32 samples. The effect of applying the decimation is reported in Fig. 3.21. It shows a cleaner signal compared to Fig. 3.18 (right) with good reconstruction for the touches of low frequency, compared to Fig. 3.19 (right). These results verify the feasibility of applying decimation to filter the signal from noise and reconstruct the frequencies of interest in the real application.

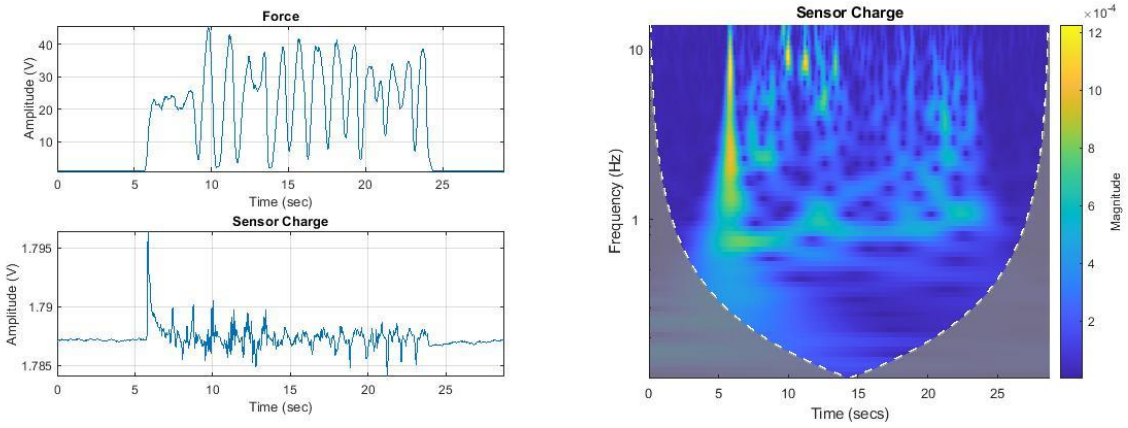

Fig. 3.21 IE with decimation filter measurments: in time (left); spectrum (right)

Filtering by Finite Impulse Response method

Finite impulse response is a well-known digital signal processing filter. The filter output is a result of discrete-time convolution process between input signal and the impulse response of the filter (filter coefficients), see fig. 3.22. The design of the filter is defined/specified by two main parameters: cutoff frequency and filter order. Also, for the purpose of reducing the noise in the IE signal, the value of cutoff frequency should be low to eliminate high frequencies from the signal spectrum. The filter order generally is recommended to be high to have more accurate results. However, high filter order means that many multiply-accumulate (MAC) operations are required to filter out one output and thus the filter will cause a delay in the IE. Therefore, this trade-off should be considered while designing the filter.

$$y(n) = \sum_{k=0}^{N-1} h(k)x(n-k)$$

Fig. 3.22 Decimation block diagram and equation

MATLAB has been used to design a FIR filter with 30 Hz cutoff frequency and an order

of 58. The MATLAB code to generate the filter coefficients is shown below:

$$H = fir1(57, 30/1000) \tag{8}$$

Where the first argument (57) is the filter order and is always one less than the desired length. The second argument is the normalized cutoff frequency where 1000 is Nyquist frequency (fm=fs/2; fs=2 kHz). The filter will have a delay of 28 samples (order/2) and cutoff frequency 30 Hz. This filter has been implemented in the IE. Fig. 3.23 shows the output of the filter where the noise spread as high frequencies components are eliminated, whereas the low frequency components are reconstructed. Note that applying FIR filter to all the IE channels (32) was quite challenging. From the controller resources perspective, the memory was limited to run just a set of 10 filters for 10 sensors.

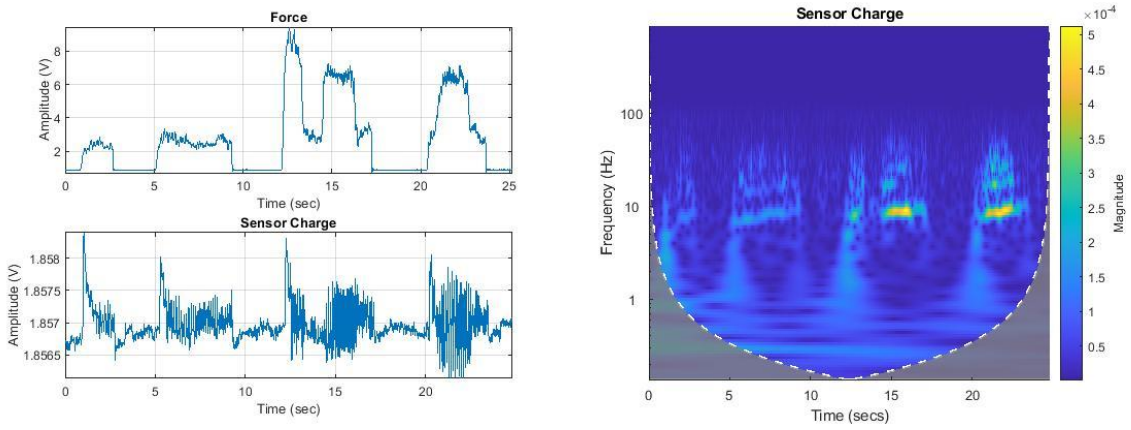

Fig. 3.23 IE with FIR filter measurments: in time (left); spectrum (right)

Filtering by Moving Average Filter

Moving average filter (MA) is one of the popular digital filtering techniques that can smoothen all kind of data and reduce random noise in the data. Exponential moving average filter (EMA) is a type of MA filter that operates with low computational burden and can be implemented easily and efficiently. EMA filter computes a weighted average of time-ordered sequence by applying to the previous inputs weights that decrease exponentially [74].

The exponential moving average filter is expressed in a simple equation:

$$y[n] = \alpha x[n] + (1 - \alpha) y[n - 1] \tag{9}$$

Where x[n] is the current input, y[n] is the current output, and y[n−1] is the previous output; α is a number between 0 and 1. If α=1, the output is just equal to the input, and no filtering takes place. Equation 9 can be demonstrated as follows:

$$y[n] = \alpha \sum_{k=0}^{n} (1 - \alpha)^k x[n - \mathrm{k}] \tag{10}$$

The output of the filter can be expressed as the convolution of the input with the impulse response. The impulse response is the output of the filter when Kronecker delta function is applied to the filter input. The definition of the Kronecker delta:

$$\delta[n] = \begin{cases} 1, & n = 0 \\ 0, & n \neq 0 \end{cases} \tag{10}$$

Then the impulse response of the EMA is:

$$h[n] = \alpha \sum_{k=0}^{n} (1-\alpha)^k \delta[n - \mathrm{k}] = \alpha(1-\alpha)^n \tag{11}$$

Thus, the output of the filter can be expressed as follows:

$$y[n] = x[n] * h[n] \tag{12}$$

Analysis of such DTLTI systems is easier in the Z-domain, in which the convolution is reduced to a simple product. It is defined as:

$$X(z) = Z\{x[n]\} = \sum_{n=0}^{\infty} x[n] z^{-n} \tag{13}$$

Then the transfer function of the system is:

$$H(z) = \frac{Y(z)}{X(z)} \tag{14}$$

The transfer function of the EMA filter can be calculated from the impulse response of the filter expressed in equation 11:

$$H(z) = Z\{h[n]\} = \sum_{n=0}^{\infty} h[n] z^{-n} = \frac{\alpha}{1 - (1-\alpha) z^{-1}} \tag{15}$$

Expressing the frequency response of the filter describes how the spectrum of the input changes as it passes through the filter. To calculate the frequency response of the EMA filter, we can evaluate the transfer function for z=$e^{-i\omega}$ and then calculate the amplitude of each frequency component in the output by taking the modulus of H($e^{-i\omega}$).

$$\left|H\left(e^{-i\omega}\right)\right|^2 = \frac{\alpha^2}{1 - 2(1-\alpha)\cos(w) + (1-\alpha)^2} \tag{16}$$

w is the normalized angular frequency in radians per sample. You can substitute it with ω=2πf/fs where f is the frequency in Hertz, and fs is the sample frequency of the system in Hertz. The filter's gain in function of the frequency in fig.3.24 is computed in dB by using the logarithmic scale.

$$A_{dB}(w) = 10\, log_{10} \left|H\left(e^{-i\omega}\right)\right|^2 \tag{17}$$

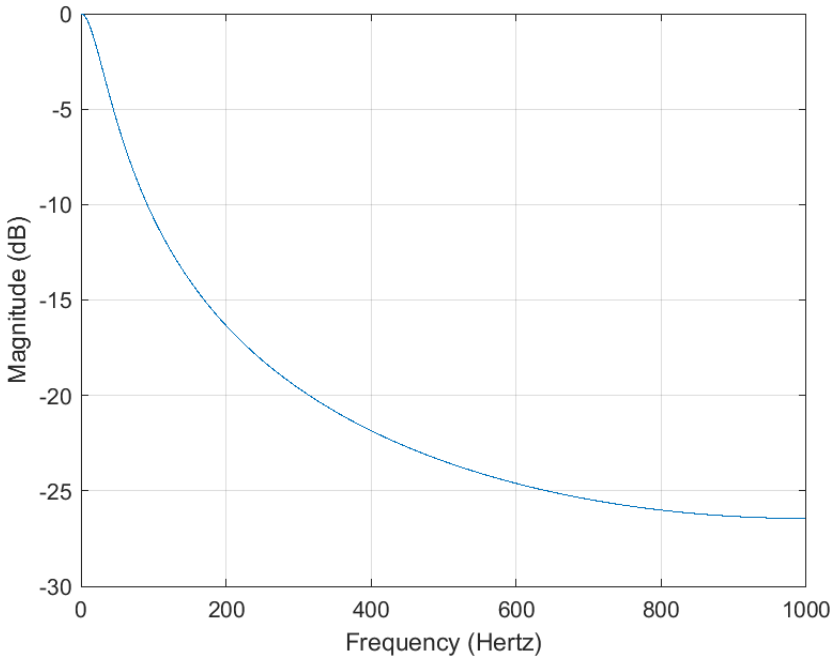

Fig. 3.24 Frequency respons of the moving average filter

The EMA behaves as a low pass filter where low frequencies have a near-unit gain, and high frequencies are attenuated. The filter has been implemented on the IE, performing filtering at around 30 Hz cut-off frequency. The filter α value has been computed and set a given value to enable the EMA to filter out signals above the cut-off frequency. To find it, the following equation has been solved where the power gain is a half:

$$\left|H\left(e^{-i\omega}\right)\right|^2 = \frac{1}{2} \tag{17}$$

Thus, the cut-off frequency is

$$w_c = \arccos\frac{\alpha^2 + 2\alpha - 2}{2\alpha - 2} \tag{18}$$

Therefore, the value of α is around 0.0909 to achieve cut-off frequency 30 Hz.

This allows the Interface Electronics (IE) to perform filtering with minimum delay and at high sampling rate without the sacrifice of losing the detection of some touches during run-time. By implementing the filter on the IE and applying it for the 32 sensors, we recognized a significant improvement in the behavior of the IE. The IE is capable at initialization to set a small decision threshold which allows the detection of more genuine touches avoiding the detection of some fake touches.

Fig. 3.25 shows sensor data acquired and filtered by the IE. The plot shows small and stable noise level compared to the touch applied and detected by the IE. This preliminary test shows the reconstruction of taping and continuous touches by the IE. For example, the first two spikes (@1.9 sec and 3.2 sec) correspond to tapping touches while the continuous touch is represented in the portion after the third spike (@ 5.1 sec).

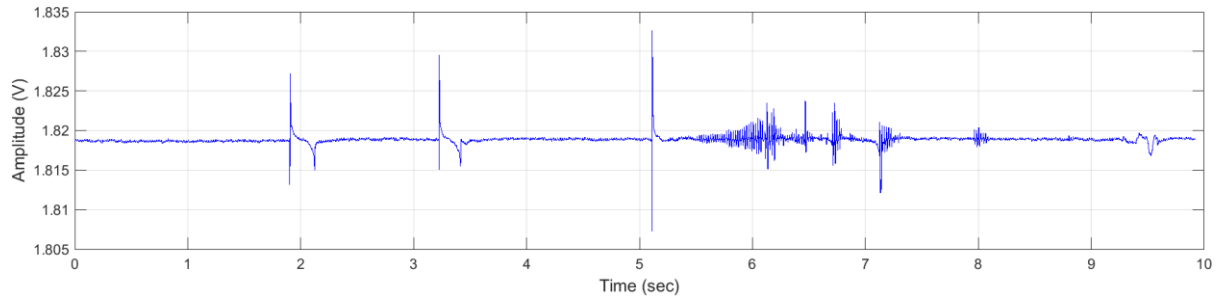

Fig. 3.25 Output of the IE after implementing EMA fiter

After all, we can conclude that the IE can be configured to operate in three modes: continuous transmission, event-driven and digital filtering mode. In the continuous transmission mode, the IE sends data packet at each time it acquires a new sample. The transmitted data is for an array of 32 sensors where each sensor data is packed within 40-bit packet, leading to 1280 (32x40 bits) overall bits for the whole array. The overall bits are transmitted at 1 Mbps baud rate through UART, which will take around 1.3 ms for transmitting the data of the whole array. However, during the 1.3 ms, around 3 arrays samples will be lost since the actual sampling rate is 2 kSps and the transmission rate is around 725 Hz (2000/725). Thus, decreasing the sampling rate down to match with the transmission rate could be a solution to avoid losing samples.

In the event-driven mode, the IE continuously acquires sensor data, but only sends the data of the touched/activated sensors. In this scenario, a threshold value should be defined/configured representing the decision boundary between touch and no touch events. The advantage of this mode is reducing the load on the transmission bandwidth, where only part of the sensor array will be touched leading to an overall number of bits smaller than 1280 bits that should be transmitted. In the third mode, filtering is enabled in the IE where the user can select to run either Decimation filter or FIR filter. FIR is a good choice for filtering noise in the sensor data, however at the cost of delay and memory storage. With the current filter order (58), the delay would be around 28 samples and the number of filters to run on the IE would be at most 10 filters. This disadvantage could be solved by combing more than senor together to represent an input to the filter. On the other hand, no memory limitations occur for applying decimation to the whole sensor array (32 sensors). Noting that mode three, filtering, can run with either continues transmission or event-driven transmission. Table 3.1 reports the specifications of the IE working in the three modes.

Table 3.1 IE SPECIFICATIONS WORKING IN THREE MODES: CONTINUOUS TRANSMISSION, EVENT-DRIVEN AND DIGITAL FILTERING

Modes	**Continuous Transmission**	**Event-driven**	**Digital Filtering**		
			FIR	**Decimation**	**EMA**

# of sensors	32	32	32	32	32
Sampling rate	2 kHz	2 kHz	2 kHz	64 Hz	2 kHz
Transmission rate	~ 725 Hz	Touch-dependent Max: 725 Hz	Cont. Mode: 725 Hz; Event-driven Max: 725 Hz	Cont. Mode: 64 Hz; Event-driven Max: 64 Hz	~ 725 Hz
Delay (trans. Time* + sampling time)	1.3 ms + 500 us	Max: 1.3 ms + 500 us	Max: 1.3 ms + 500 us + 14.5 ms**	Max: 1.3 ms + 15.625 ms	1.3 ms + 500 us
Lost samples	~ 3 arrays***	Max: ~ 3 arrays	Max: ~ 3 arrays	No loss	~3 arrays***
# of bits of packet	40 bits x array	Max: 40 bits x array	Max: 40 bits x array	Max: 40 bits x array	40 bits x array
Memory limitations	No	No	Yes; 10 sensors of the array are filtered	No	No

* time to transmit data of 32 sensors; reciprocal of transmission rate

** this time is due to the delay resulted from filter (order/2) x sampling time

*** array contain 32 sensors

3.7 Summary

The design, implementation and experimental evaluation of miniaturized, low power and real-time interface electronics for PVDF-based piezoelectric sensors is presented in this chapter. The circuit design has been developed according to the sensing system requirements, task and hardware related. The IE is composed of low-power ARM-Cortex M0 microcontroller and a DDC232 analog-to-digital converter to interface 32-input tactile sensors and acquire their data simultaneously. The sensing system has been introduced by presenting the sensor structure with its model and by describing in details the building components and implementation process of the IE. After implementation, IE has been tested with a sensing array for a range of normal forces 0.01 to 1.2 N (10 kPa – 1.4 MPa) and frequency (20 Hz - 350 Hz). Where the generated charges have been acquired and measured by the IE with 56 dB signal-to-noise ratio and 14 bits of ENOB. This show that the IE can measure range of charge that corresponds to range force (order up to 100 kPa) for normal manipulation tasks and stresses. Moreover, the energy consumption of the IE system has been measured showing encouraging results of about 22h of battery lifetime. Furthermore, enhancement methods have been implemented toward improving the IE behavior by reducing the effect of noise in the design. Two filters, decimation and finite impulse response has been used and their results have been discussed. The IE provides three

operational modes that could be tested in the future as its integrated in a sensory feedback system. In the next chapter we will demonstrate a sensory feedback system based on the proposed IE. Then we will study the behavior of the IE in delivering tactile information to the user//participant.

Chapter 4 Interface Electronics in the Sensory Feedback of Prosthetics

4.1 Introduction

The tactile sensing system is the basis for enabling the sensory feedback system to deliver tactile information to the prosthetic user. Sensory feedback systems are usually composed of: i) tactile sensing arrays, ii) Interface Electronics (IE), and iii) stimulation system. The stimulation system delivers sensory information from tactile sensors through electrical stimulation on the forearm of an amputee. The system must be robust and embedded to be integrated into a prosthetic hand or used by patients with sensory deficits. As such, the system should include flexible tactile sensors of high electro-mechanical frequency bandwidth, with hopefully spatial resolution of 1mm for fingertips.

Some researchers developed sensing systems [40], while others proposed PC controlled stimulation systems [41]. Few studies in the literature proposed embedded-real time feedback systems that incorporate the two systems. Pamungkas and Ward. [42] developed a sensory feedback system based on sixteen polymer film force sensors fitted to the fingers and palm of a prosthetic hand. Six electrotactile feedback channels were used for force feedback. A host PC was used to monitor the sensor data and to deliver appropriate pulses to the six electrodes. Whereas Franceschi et al. [35] and Hartman et al. [43] investigated the possibilities of communicating tactile information such as touch position from artificial skin (PVDF based sensor array) through a host PC. Information from an array of 64 piezoelectric sensors is translated into electro-cutaneous stimulation patterns and conveyed to the subject through 32 electrodes or concentric electrodes attached to the subject's arm skin.

The speed in communicating sensation information has not been widely reported on when examining the performance of a sensory feedback system. A healthy nervous system can take approximately 14-25 ms to deliver tactile information to the brain [44]. A change in the dynamics of a prosthetic feedback system (e.g., response time constants, pure time delays) affects the overall system behavior, even its stability. One example of this is the integration of advanced haptic intelligence within the feedback loop. The authors in [45] examined a multi-modal sensory feedback system with three amputees. Sensory information from five piezoelectric barometric sensors was mapped into stimulations through vibrotactile or mechanotactile feedback. The developed system can communicate sensory information to the remaining stump of the amputees within 85 ms. Schoepp et al. [46] used a microcontroller (ATmega32u4) to map force level from two SingleTact sensors into one tactor fixed on the upper arm. The system operates with a time delay of 200 ms between touch instant and activation of the tactor.

With respect to previous PC-based systems presented in the literature e.g. [35]-[43], this chapter demonstrates an embedded sensory feedback system based on the IE design developed and explained in chapter 3. The system can artificially convey to the user the position and the level of any touch applied on a flexible distributed electronic skin. The system is portable and capable of delivering the tactile information to the user within a delay comparable to the healthy nervous system [44]. The system was preliminarily tested on three healthy subjects.

4.2 Feedback System Architecture

The sketch of the proposed feedback system is shown in fig. 4.1. It consists of a) the tactile sensor arrays with three sensing patches, b) an IE, c) a master Bluetooth module [75], and d) a fully programmable 24-channel electro-cutaneous stimulator equipped with three concentric electrodes. In the following the details of each part.

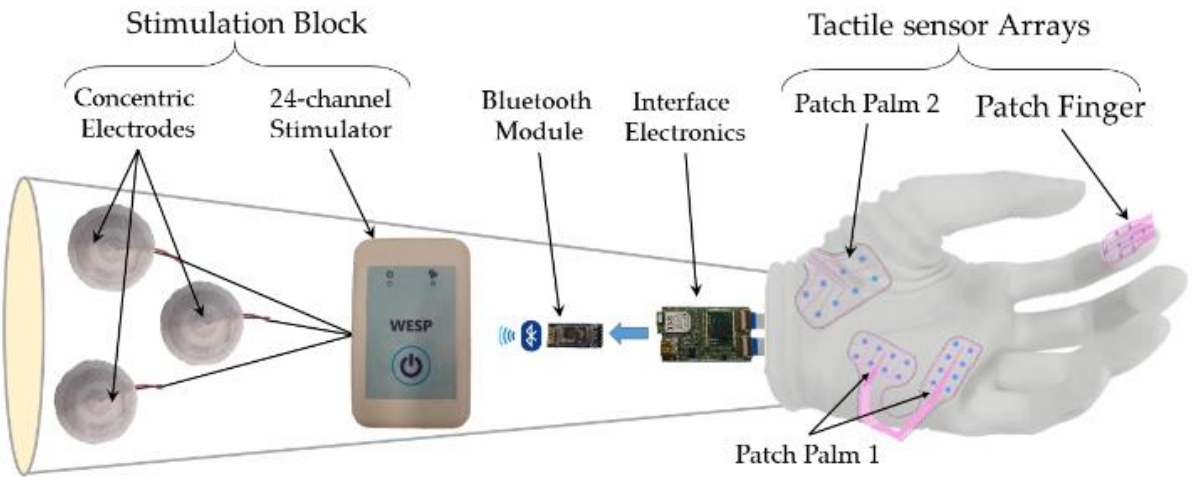

Fig. 4.1 Sketch of the sensory feedback system

4.2.1 Tactile sensor arrays

The presented sensing patches are composed of three sensor arrays (32 sensors in total), i.e. palm left1 (16 sensors), palm left2 (8 sensors), and single finger (8 sensors). The three patches were chosen following the number of channels offered by the IE (32 channels). These sensors have been fabricated as described in chapter 3 and fig. 4.1 shows their shape.

4.2.2 Interface electronics

The IE performs three tasks: 1) detection and identification of the position of the touch with its charge level (three intervals of charge were selected as the identification of three force levels); 2) translation of the charge value into its corresponding electrotactile commands; 3) transmission of the commands to the stimulator through the HC-05 Bluetooth module. The HC-05 is a master/slave configurable UART-to-Bluetooth converter. It supports Bluetooth standard 2.0 and provides UART serial interface for configuration and data transfer [76].

4.2.3 Stimulation device

The stimulation block employs a 24-channel programmable battery-powered stimulator (WESP, Tecnalia Serbia [77]). It generates current-controlled waveforms with a current magnitude in the range of 0-10mA with 0.1mA step, a frequency from 1 to 400 Hz, and a pulse width from 50 to 500 μs. The WESP produces simultaneous charge-balanced biphasic continuous electrostimulation pulses in any combination of electrodes or individually in each electrode. Three self-adhesive concentric electrodes (CoDe 1.0, OT Bioelettronica, IT [78]) were used to deliver the electrical stimulation to the user.

4.3 Experimental Setup and Protocol

Experimental setup

To test the effectiveness of the system, localization and identification tests have been performed. The localization tests the subject's ability to localize the touched sensing patch while the intensity identification tests the subject's ability to distinguish between touch pressure values.

Three healthy subjects (3 males, 28 ± 8 years) participated in the experimental tests. The experimental setup of the conducted tests is shown in fig. 4.2. The three sensing patches were fixed on a table and connected to the IE. The subject was comfortably seated on a chair in front of a table in a quiet environment to avoid distraction. With the forearm on the table, the three electrodes were put on the volar side and aligned with the position of the sensor patches in the prosthetic hand. A sheet of paper was placed in front of the subject with a schematic drawing of the position and names of the electrodes. The experimental procedure was then explained to the subject. For each electrode, the subject received stimulation at a comfortable intensity to familiarize him/her with electro-cutaneous stimulation. The electrode locations remained fixed during the experimental sessions because they affect the perceptual thresholds.

For each subject, the Sensation Threshold (ST) and Pain Thresholds (PT) for electrotactile stimulation have been determined for the three electrodes using the method of limits [79]. The current amplitude and frequency were constant and set to 3 mA and 100 Hz respectively. While the pulse width was adjusted to regulate the intensity of stimulation. The mean ST and PT calculated among all subjects were equal to 140±50 μs and 350±50 μs respectively. Previous experiments in [41] demonstrated that stimulation with these parameters allowed good perception and modulation of the elicited tactile sensations.

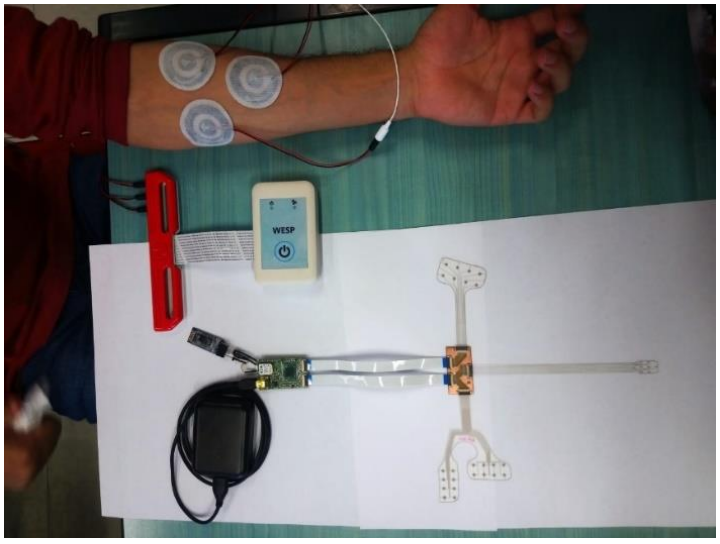

Fig. 4.2 Experimental setup for the system

Testing methodology

The stimulation parameters were chosen to maximize the differences in the intensities of the stimuli. The pulse widths for the low (LE), medium (ME) and high (HE) electrotactile stimuli were: LE = 1.2×ST, ME = LE+0.3× (HE-LE) and HE = 0.8×PT, respectively. The sketch shown in fig. 4.3 illustrates the mapping of tactile information into stimulation patterns. Each subject received 9 different configurations of stimulation shown in Table 4.1. Where electrode F corresponds to patch Finger, electrode P1 corresponds to patch Palm1, and electrode P2 corresponds to patch Palm2. Each experimental session was divided into three phases: pre-training, reinforced learning, and validation. During the three phases, each trial consisted of 2-second of continuous stimulation.

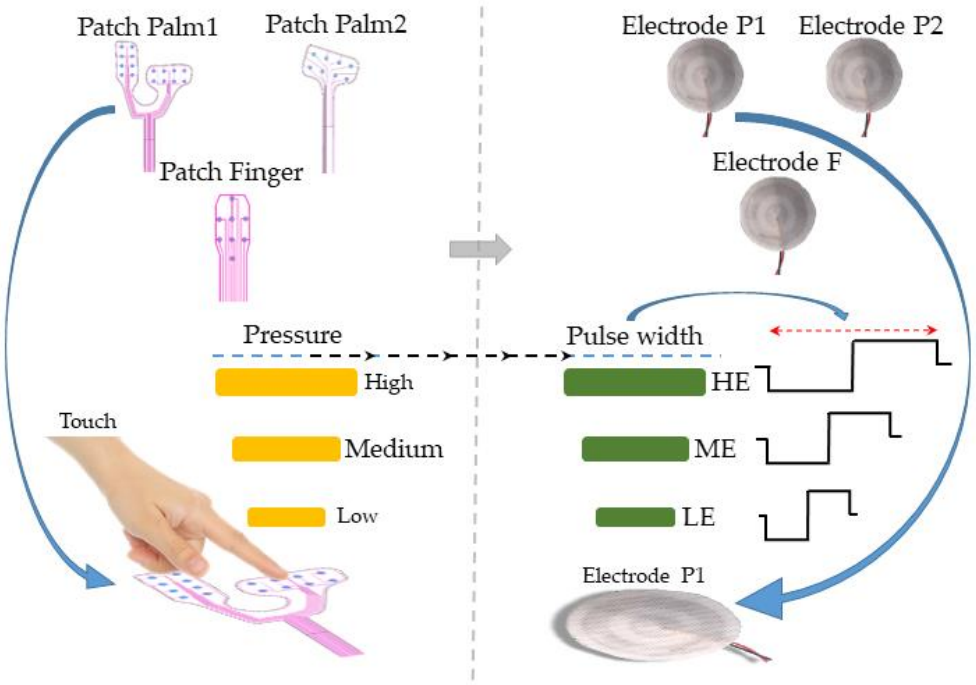

Fig. 4.3 Mapping of tactile information into stimulation patterns at the subject side.

Phase 1: subjects were instructed to focus on the stimulation and build a tactile mental map between sensation, level of stimulation, and the position of the activated electrode. The subjects were introduced to the nine configurations. The experimenter announced to the subject the electrode/patch that will be activated and the level of touch, then started the stimulation by touching the corresponding patch. In total 18 stimulations trails were presented (two repetitions per configuration).

Phase 2: one of the stimulation configurations was randomly selected and delivered to the subject (three repetitions per configuration). The subjects were asked to guess the configuration, and verbal feedback about the correct response was provided by the

experimenter.

Phase 3: the protocol of phase 2 was repeated, except that each stimulation configuration was delivered five times (45 stimulation trials in total) and the subjects did not receive the verbal feedback about the correct answer.

The Recognition Rate (RR) has been selected as a metric to recognize the ability of the subject in identifying the touch positions and the value of the applied pressure. RR is defined as:

$$RR = \frac{number\ of\ correctly\ identified\ trails}{number\ of\ total\ trails} \times 100 \quad (9)$$

Table 4.1 NINE DIFFERENT STIMUALTION CONFIGURATIONS

Categories		Pressure Levels		
		Low (L1)	**Medium (L2)**	**High (L3)**
Touch Position	**Palm 1 (P1)**	P1. L1	P1. L2	P1. L3
	Palm 2 (P2)	P2. L1	P2. L2	P2. L3
	Finger (F)	F. L1	F. L2	F. L3

4.4 Experimental results

4.4.1 Recognition Rate

Three subjects took an experiment on recognition of touch position and applied pressure. The average RR has been calculated using the following equation: RR = mean ± standard deviation was 86.66 ± 2.22 %. The confusion matrix presented in fig. 4.4 is used to evaluate the overall performance and identify prevalent classification errors. The confusion matrix demonstrates a visible diagonal line standing for a correct class (position) recognition. Whereas typical errors were observed due to the misjudgments of the level of the stimulus at electrodes P1 and P2 (the 2×2 squares along the main diagonal) and less frequently of the electrical stimulus at electrode F (the parallel diagonals above and below the main diagonal) for one level up or down from the presented (correct) level. The subject's answers were therefore distributed within several levels around the correct stimulus. Subjects were significantly better in discriminating low and high levels of pressure i.e. pulse width values with respect to the intermediate level. One reason is the small difference between two consecutive levels of pulse width. Which in turn depends on the PT and DT of each electrode separately. These results indicate the ability of the system in delivering meaningful information to the subjects. The high accuracies in discriminating different touch positions and levels demonstrate the feasibility of an embedded system in coding different touch

modalities for example light and strong touches.

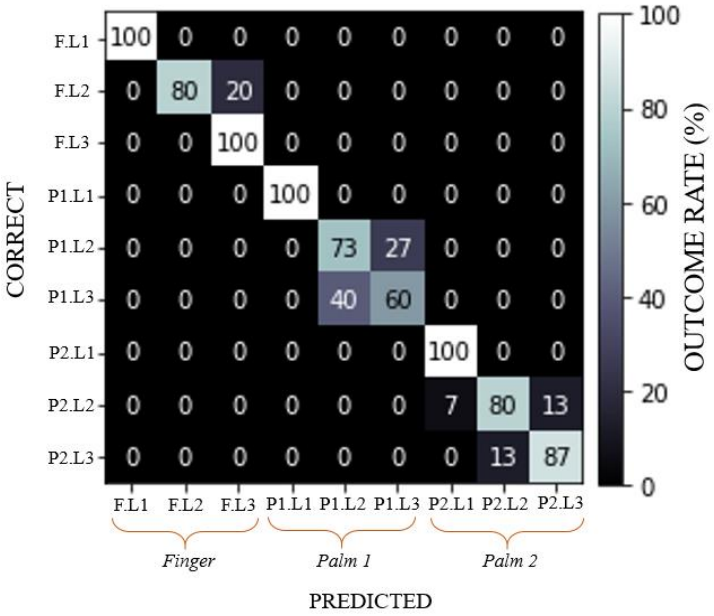

Fig. 4.4 Confusion matrix for the RR of 9 configurations in the validation phase. The matrix demonstrates the superior performance in recognizing touch positions.

4.4.2 System time latency

The total delay from the applied pressure to the stimulation is the summation of the delays starting from the sensor, to the IE different tasks until the activation of the stimulation. A 2.2 kΩ load resistor was connected between the stimulator electrode and the oscilloscope probe to visualize the stimulation signal. Fig. 4.5 shows the setup and the response of the system when a touch is applied to one of the sensor arrays. The total time latency is around 32 ms. This indicates that the response of the system is fast enough to transmit the desired signal without a perceivable delay.

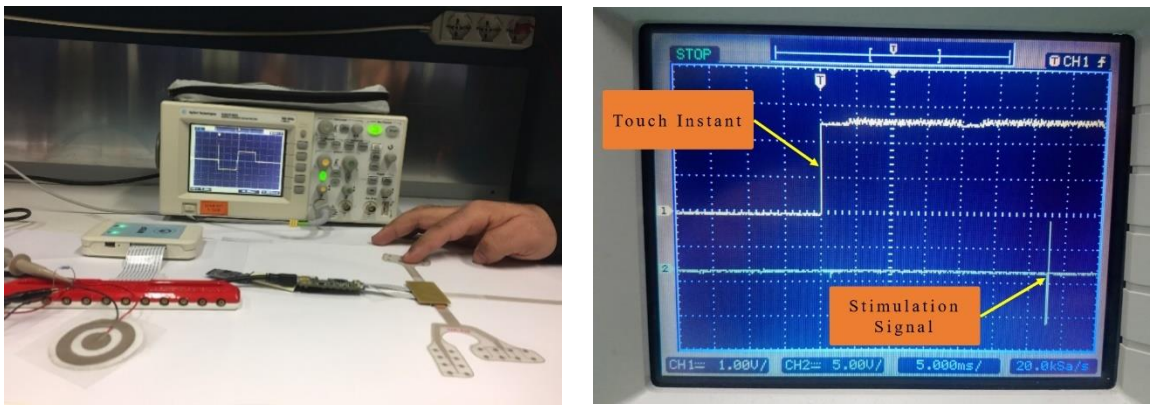

(a) (b)

Fig. 4.5 (a) Picture of the system responding to a contact on one sensor array; (b) CH1 signal represents a touch event

on the sensor array; CH2 signal is the corresponding electrical stimulation waveform.

4.5 Summary

A portable sensory feedback system has been proposed incorporating tactile sensors, interface electronics, and a programmable electro-cutaneous stimulator. The purpose is to demonstrate the functionality of the IE in the feedback system, showing its potential in providing tactile information to the user. The power consumption and time latency of the system have been measured. The proposed system operates in real-time with 32 ms delay (from touch to stimulation) and low power consumption of 300 mW. Although more extensive experimentation is needed to fully evaluate our system, the preliminary demonstration on three healthy subjects showed an accuracy of 86.66% recognition rate. The results of this study are important for sensory feedback design. They have shown the effectiveness of using a real-time embedded feedback system to extract and deliver tactile information to the users. The system is an important step toward integrating a distributed sensing system into a prosthetic hand and deliver tactile information to the user. In the next chapter we will introduce a tensorial-based machine learning algorithm that can extract from the acquired tactile data the type of touch modality applied on the sensor array. Then, we will study the performance of the algorithm on embedded hardware and propose an optimization method to reduce the algorithm complexity for efficient embedded implementation.

Chapter 5 Embedded Machine Learning Algorithm for Tactile Data Processing

5.1 Introduction

Employing Machine learning algorithms in tactile sensing systems have emerged recently to recognize/classify touch patterns. The high computational complexity of the ML algorithms makes challenging the embedded implementation of tactile data processing. The requirements for embedding ML into hardware devices vary according to the complexity of each algorithm. Thus, hardware designers compromise between hardware complexity and classification accuracy of the ML algorithms in order to achieve efficient embedded implementations.

A tactile sensing system comprises three main parts: 1) tactile sensors array, 2) interface electronics (IE), and 3) processing unit, as presented in Fig. 5.1. The sensors array – connected to the IE – generates electrical charges after applying a touch on its surface. The IE acquires and digitizes these charges and sends them for further processing. Then, the processing unit runs a ML algorithm to process and extract structured information e.g. classifying touch modalities from raw tactile data.

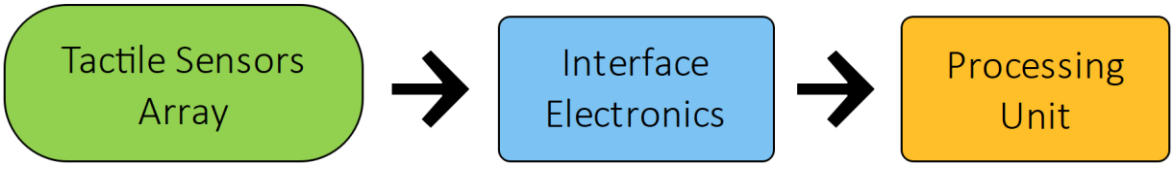

Fig. 5.1 Block diagram of the tactile sensing system

Many researches have focused recently on optimizing the machine learning algorithms due to the need in enabling intelligent tasks in embedded hardware platforms. Support Vector Machine (SVM) method is a widely used classifier and has gained momentum for its efficiency in various application domains. An optimized SVM approach is proposed in [80] to solve the global parameters optimization problem for ship systems state estimation. In the problem of the SVM classification of imbalanced datasets, authors in [81] suggested an approach to optimal parameters selection for the synthetic minority over-sampling technique algorithm. Authors in [82] proposed an improved version of the Whale Optimization Algorithm aiming to choose the best model for SVM by looking for the optimal parameter values. In [83], authors proposed a bio-inspired optimization tool for SVM for hyperparameters tuning demonstrating better results in terms of speed and simplicity compared to state of art works. An optimized linear-kernel SVM is proposed in [84] to deal with the key issue in smart grids i.e. to reduce the gap between generation and consumption of electricity. However, these optimization techniques were proposed for linear SVM and in some cases for improving the classification accuracy and not targeting the hardware implementation.

Tactile sensors deal with 3-dimension tensor structure data i.e. similar to videos, in which the first two dimensions are defined the area of tactile sensors while the third dimension represents the time. A tensorial SVM approach is proposed in [10] and has proven its effectiveness in classifying input touch modality. Ibrahim et al. [56] has presented the hardware architectures and implementation of the tensorial SVM presented in [10]. The system has achieved a peak performance of 302 G-ops and demonstrated the feasibility for real-time classification. However, the complexity of the implementation in terms of hardware resources and power consumption was dramatically increasing when the system scales up.

This chapter proposes an efficient tensorial-based Support Vector Machine (SVM) machine learning algorithm for embedded tactile data processing. The main contributions of this work are summarized as follows:

- It introduces a novel method for data organization of the tensors produced from a tactile sensing array.
- It achieves, with respect to state of art [55], a reduction in the complexity of the tensorial-based algorithm in terms of number of operations per inference by 96.6% and the memory storage by 96.7%.
- It demonstrates the feasibility of the proposed algorithm for real-time tactile data classification by providing a prediction speedup of 43× compared to [6] with an

accuracy loss less than 2%.

5.2 Tensorial Based Data Processing Algorithm

This section presents the architecture of the tensorial-based machine learning algorithm for touch recognition proposed in [10]. Tactile data are acquired in 3-dimensional representation known as tensor. The first two dimensions of the tensor represent the sensor array, while the third one represents the time. Gastaldo et al. [10] proposed a tensorial-based ML approach for touch modality classification. The ML model is based on support vector machine method that was trained to discriminate between three classes: “sliding”, “rolling” and “brushing”. Fig. 5.2 depicts the algorithm block diagram. It is composed of three main processes: 1) Tensor unfolding, 2) Jacobi process, and 3) SVM classification.

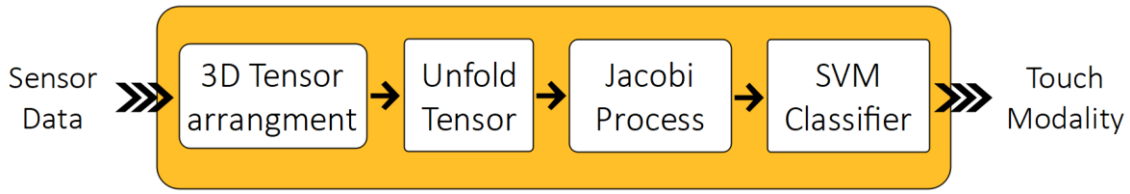

Fig. 5.2 Tensorial based machine learning algorithm

5.2.1 Tensor unfolding

The Tensor Unfolding process converts the tensor T (m1 × m2 × m3) to three matrices: A1 (m1 × m2.m3), A2 (m2 × m1.m3) and A3 (m3 × m1.m2), where mi < mj.mk e.g. m1 < m2.m3. The first 2 matrices A1 and A2 stack the information of the tensor rows and columns, respectively. The third matrix A3 stacks the row and columns of the third dimension.

5.2.2 Jacobi process

The Jacobi process computes the singular values of the three unfolded matrices (A1, A2, and A3). It constitutes two subprocesses: symmetrization and singular value decomposition. Equation (1) is used to symmetrize the unfolded matrices:

$$A_{\text{xsym}} = A_x^T \times A_x \tag{1}$$

Where A_x^T is the transpose matrix of A_x and x ∈ {1, 2, 3}.

Symmetrization outputs three matrices $\boldsymbol{A_{1\text{sym}} = A_1^T A_1}$ (m2.m3 × m2.m3), $\boldsymbol{A_{2\text{sym}} = A_2^T A_2}$ (m1.m3 × m1.m3) and $\boldsymbol{A_{3\text{sym}} = A_3^T A_3}$ (m1.m2 × m1.m2).

The Asym eigen vectors and eigen values are calculated using the singular value decomposition method. Matrix A_{sym} is decomposed into a multiplication of three matrices:

two matrices contain the left and right singular vectors (U and V) and diagonal matrix (S) contains the singular values. The mathematical representation of this process is expressed as follow:

$$A_{\text{sym}} = USV^T \tag{2}$$

The singular value decomposition method is based on one sided Jacobi algorithm. The Jacobi algorithm iterates to diagonalize matrix A_{sym} until the convergence point is reached.

5.2.3 Classification

The support vector machine classifier finds the maximum and best gap (hyperplane) between two set of classes, linearly or non-linearly separable [85]. Tensor-based models cannot be separated by a hyperplane; thus, a nonlinear classifier is required. The designed classifier is based on a nonlinear kernel function of Gaussian distribution. The kernel for the two tensors (X_i, Y_i) is formulated as follow:

$$K\ (X_i, Y_i) = \prod_{n=1}^{N} k^n(X_i, Y_i) \tag{3}$$

Where the kernel factor $k^n(X_i, Y_i)$ is defined as:

$$k^n(X_i, Y_i) = exp\left(-\frac{1}{2\sigma^2}(Im\ - trace(Z^T Z))\right) \tag{4}$$

$$\text{Z} = V_x^T V_y \tag{5}$$

Where V_x is the SVD eigen vector right matrix during the prediction phase, and V_y is the eigen vector right matrix obtained during the training phase. Now, the classification function would be expressed as:

$$class = f(x) = \sum_{i=1}^{N} W_i K(X_i, Y_i) + b \tag{6}$$

Where class is the predicted category and W_i are the weights obtained during the training phase.

5.3 Implementation and optimization

5.3.1 Data set and pre-processing

The dataset obtained in [48] was used to train the model and to perform classification between two different modalities, labeled “rolling” and “sliding”. The dataset collection is expressed by a 3-D tensor – extracted from the 4×4 tactile sensors array. The tensor size (T)

is 4×4×30000 which corresponds to 10s acquisition at 3 KSps sampling rate [48]. In fact, with such large number of elements represented by the 3rd component of the tensor (30000), the computation of the SVD matrix is impractical. For that, preprocessing methods [10] were applied to reduce the size of the tensor to be T (4×4×20).

5.3.2 Training phase

Prior implementation, the algorithm has been trained and used as a benchmark to test the proposed optimized algorithm. For fair comparison, the cross-validation method was used during training phase: the dataset composed of 260 samples was divided into five folds, each fold is partitioned into training and test sets; where 80% of the dataset represents the training set (208 samples) and 20% for the test set (52 samples).

5.3.3 Hardware configuration

The Zed-board hardware platform was chosen to run the algorithm. It contains a Xilinx Zynq XC7Z020 SoC which is composed of processing system together with programable logic. The processing system includes a dual ARM cores of A9 family with standard peripheral interfaces. The programable logic contains logic units that are accessible and can be configured. These features enable the Zed-board to run an operating system (OS) host and to perform tasks in real-time.

The implementation steps are as follows: first, the Zynq has been configured to boot an Ubuntu Linux-based operating system; second, the algorithm C code has been installed and compiled into the OS; third, the C code was executed to predict the output modality class of the test set (five folds each of 52 samples); finally, the model accuracy and prediction time have been recorded. Results show that for every input sample, the algorithm requires around 1.2 seconds to classify a touch modality.

5.3.4 Code profiling

The Linux provides a profiling tool that allows to extract detailed information about the execution of a program (execution time, number of function calls, etc.). This tool was used to profile the algorithm code and to record the execution time of every single process in the code. Table 5.1 reports the time required by the main functions to predict the output touch modality for 52 input samples. Results show that the Jacobi process dominates around 96% of the total run time of the code. Hence, this process is computationally expensive and should be optimized to speed up the inference time.

Table 5.1 CODE PROFILE AFTER PREDICTING 52 SAMPLES ON ZYNQ

Function Name	Time %	seconds
Jacobi	96.06	63.33
KernalTrace	3.52	2.32

5.3.5 Algorithm optimization

Fig. 5.3 illustrates the four steps needed to compute the tensorial SVM algorithm. The number of iterations required by the SVD process to compute the diagonal matrix depends on two parameters: the matrix size (mj.mk × mj.mk) and the convergence factor k. The code profiling results show that the SVD is the computational bottleneck. For that, reducing the computational load of the SVD process should be addressed.

The subsampling method applied in [10] reduced the elements of the third component of the tensor. This method has reduced the number of iterations required by the algorithm and the iterations required by the SVD. However, this method is customized to the specified application where the subsampling factor is dependent on the datasets. This motivates the development of a generalized method for all data dimensions that can significantly reduce the computational complexity of the algorithm.

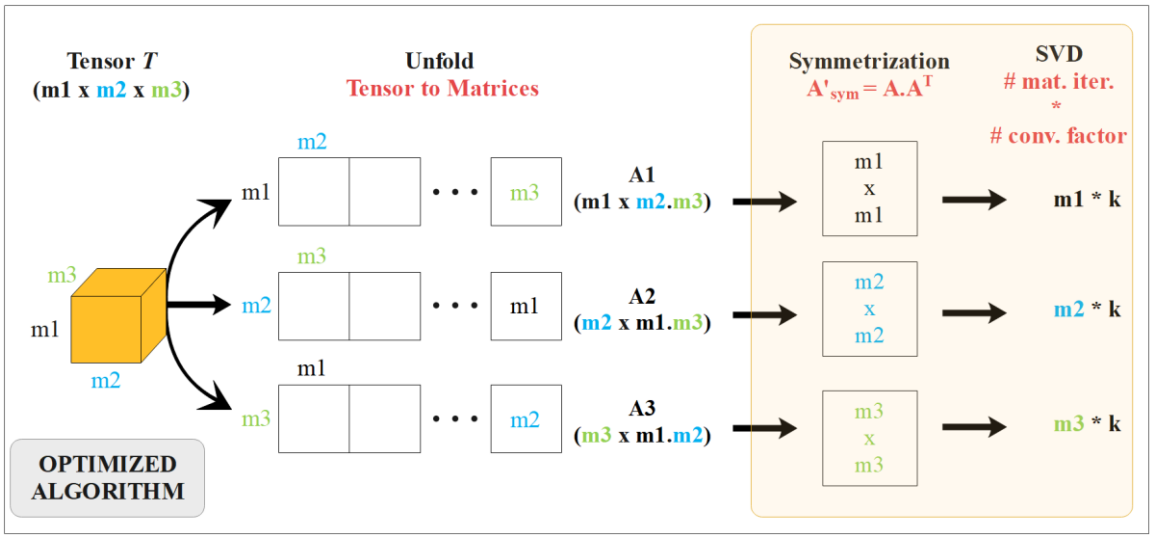

Fig. 5.3 Sketch of the proposed method for data organization of the tensorial SVM approach.

In the original algorithm, the unfolded Ax ∈ Rmi ⊗ Rmj.mk (mi, mj and mk are the tensor 3-dimensional components); Asym ∈ Rmj.mk ⊗ Rmj.mk, where AxT ∈ Rmj.mk ⊗ Rmi. In the optimized algorithm, after flipping the symmetrization multiplication elements, the new matrix A'sym ∈ Rmi ⊗ Rmi where A'sym matrix size is smaller than Asym because mi < mj.mk is always valid. This method optimizes the algorithm whatever is the tensor data size. Fig. 5.3 shows a reduced number of iterations (mi*k < mj.mk*k) after optimization compared to the original algorithm.

5.4 Experimental Results

5.4.1 Computational analysis

The algorithm is implemented on Zynq which deals with an input tensor T (4 × 4 × 20). After unfolding T into three matrices (A1 (4×80), A2 (4×80), and A3 (20×16)), For the obtained symmetric matrices, SVD operates on three matrices (A1sym (80×80), A2sym (80×80), and A3sym (16×16)). Then the same implementation was repeated by applying the optimization method where SVD operates on three matrices (A'1sym (4×4), A'2sym (4×4), and A'3sym (20×20)). Table II shows the complexity of SVD function in terms of matrices size and the corresponding number of iterations required to operate them (number of samples × k × size of symmetrized matrices). Results show that the optimized algorithm performs the same task as the original one with 30× reduction in number of iterations.

To further assess the feasibility of the proposed approach and its impact on the scalability of the system, different tensor sizes have been analyzed. The complexity analysis presented in [12] for the tensorial kernel approach has been adopted to compute the number of operations required for each algorithm. Fig. 5.4 shows how the proposed approach decreases dramatically the number of operations even when the number of operations in the original algorithm have been normalized to 1:1000. Moreover, the percentage reduction in the number of operations is reduced of 99% which will reduce as consequences the hardware complexity, time latency, and energy consumption of the system.

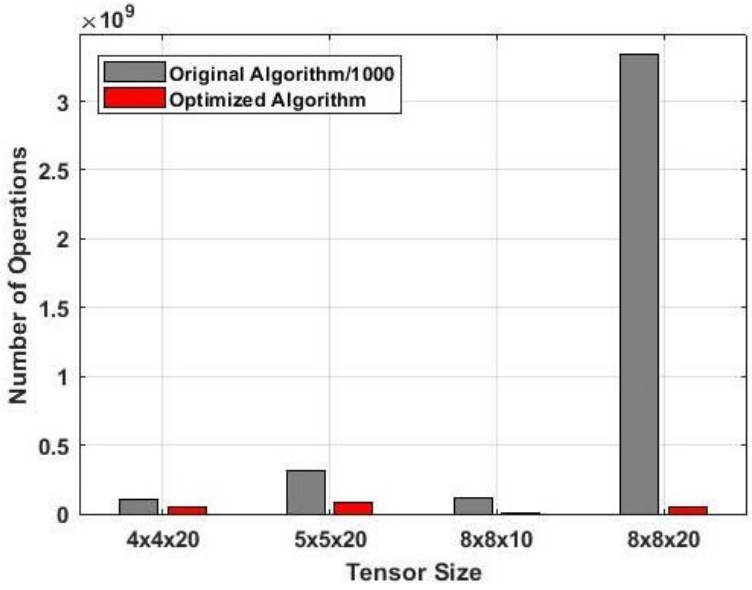

Fig. 5.4 Scalability analysis for the original versus optimized approach

5.4.2 Case study

The algorithm has been implemented on Zynq platform and the accuracy and inference

time have been analyzed. Table 5.2 compares the average results of the original algorithm [55] with the proposed optimized version for five data folds each with 52 input samples. Results show that after optimization, the algorithm can predict faster by 43× with an accuracy loss less than 2%. The optimized algorithm achieves around 28 ms in predicting one output class enabling real time classification. Compared to the recent works [55], the proposed method significantly reduces the number of operations per inference from 545 M-ops to 18 M-ops when dealing with an input tensor. In addition, the required memory size to store the tensor data is reduced as shown in Table 5.3.

Table 5.2 PERFORMANCE ASSESSMENT

	Original Algorithm [55]	Proposed Approach
SVD number of iterations	5,431,296	179,712
Accuracy %	72.884	70.961
Time latency (sec)	65.930	**1.473**

Table 5.3 COMPARISON RESULTS FOR INPUT TENSOR (4 × 4 × 20)

	[55]	This work
Number of Operations (M-OPS)	545	18
Memory size (kB)	52.2	1.7
Inference time	3.3 sec	**28 ms**

5.5 Summary

This chapter proposed an optimized tensorial-based machine learning algorithm for touch modality classification. Aiming to reduce the algorithm complexity, the proposed optimization technique has been applied and implemented on Zynq SoC to confirm the validity of the approach. Achieved results demonstrate that the proposed approach has reduced the computational complexity with respect to the original algorithm presented in the state of the art. First, the number of operations is decreased from 545 M-ops to 18 M-ops. This has affected the time latency achieving a prediction speedup of 43×. Moreover, the needed amount of memory storage has been minimized from 52.2 KB to 1.7 KB; These results have been reached at a 2% of accuracy loss with respect to the literature [55]. The results have been compared with recent implementations and showed a performance superiority of our proposed approach.

Chapter 6 Tactile Data Communication

6.1 Introduction

The main target of the tactile sensory feedback system in prosthetics and robotics is to enable the delivery of tactile data/information to the user/controller end [59]. These tactile data aggregate as the number of sensors in the system increases, thus, placing some constraints on the system related to data transmission. The path of data from the sensing elements towards the user/controller could goes through several communication channels/buses of different protocols. Where the choice of these channels is mainly affected by several factors such as the desired transmission speed, noise, data reliability, amount of wires and most importantly channel bandwidth and power consumption. Therefore, providing the sensory system with a wide-bandwidth and low power consumption channel would allow an effective utilization of tactile data for sensor arrays that are distributed over prosthetic/robotic body.

Several communication protocols have been used for tactile data transfer (check chapter 2) either wired buses or wireless channels. For wired buses, serial communication protocols (e.g. I2C, SPI, CAN) are used for short distances and less wiring, such as collecting data from sensor arrays. However, they suffer from low bandwidth which not suitable for the data transmission of many sensors. While the wireless data transmission, in addition to the low bandwidth, has some power disadvantages with some safety issues that can’t be bearable by critical applications working with human such as robots and prosthetics.

This chapter demonstrates the implementation of a novel architecture based on the use of an optical fiber communication link for data transmission in the tactile sensory feedback systems for the prosthetic applications. The proposed solution, implemented on FPGA

boards, is capable of acquiring data coming from a sensor array and transmitting them through the optical communication channel to a prosthetic user through an electrotactile stimulation after coding the data by a UWB-inspired pulsed modulation technique [86], [87]. The sensory system with the advantage of this channel, can acquire, process and transmit the information of 32 sensors with 100 Mbps transmission data rate while consuming 50 pJ/bit. Compared to the standard communication protocols [88], [89] such as Bluetooth, CAN bus, SPI and UART, the presented architecture provides higher transmission rate and lower power consumption.

The chapter includes a description of the sensory system with additional details on each block. In addition, the communication protocol is fully explained, and a prototype that transmits data information measured from real sensors to the electrotactile stimulator has been experimentally validated. Chapter is organized as follows: Section 5.2 introduces sensory feedback systems blocks with the architecture of the proposed communication channel protocol. The implementation of the communication channels is presented in Section 5.3. Section 5.4 describes the experimental setup used to evaluate the overall system and present the test results. Finally, Section 5.5 summarizes the chapter.

6.2 System Architecture and Communication Protocol

The proposed feedback system architecture based on the optical communication channel is shown in Fig. 6.1. The system mainly consists of a transmitter and a receiver connected through an optical communication link. The transmitter board is connected to a data acquisition system that interfaces the tactile sensors. On the other side, the receiver board is connected to an electrotactile stimulator. Interfacing multiple tactile sensors is challenging since continuous sampling is required. This challenge is addressed by adopting a data acquisition circuit that integrates, converts and stores charge measurements of all input sensors simultaneously as detailed in the following subsections. The transmitter is designed to perform a data coding by a UWB-inspired pulsed modulation technique. Whereas, the receiver communicates directly with the prosthetic user through the electrotactile stimulation by means of a direct connection through a USB port translating the tactile sensor data into stimulator commands. The receiver has a shared global data buffer to store the decoded/recovered data and can send the processed data also to a PC (through a UART INTERFACE) and/or an oscilloscope for visualization.

In the following sub-sections, we will describe, more in detail, each part composing the complete system.

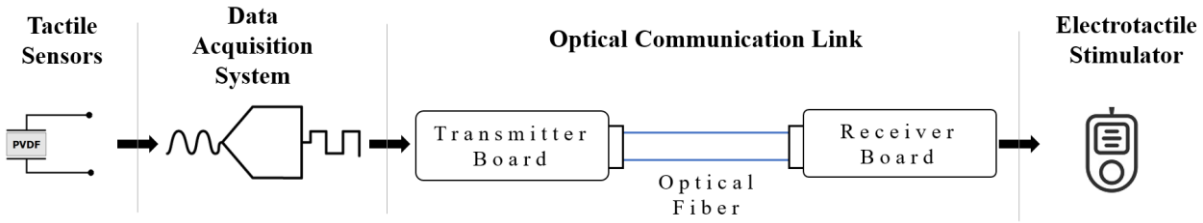

Fig. 6.1 Block diagram of the overall sensory feedback system based on optical communication channel.

6.2.1 Tactile sensors

A PVDF-based sensory array was used to demonstrate the proposed system architecture. Their structure and fabrication process are described in chapter 3, section 3.2.1. Noting that these sensors have been exposed to a validation process where an electromechanical test has been performed on a set of sensing patches [90]. Continuous indentation has been applied on the sensor taxel for the whole frequency range of interest for tactile applications [65] (< 1 Hz - 1 kHz). Then, the (d33) coefficient has been estimated to define the behavior of the sensor. Results show an average value of the d33 that matches with the literature values and thus allowing our proposed system to be tested with real sensor data.

6.2.2 Data Acquisition system

The data acquisition design mainly consists of two components: an offset circuit and DDC232 [71] as a current input analog-to-digital converter. The architecture of both components has been demonstrated in chapter 3, section 3.2.2. However, the mechanism of acquiring, digitizing and retrieving data is controlled by an FPGA controller, which will also host the transmission block of the system and apply its protocol.

6.2.3 Optical communication link

Fig. 6.2 shows the block scheme diagram of the Optical Communication Link composed by two sub-systems: the transmitter board and the receiver board that are linked together through the optical fiber-based communication channel.

The Transmitter board is composed of two blocks: TX MODULE and ANALOG UNIT. In the TX MODULE, the ADC INTERACE subblock controls the Data Acquisition System and generates from the acquired data a Data Package. Once the acquisition is accomplished, Serial Data Package bit stream is transmitted, and the Data Coding block is enabled performing the UWB pulsed coding of the data. Fig. 6.3 presents the coding technique, where it always generates a “synchronism pulse” (used for the clock recovery operation in the RX module) in correspondence to the rising edge of a clock signal (synchronous with the data to be transmitted) and a “data pulse” on the falling edge of the same clock signal

only if the bit to be coded from the serial data is equal to “1”. Thus, the output of this block is an aperiodic sequence of voltage pulses (i.e., the Transmitted Pulsed Signal) that contains also a synchronization clock signal needed to properly receive the information/data contained in the signal generated by the sensors.

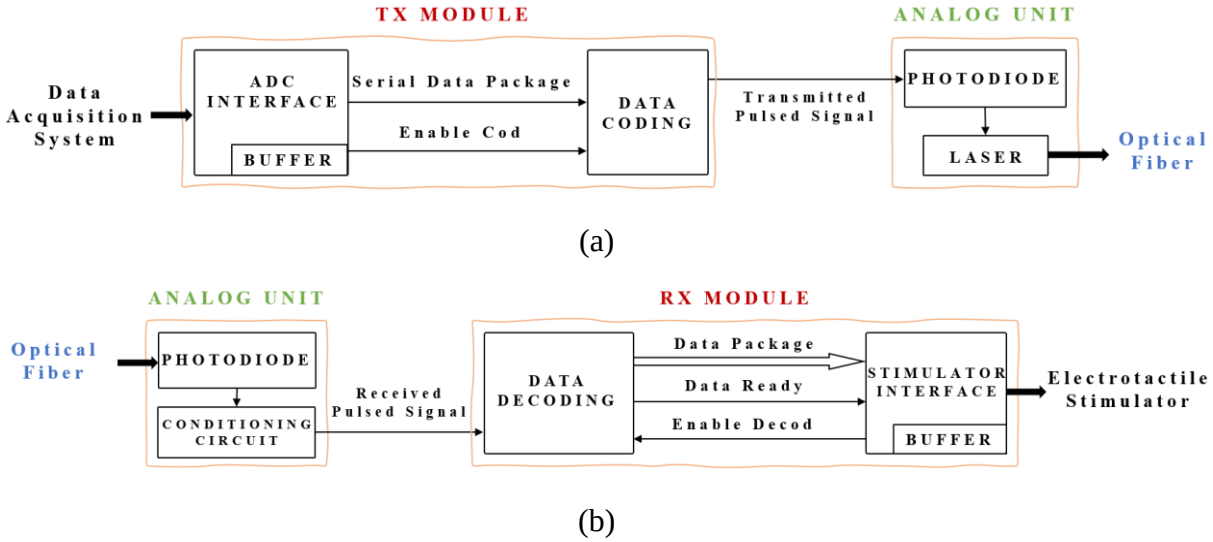

Fig. 6.2 Block scheme of the Optical Communication Link; (a) Transmitter board; (b) Receiver board

The second block in the Transmitter board, named ANALOG UNIT, is composed by a Vertical Cavity Surface Emitting Laser (VCSEL) and a LASER DRIVER that receives in input the sequence of the coded pulses and transforms them in a sequence of current pulses. This sequence of current pulses must have an amplitude greater than the threshold level to activate the VCSEL laser action (i.e., the amplitude of each current pulse of the sequence must exceed the value of the VCSEL threshold current). The generated laser pulses are coupled to the optical fiber.

On the other hand, the Receiver board includes two main blocks: ANALOG UNIT and RX MODULE. The first one (Analog Unit) is composed by an analog conditioning circuit and an optoelectronic device, the Photodiode (PD). The PD has a frequency bandwidth equal or larger than that one of the VCSEL and generates current pulses that follow the same temporal shape of the transmitted laser pulses with amplitudes proportional to their intensities. Starting from the incoming pulsed current, the CONDITIONING CIRCUIT generates a sequence of voltage pulses and transmits the Received Pulsed Signal to another block of the Receiver board (RX MODULE) that performs the decoding operation. Once the Data Package has been regenerated by the DATA DECODING sub-block, it is sent to the STIMULATOR INTERFACE that is able to establish an UART communication with the Electrotactile Stimulator.

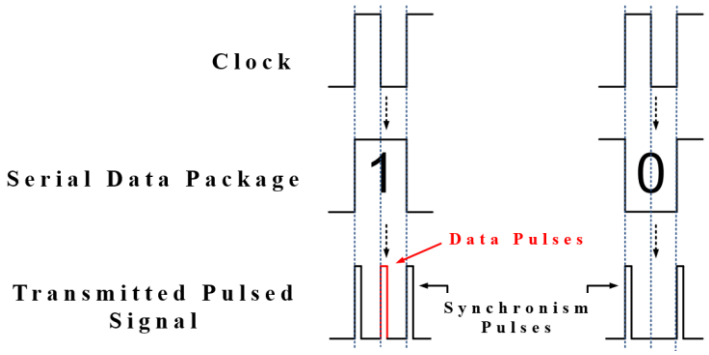

Fig. 6.3 Example of the timing diagram of the optical UWB-based pulsed data coding technique.

6.2.4 Electrotactile stimulation

The WESP stimulator, fabricated by Tecnalia Serbia, is a battery-powered device that offers 24-programmable channels. The stimulator generates current pulses in the range of 0-10 mA of intensity and 1-400 Hz of frequency with pulse width of range from 50ms to 500ms. This allows the stimulator to produce electrotactile pulses with different parameter combinations. The stimulator is controlled by the stimulator interface block of the RX MODULE. When the system detects a touch, the receiver delivers the information to the stimulator by transmitting the corresponding commands. These commands order the stimulator to generate electrotactile pulses at given parameters.

6.3 System Implementation

This section presents the implementation details of the optical communication link blocks of the transmitter, optical channel drivers and the receiver.

6.3.1 Transmitter module

The TX MODULE architecture has been implemented in a Spartan6 FPGA (SP601 by Xilinx), as shown in Fig. 6.4. It works at a main clock frequency (i.e., Clock) equal to 100 MHz. The ADC INTERFACE is the first subblock that activates after the Start signal goes high and it generates a proper Clock ADC signal connected to the DCLK pin of the DDC232 previously described.

Every time the ADC INTERFACE toggles the signal Start Conv, the external A\C simultaneously scans and convert the analogue signals generated by the array of sensors. The converted signals are shifted out to the acquisition module (i.e., the ADC INTERFACE block) through the Digital Data port at 2 kS/s every time the Data Valid signal, connected to the DVALID pin of the acquisition module, is set to a logic state low. Thus, when the data are stored in the BUFFER, the ADC INTERFACE generates a Data Package containing the data that must be transmitted (16 bits for each one of the 32 channels) and a fixed sequence

used as HEADER (i.e. the begin of the package). Then, the signal Enable_Cod goes high enabling the Data Coding block to perform the coding of the BUFFER data into a digital pulsed signal. The coding process and the composition of the Transmitted Pulsed signals are shown in Fig. 6.5. Its upper part shows the Serial Data Package, which consists of an orderly sequence of samples (each one corresponding to the related sensor of the input array) packed with a header used to detect the beginning of this package. While, the lower part of Fig. 6.5 reports the coding of the Serial Data Package into the Transmitted Pulsed Signal which are received by the ANALOG UNIT block of the transmission board. Only when a Serial Data Package has been transmitted, another acquisition can be performed. All the control signals of the ADC INTERFACE block are managed by a CONTROL UNIT that uses the ALU unit for the timing operations.

According to Fig. 6.4, the DATA CODING block has been implemented by using a Phase-Locked Loop (PLL) and few logic gates. The PLL, already realized as a basic block inside the FPGA, generates two pulsed signals starting from the input Clock signal. The first pulse at the PLL terminal A is generated in correspondence of the rising edges of the Clock signal, and the second pulse at the PLL terminal B is generated synchronized with the falling edges of the Clock signal. These two pulsed signals have the same frequency of 100 MHz with a relative phase difference of 180° and a selectable duty-cycle in order to guarantee the desired pulse width (about 1 ns in this application). Combining the Serial Data Package with the signals A and B, the DATA CODING block is able to send the Transmitted Pulsed Signal at 100 Mbps.

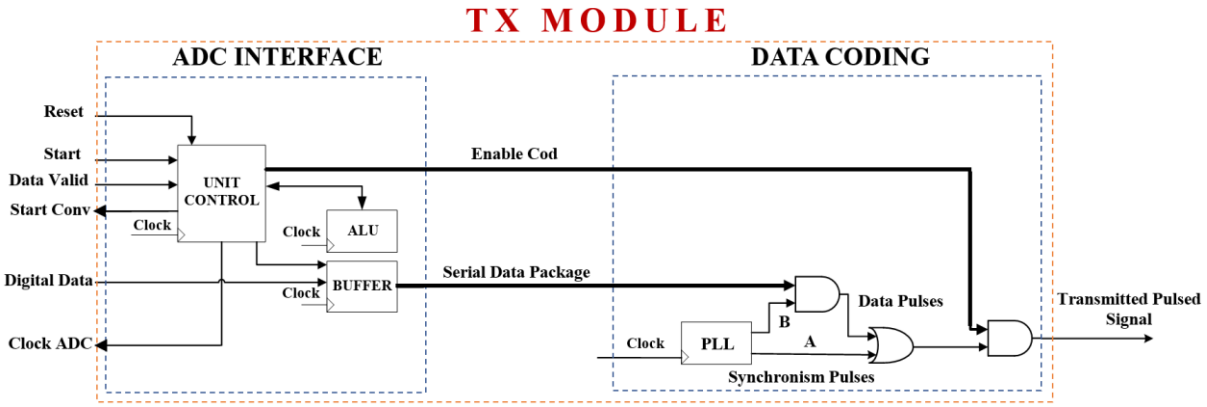

Fig. 6.4 Block scheme of the TX MODULE.

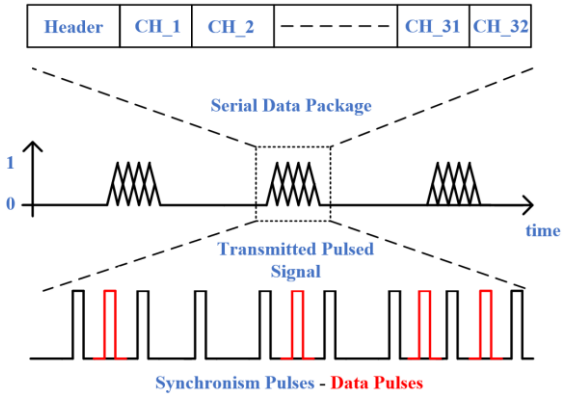

Fig. 6.5 Structure/composition of the Serial Data Package.

6.3.2 Optical link drivers

On the Transmitter board, the Analog Unit has been composed by a driver circuit (i.e., LASER DRIVER) that converts the voltage digital pulses into current pulses to drive the VCSEL (OPV314AT by TT Electronics) emitting at λ = 850 nm with a response time lower than 100 ps. In this way, the laser pulses are the optical replica of the current pulses. Fig. 6.6 shows the schematic circuit of the Laser Driver based on a simple current-mirror topology. The variable resistors R1 and R2 (i.e., 470 □ trimmers) allow for the regulation of the current pulses DC level and AC amplitudes, respectively. The devices Q1, Q2 and Q3 are BFT92 5 GHz wideband PNP BJT transistors while R3=R5=R6=33 Ω and R4=100 Ω. The VCSEL is coupled to one end of a 1 m length 50/125 µm multi-mode optical fiber while the other end is coupled to a high-speed Si-based photodiode (PD, DET025AFC/M by Thorlabs) with rise/fall times of about 150 ps. This photodiode, inside the Receiver Board, detects the laser pulses and generates their replica as photocurrent pulses. The PD is finally interfaced with a signal conditioning circuit that converts current pulses into voltage pulses (i.e., Received Pulsed Signal) to be decoded by the RX MODULE. Its schematic circuit, based on a transimpedance amplifier configuration, is reported in Fig. 6.7. It employs BFG520 9 GHz wideband NPN BJT transistors (i.e., Q1-Q5) while R1=R2=1.2 kΩ, R3=390 Ω, R4=470 Ω, R5=680 Ω, R6=2.7 kΩ. It provides a suitable amplification of the pulsed signal to reach amplitudes matching with the logic threshold levels of the standard I/O LVCMOS25 considered and employed for the transmitter and the receiver module.

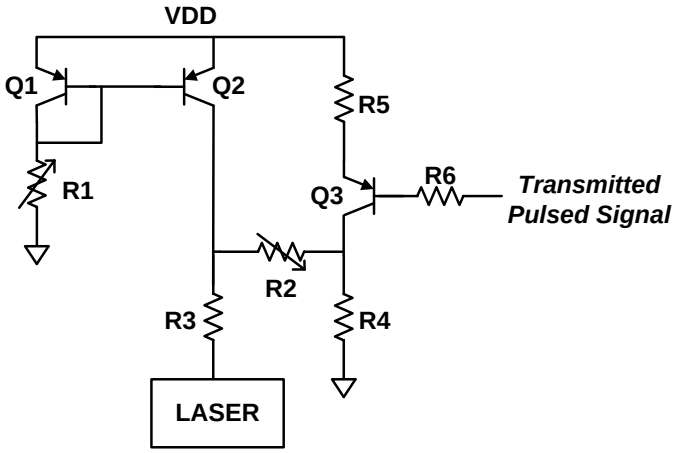

Fig. 6.6 Schematic circuit of the LASER DRIVER.

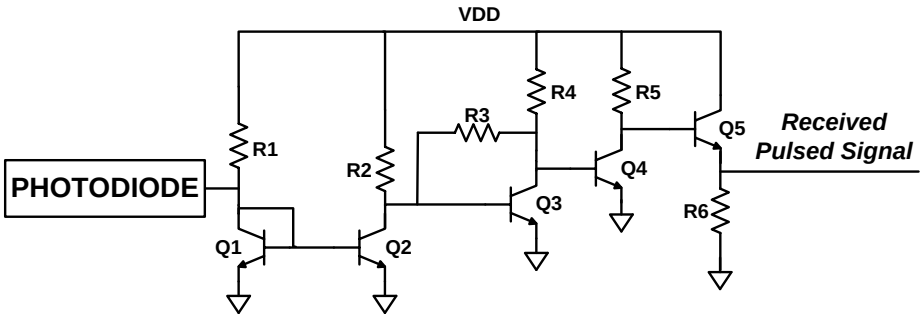

Fig. 6.7 Schematic circuit of the CONDITIONING CIRCUIT.

6.3.3 Receiver module

In the Receiver board, the RX MODULE has been implemented on a Virtex6 FPGA (ML605 by Xilinx) and shown in Fig. 6.8. The main Clock signal in this block is equal to 100 MHz. Starting from the Received Pulsed Signal provided by the CONDITIONING CIRCUIT, the CLOCK RECOVERY sub-block recovers and regenerates the 100 MHz clock signal starting from the received “Synchronism Pulses”. Simultaneously, the IDELAYE3 primitive block processes the same Received Pulsed Signal to start the data recovery procedure. This is a programmable time delay line implemented into the I/O blocks of the FPGA that provides a finite and discrete time delay to be added to the input pulsed signal. Consequently, the IDDR primitive block allows to achieve the Recovered Data Package starting from the Data Pulses, acquired at the falling edge of the Recovered Clock, of the properly delayed Received Pulsed Signal.

At the starting time of the DATA DECODING block, the control unit DECOD (C.U. DECOD) gradually increases the time delay introduced by IDELAYE3 until the rising edge of the Recovered Clock is in-phase (i.e., synchronous) with the Synchronism Pulses. In this way, the falling edge of the Recovered Clock allows to recover the bit stream from the received Data Pulses. Furthermore, in order to perform a compensation of the time delay

variations of the IDELAYE3 due to supply voltage and/or operating temperature drifts, the C.U. DECOD properly enables and controls also the IDELAYCTRL block that is a further primitive used for this specific purpose implemented on the FPGA. The Recovered Data Package provided by the IDDR is stored in a specific buffer (BUFFER) when the HEADER sequence is correctly detected/recognized by the HEADER DETECTOR block. Thus, the Data Ready signal is set to a high logic state so indicating that the operation has been correctly performed and the data package has been acquired. At this time the Data Package is acquired by the STIMULATOR INTERFACE that suitably process and sent it to a stimulator and/or to a PC monitor through a standard UART communication protocol.

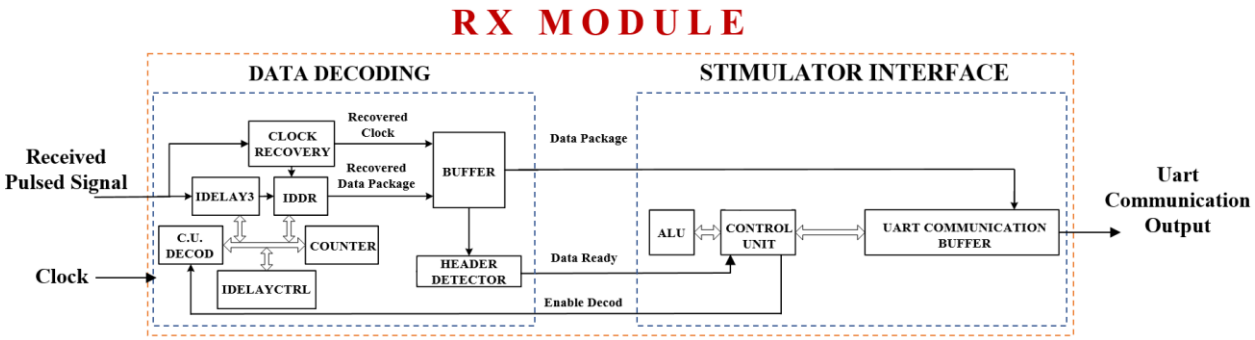

Fig. 6.8 Block scheme of the RX MODULE.

In particular, the data are processed to provide proper control commands to the stimulator device together with the generation of stimuli corresponding to the touch detected by the input tactile sensors. Once the UART transmission is accomplished, the CONTROL UNIT of the STIMULATOR INTERFACE block enables the acquisition of the subsequent Data Package with the signal Enable Decod. Moreover, the control commands carry out the parameters related to the stimulations to be generated (e.g., stimulation pulse intensity, frequency and electrode channel position, etc.) that could change according to the type and the force intensity of the touch of the sensing elements (i.e., their physical stimulation).

6.4 Experimental Setup and Results

The experimental setup was implemented as shown in Fig. 6.9. It incorporates an array of 32 tactile sensors (taxels) along with the ADC INTERFACE. The TX and RX modules are implemented on two FPGA boards with the optoelectronic devices (laser driver and conditioning circuit) and circuits of the optical communication link. The overall system, operating at 100 Mbps transmission data rate through the Optical Communication Link, is connected to a PC through USB cable to 1) to collect the sensor's data and plot them using MATLAB and 2) to display the touch information onto a graphical user interface (GUI). The GUI interface layout has the structure of the sensor array, which allows to easily

identify the location of touch on the screen.

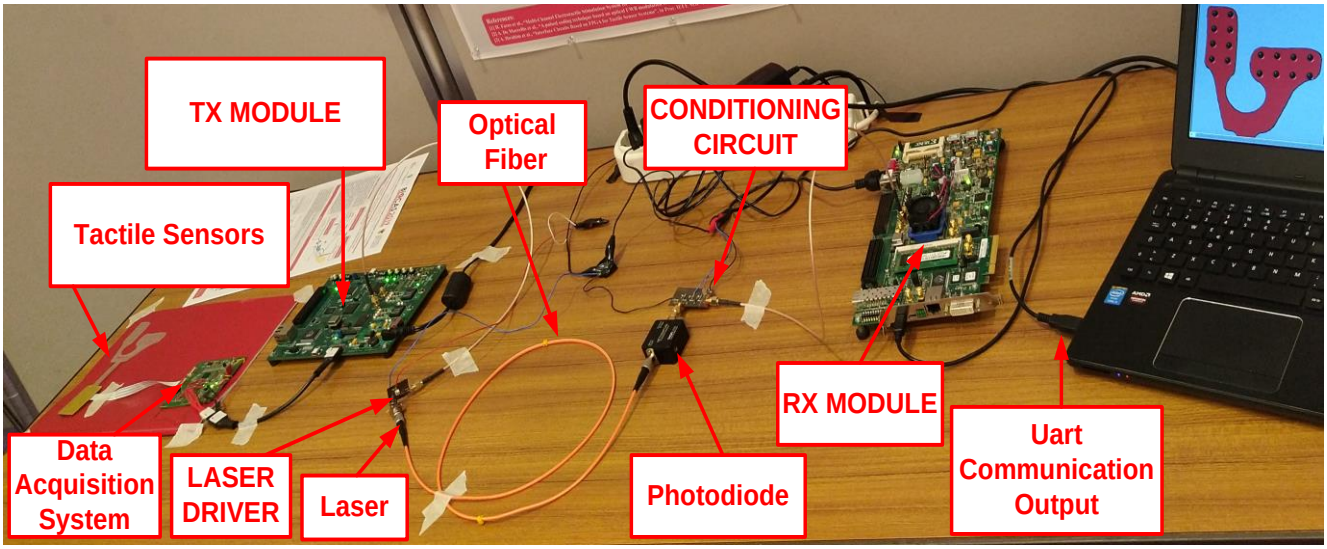

Fig. 6.9 Photo of the experimental set-up showing the two FPGA boards and the optical communication link composed by the optoelectronic devices and circuits together with the optical fiber.

Three tests have been conducted. The first was a preliminary test of the designed communication architecture, where a package of 512 bits made by a repeated sequence of {0,1} has been employed to verify the correctness of the data transmission and, so, of the overall Optical Communication Link. All the signals have been evaluated and acquired through the 6 GHz bandwidth digital oscilloscope LeCroy Master 8600A. Fig. 6.10 shows the initial part of the transmitted bits of the Serial Data Package, generated starting from the chosen repeated sequence {0,1}, and the related pulsed coded sequence measured at the output of the PD. In this way it is possible to mainly observe the correct functionality of the DATA CODING block and of the LASER DRIVER block. In the lower part of the Fig. 6.10, it is also possible to observe the Received Pulsed Signals generated by the Conditioning Circuit that are subsequently read by the RX MODULE. As shown, the Conditioning Circuit are able to correctly amplify the signal coming from the PD.

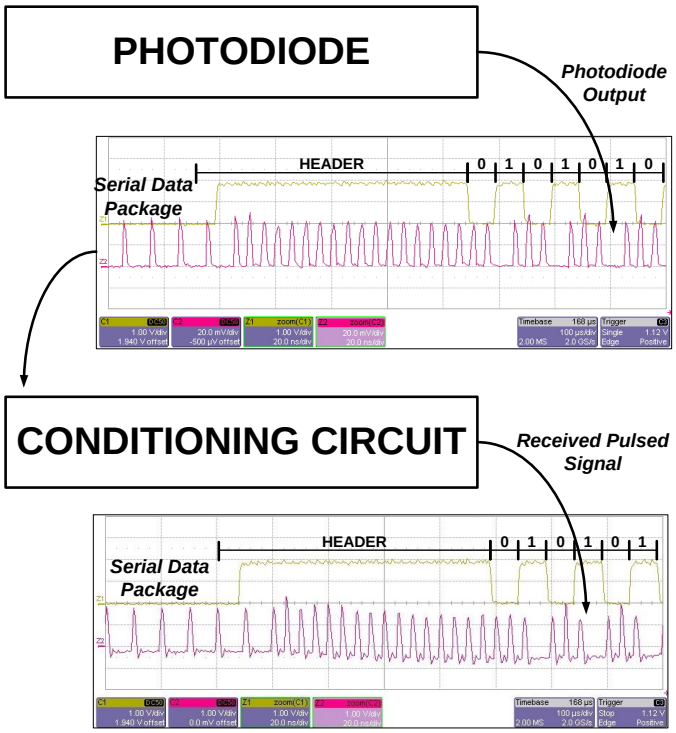

Fig. 6.10 Experimental measurement: Serial Data Package related to a repeated {0,1} bit serial sequence and the subsequent Transmitted Pulsed Signal operating at 100 Mbps. The Transmitted Pulsed Signal is observed at the output of the PD and at the output of the Conditioning Circuit (i.e., Received Pulsed Signal).

The second test was carried out to evaluate the correctness of the decoding process of the transmitted serial data operated by the RX MODULE and to verify the Uart Communication Output. A package of 512 bits containing the samples of a ramp voltage signal has been assembled and periodically sent from the transmitter to the receiver. After the data decoding and processing was performed by the receiver module, the recovered data have been transmitted through a UART communication protocol, implemented on the receiver FPGA, to the PC. As shown in Fig. 6.11, MATLAB environment has been used to receive the decoded data package and to plot the corresponding samples.

Finally, Fig. 6.12 shows an example of measurement results achieved by the third test which was conducted on the complete proposed system. The green channel is the Transmitted Pulsed Signal generated starting from the data coming from the Tactile Sensors (digitalized and collected into the Serial Data Package). The purple and blue channels show the clock and the data recovered by the DATA DECODING block, respectively. Moreover, in the magnified sections of Fig. 6.12 the HEADER and the begin of the Serial Data Package are highlighted, while in the lower part are shown the last bits acquired and the signal that indicates the correct detection of the HEADER.

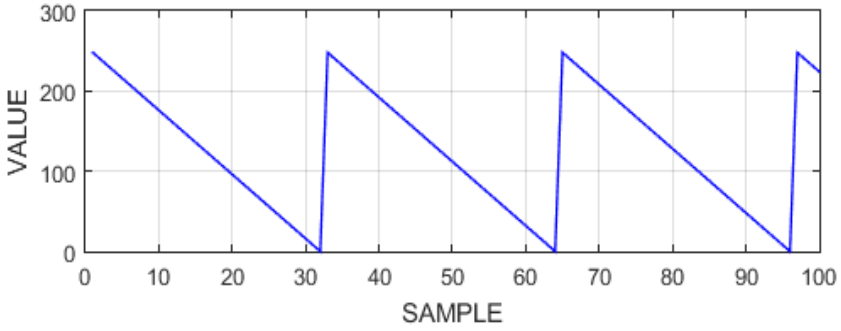

Fig. 6.11 Example of samples of a periodic ramp voltage signal that has been coded, transmitted via optical fiber, decoded, sent to a PC through a UART communication protocol (implemented in the RX MODULE on FPGA) and plotted in MATLAB environment.

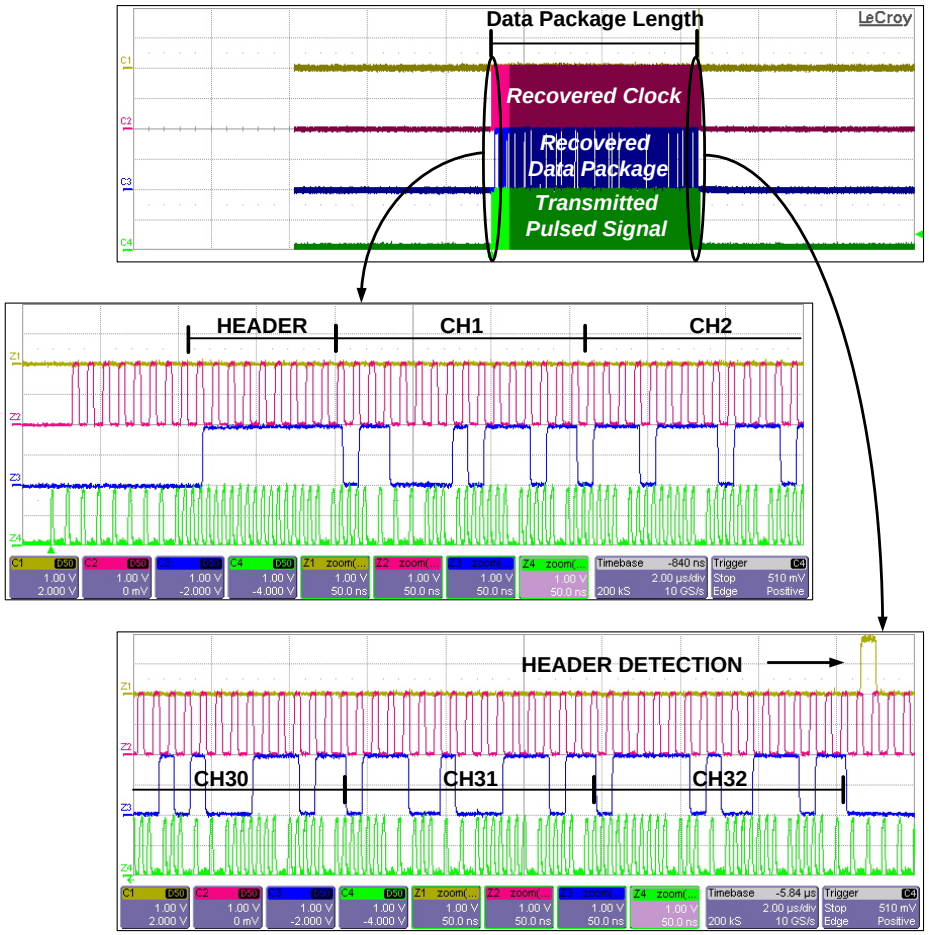

Fig. 6.12 Experimental measurement of the overall system operating at 100 Mbps: the green channel is the Transmitted Pulsed Signal related to the data coming from the Tactile Sensors; the purple and blue channels are the Recovered Clock and the Recovered Data Package, respectively; the yellow channel is the detection signal of the header.

Table 6.1 PROPOSED TACTILE SENSORY FEEDBACK SYSTEM: MAIN SPECIFICATIONS, PERFORMANCES AND CHARACTERISTICS

Number of tactile sensors	32
Sensor data sampling rate	2 kHz
Optical transmission data rate	100 Mbps
Optical link power consumption	5 mW
Transmission power efficiency	50 pJ/bit
FPGA LUTs for the Tx + Rx	1420 + 1320
FPGA FFs for the Tx + Rx	2230 + 2860

6.5 Summary

A tactile sensory feedback system based on an optical fiber communication link for the prosthetic application was described and implemented. The UWB-based pulsed data coding technique of the optical channel allows the system to operate with high data rate while showing low power transmission. The assembled system is composed of both digital transmitter and receiver block, and an acquisition circuit which interfaces 32 piezoelectric sensors. The transmitter acquires, encodes and sends sensor data via the optical channel. Whereas, the receiver decodes, recovers and translate the sensor data into commands. These commands control an electrotactile stimulator, conveying the tactile information to the user as electrotactile stimulations. The transmission performances have been evaluated by emulating the data coming from 32 sensors sent to an external apparatus (i.e., PC and/or oscilloscope) that represents a possible stimulator. A summary of the main overall system specifications, performances and characteristics is reported in Table 6.1. Results showed a correct functionality of the proposed system and validated that the system can transfer large number of data at 100 Mbps while low power consumption 50 pJ/bit. Moreover, thanks to the higher bandwidth obtained with the combination of the optical link and data coding used, a larger number of tactile sensors can be easily employed for the proposed sensory feedback system while maintaining a real-time operation.

Chapter 7 Summary and Future Perspectives

7.1 Summary

The main target of the tactile sensory feedback system in prosthetics and robotics is to deliver tactile information to the user and controller respectively. The tactile information represents touches that usually occur during object manipulation and exploration tasks. However, utilizing tactile information effectively requires a tactile sensing system that fulfils the prosthetic system requirements in terms of portability and functionality. Tactile sensors are the main block of the tactile sensing system, where in most cases should cover wide areas of prosthetic/robot surface. Thus, developing tactile sensing system is quite challenging due to set of issues related to hardware and algorithmic levels. For hardware requirements, the electronic circuits of the sensing system should be capable of interfacing large number of tactile sensors; acquiring sensors data with minimum delay and at high sampling rate; processing and transmitting large amount of data through reliable communication channels/buses. The algorithmic requirements include tactile data processing algorithms that can extract meaningful information from data. The algorithm structure and complexity should provide the desired processing task with minimum hardware resources at which will be employed.

This thesis focused on developing a tactile sensing system, taking into consideration most of the mentioned requirements. This work paves the way toward embedding the tactile sensing system in prosthetic/robotic allowing the user to restore sense of touch in real-life.

In this regard, three approaches have been proposed.

In the **first approach** we developed low power and real-time interface electronics for tactile sensing system for prosthetic application. The IE design is miniaturized and suitable to carry up to 32 PVDF-based piezoelectric tactile sensors. The design has been implemented including component-off-the-shelf DDC232 converter for signal conditioning and data acquisition with low-power ARM-Cortex M0 microcontroller. This implementation allowed the IE to perform simultaneous sampling, which is suitable for achieving real-time operation. Moreover, we conducted two types of tests to evaluate the behavior of the IE.

In the first test, real sensing array has been connected to the IE, together held on an experimental setup where a shaker instrument has been used to generate normal forces indentation. We analyzed the charges acquired by the IE, where results show that the IE can measure range of charge related to normal manipulation tasks and stresses (forces up to 100 kPa) at 56 dB signal-to-noise ratio and 14 bits of effective number of bits (ENOB). For the second test, we integrated the IE in a sensory feedback system to demonstrate the functionality of the IE in the feedback system, showing its potential in providing tactile information to the user. The proposed system operates in real-time with 32 ms delay (from touch to stimulation) and low power consumption IE for 300 mW. Although more extensive experimentation is needed to fully evaluate our system, the preliminary demonstration on three healthy subjects showed an accuracy of 86.66% recognition rate.

Furthermore, enhancement methods have been implemented toward improving the IE behavior by reducing the effect of noise in the design. Two filters, decimation and finite impulse response has been used and their results have been discussed. The results of this approach are important for sensory feedback design. They have shown the effectiveness of using a real-time embedded feedback system to extract and deliver tactile information to the users. The system is an important step toward integrating a distributed sensing system into a prosthetic hand and deliver tactile information to the user.

In the **second approach**, we have implemented a touch modality classification algorithm on embedded hardware platform. The algorithm is a tensorial-based machine learning algorithm based on support vector machine classifier (SVM). Then, we analyzed the performance of the algorithm (classification time, accuracy, number of operations) and studied the complexity and its effects on the hardware. In this regard, we proposed an optimized version of algorithm aiming to reduce the its complexity and improve the algorithm performance on the hardware. The proposed optimization technique has been applied and implemented on Zynq SoC to confirm the validity of the approach. Achieved results demonstrate that the proposed approach has reduced the computational complexity

with respect to the original algorithm presented in the state of the art. First, the number of operations is decreased from 545 M-ops to 18 M-ops. This has affected the time latency achieving a prediction speedup of 43×. Moreover, the required amount of memory storage has been minimized from 52.2 KB to 1.7 KB; These results have been achieved at a 2% of accuracy loss with respect to the literature [6]. The results have been compared with recent implementations and showed a performance superiority of our proposed approach. This approach allows the tactile sensing system to acquire, process data and extract touch modality on embedded hardware near the sensor and in real-time.

In the **third approach** we proposed a tactile sensory feedback system based on an optical fiber communication link for the prosthetic application. The optical communication protocol is based on UWB-based pulsed data coding technique which allows the system to operate with high data rate while showing low power transmission. The assembled system is composed of both digital transmitter and receiver block, and an acquisition circuit which interfaces 32 piezoelectric sensors. The transmitter acquires, encodes and sends sensor data via the optical channel. Whereas, the receiver decodes, recovers and translate the sensor data into commands. These commands control an electrotactile stimulator, conveying the tactile information to the user as electrotactile stimulations. We implemented the system including the data acquisition circuit and the communication channel. Then we evaluated the transmission performances by emulating the data coming from 32 sensors sent to an external apparatus (i.e., PC and/or oscilloscope) that represents a possible stimulator. Results showed a correct functionality of the proposed system and validated that the system can transfer large number of data at 100 Mbps while low power consumption 50 pJ/bit. Moreover, among the standard communication protocols (I2C, CAN, Bluetooth) this approach allows the tactile sensing system to employ large number of tactile sensors and transfer their data in the system through high bandwidth and low power communication channel while maintaining a real-time operation.

7.2 Future Perspectives

The aforementioned approaches contribute to the tactile sensing system where the first approach deals with the sensors and the interface electronics (data acquisition) block. This approach allows employing large number of sensors with low-power and real-time operation. These results motivate the integration of the proposed IE design in a prosthetic hand where sensor array will be connected to the IE mounted on the hand. On the other hand, the IE will be extended to handle 64 sensors and then will be implemented in a sensorized glove which will be used in an experimental campaign on a post-stroke patient. With respect to the power consumption aspect, the DDC232 circuit architecture would be

modified and implemented on ASIC design to operate in event-driven mode. This allows the chip to scan all input channels with consuming minimal energy.

The second approach is related to the processing unit of the sensing system where tactile information are extracted from the acquired sensor data. The approach introduces an optimized touch modality classification algorithm that can be embedded on hardware and execute the output classification with minimum delay and minimum hardware resources. From co-design perspective, a future approach would improve the performance of the algorithm by adding hardware accelerators and proposing new architectures (parallel computations) for several blocks of the algorithm. For instance, adding hardware IPs (i.e. Support Vector Decomposition) on the FPGA field of the Zynq SoC, which would speed up the classification task. Furthermore, storing the algorithm parameters requires enough storage which in embedded sensing system would be challenging due the limited memory storage. In addition to the high memory accesses that are required during the algorithm run-time imposing additional burden in terms of power consumption. Therefore, approximate memory approaches could be applied to reduce the memory read/write accesses and thus improving the power requirements of the sensing system.

The last approach is proposed to deal with the transmission of tactile data in the sensing system, especially in case of large amount of data received from large number of sensors. The communication channel allowed the system to transfer tactile data with low power consumption and wide bandwidth transfer. These results motivate the integration of the communication channel (ASIC design) which can be embedded in the tactile sensing system. Finally, combining the above three approaches in one system could paves the way toward an efficient embedded electronic system for tactile sensing system that could be integrated in electronic-skin applications (i.e. prosthetic).

References

[1] R. S. Johansson and J. R. Flanagan, “Coding and use of tactile signals from the fingertips in object manipulation tasks,” *Nat. Rev. Neurosci.*, vol. 10, no. 5, pp. 345–359, May 2009, doi: 10.1038/nrn2621.

[2] I. Saunders and S. Vijayakumar, “The role of feed-forward and feedback processes for closed-loop prosthesis control,” *J. Neuroeng. Rehabil.*, vol. 8, no. 1, p. 60, 2011, doi: 10.1186/1743-0003-8-60.

[3] R. S. Dahiya, P. Mittendorfer, M. Valle, G. Cheng, and V. J. Lumelsky, “Directions Toward Effective Utilization of Tactile Skin: A Review,” *IEEE Sens. J.*, vol. 13, no. 11, pp. 4121–4138, Nov. 2013, doi: 10.1109/JSEN.2013.2279056.

[4] A. Charalambides and S. Bergbreiter, “A novel all-elastomer MEMS tactile sensor for high dynamic range shear and normal force sensing,” *J. Micromechanics Microengineering*, vol. 25, no. 9, 2015, doi: 10.1088/0960-1317/25/9/095009.

[5] P. Dario and D. De Rossi, “Tactile Sensors and the Gripping Challenge.,” *IEEE Spectr.*, vol. 22, no. 8, pp. 46–52, 1985, doi: 10.1109/mspec.1985.6370785.

[6] L. Zou, C. Ge, Z. J. Wang, E. Cretu, and X. Li, “Novel tactile sensor technology and smart tactile sensing systems: A review,” *Sensors (Switzerland)*, vol. 17, no. 11, pp. 1–24, 2017, doi: 10.3390/s17112653.

[7] S. Luo, J. Bimbo, R. Dahiya, and H. Liu, “Robotic tactile perception of object properties: A review,” *Mechatronics*, vol. 48, no. December, pp. 54–67, 2017, doi: 10.1016/j.mechatronics.2017.11.002.

[8] J. M. Gandarias, A. J. Garcia-Cerezo, and J. M. Gomez-De-Gabriel, “CNN-Based Methods for Object Recognition with High-Resolution Tactile Sensors,” *IEEE Sens. J.*, vol. 19, no. 16, pp. 6872–6882, Aug. 2019, doi: 10.1109/JSEN.2019.2912968.

[9] G. Saggio, B. Gupta, M. Quagliani, M. De Sanctis, E. Cianca, and T. Rossi, “Power efficient wireless connectivity of a wearable data glove,” *2010 3rd Int. Symp. Appl. Sci. Biomed. Commun. Technol. ISABEL 2010*, pp. 1–5, 2010, doi: 10.1109/ISABEL.2010.5702927.

[10] P. Gastaldo, L. Pinna, L. Seminara, M. Valle, and R. Zunino, “A Tensor-Based Pattern-Recognition Framework for the Interpretation of Touch Modality in Artificial Skin Systems,”

IEEE Sens. J., vol. 14, no. 7, pp. 2216–2225, Jul. 2014, doi: 10.1109/JSEN.2014.2320820.

[11] H.-K. Lee, S.-I. Chang, and E. Yoon, "A Flexible Polymer Tactile Sensor: Fabrication and Modular Expandability for Large Area Deployment," *J. Microelectromechanical Syst.*, vol. 15, no. 6, pp. 1681–1686, Dec. 2006, doi: 10.1109/JMEMS.2006.886021.

[12] K. Weiss and H. Worn, "Resistive tactile sensor matrices using inter-electrode sampling," in *31st Annual Conference of IEEE Industrial Electronics Society, 2005. IECON 2005.*, 2005, vol. 2005, p. 6 pp., doi: 10.1109/IECON.2005.1569203.

[13] R. S. Dahiya, M. Valle, G. Metta, and L. Lorenzelli, "POSFET Based Tactile Sensor Arrays," in *2007 14th IEEE International Conference on Electronics, Circuits and Systems*, Dec. 2007, pp. 1075–1078, doi: 10.1109/ICECS.2007.4511180.

[14] F. Maita *et al.*, "Ultraflexible Tactile Piezoelectric Sensor Based on Low-Temperature Polycrystalline Silicon Thin-Film Transistor Technology," *IEEE Sens. J.*, vol. 15, no. 7, pp. 3819–3826, Jul. 2015, doi: 10.1109/JSEN.2015.2399531.

[15] A. Spanu *et al.*, "A high-sensitivity tactile sensor based on piezoelectric polymer PVDF coupled to an ultra-low voltage organic transistor," *Org. Electron.*, vol. 36, pp. 57–60, Sep. 2016, doi: 10.1016/j.orgel.2016.05.034.

[16] D. Johnston, P. Zhang, J. Hollerbach, and S. Jacobsen, "Full tactile sensing suite for dextrous robot hands and use in contact force control," *Proc. - IEEE Int. Conf. Robot. Autom.*, vol. 4, no. April, pp. 3222–3227, 1996, doi: 10.1109/robot.1996.509203.

[17] J. G. Rocha, C. Santos, and J. M. Cabral, "3 Axis Capacitive Tactile Sensor and Readout Electronics," vol. 4, no. 4, 2006.

[18] L. Yu *et al.*, "A Flexible Compound Sensing System for Tactile Detection in Prosthetic Hands∗," *2018 IEEE Int. Conf. Cyborg Bionic Syst. CBS 2018*, pp. 75–79, 2019, doi: 10.1109/CBS.2018.8612207.

[19] M. Acer, M. Salerno, K. Agbeviade, and J. Paik, "Development and characterization of silicone embedded distributed piezoelectric sensors for contact detection," *Smart Mater. Struct.*, vol. 24, no. 7, p. 75030, 2015, doi: 10.1088/0964-1726/24/7/075030.

[20] P. Yu, W. Liu, C. Gu, X. Cheng, and X. Fu, "Flexible piezoelectric tactile sensor array for dynamic three-axis force measurement," *Sensors (Switzerland)*, vol. 16, no. 6, 2016, doi: 10.3390/s16060819.

[21] A. Drimus, M. Borlum Petersen, and A. Bilberg, “Object texture recognition by dynamic tactile sensing using active exploration,” *Proc. - IEEE Int. Work. Robot Hum. Interact. Commun.*, pp. 277–283, 2012, doi: 10.1109/ROMAN.2012.6343766.

[22] T. Someya, T. Sekitani, S. Iba, Y. Kato, H. Kawaguchi, and T. Sakurai, “A large-area, flexible pressure sensor matrix with organic field-effect transistors for artificial skin applications,” 2004. Accessed: Jul. 22, 2020. [Online]. Available: www.pnas.orgcgidoi10.1073pnas.0401918101.

[23] L. Barboni, R. S. Dahiya, G. Metta, and M. Valle, “Interface electronics design for POSFET devices based tactile sensing systems,” *Proc. - IEEE Int. Work. Robot Hum. Interact. Commun.*, pp. 686–690, 2010, doi: 10.1109/ROMAN.2010.5598610.

[24] L. PINNA and M. VALLE, “CHARGE AMPLIFIER DESIGN METHODOLOGY FOR PVDF-BASED TACTILE SENSORS,” *J. Circuits, Syst. Comput.*, vol. 22, no. 08, p. 1350066, Sep. 2013, doi: 10.1142/S0218126613500667.

[25] L. Pinna, A. Ibrahim, and M. Valle, “Interface Electronics for Tactile Sensors Based on Piezoelectric Polymers,” *IEEE Sens. J.*, vol. 17, no. 18, pp. 5937–5947, Sep. 2017, doi: 10.1109/JSEN.2017.2730840.

[26] “DDC112 Dual Current Input 20-Bit ANALOG-TO-DIGITAL CONVERTER FEATURES,” 2000. Accessed: May 02, 2019. [Online]. Available: www.ti.com.

[27] A. Ibrahim, L. Pinna, and M. Valle, “Experimental characterization of dedicated front-end electronics for piezoelectric tactile sensing arrays,” *Integration*, vol. 63, no. July, pp. 266–272, 2018, doi: 10.1016/j.vlsi.2018.07.007.

[28] M. Rossi, M. Nardello, L. Lorenzelli, and D. Brunelli, “Dual Mode Pressure Sensing for Lower-Limb Prosthetic Interface,” *Eurosensors 2017 Proc.*, vol. 1, no. 4, p. 593, 2017, doi: 10.3390/proceedings1040593.

[29] Y. Ohmura, Y. Kuniyoshi, and A. Nagakubo, “Conformable and scalable tactile sensor skin for a curved surfaces,” *Proc. - IEEE Int. Conf. Robot. Autom.*, vol. 2006, no. May, pp. 1348–1353, 2006, doi: 10.1109/ROBOT.2006.1641896.

[30] O. Oballe-Peinado *et al.*, “FPGA-Based Tactile Sensor Suite Electronics for Real-Time Embedded Processing,” *IEEE Trans. Ind. Electron.*, vol. 64, no. 12, pp. 9657–9665, 2017, doi: 10.1109/TIE.2017.2714137.

[31] A. Schmitz, P. Maiolino, M. Maggiali, L. Natale, G. Cannata, and G. Metta, “Methods and Technologies for the Implementation of Large-Scale Robot Tactile Sensors A Schmitz IEEE Robotics 2011.pdf - Unknown.pdf,” *Robot. IEEE Trans.*, vol. 27, no. 3, pp. 389–400, 2011.

[32] V. Tyzhnevyi, G.-F. D. Betta, L. Rovati, G. Verzellesi, and N. Zorzi, “BJT detector with FPGA-based read-out for alpha particle monitoring,” *J. Instrum.*, vol. 6, no. 01, pp. C01051–C01051, Jan. 2011, doi: 10.1088/1748-0221/6/01/C01051.

[33] H. Kruger, M. Rabe, E. Ebert, P. Busch, N. A. Damaschke, and H. Ewald, “A flexible measurement system for absorption spectrometry using LED light sources and a high accuracy two-channel ADC for simultaneous sampling,” *Proc. Int. Conf. Sens. Technol. ICST*, vol. 2016-March, pp. 652–655, 2016, doi: 10.1109/ICSensT.2015.7438478.

[34] H. Fares, L. Seminara, H. Chible, S. Dosen, and M. Valle, “Multi-Channel Electrotactile Stimulation System for Touch Substitution: A Case Study,” in *2018 14th Conference on Ph.D. Research in Microelectronics and Electronics (PRIME)*, Jul. 2018, pp. 213–216, doi: 10.1109/PRIME.2018.8430345.

[35] M. Franceschi, L. Seminara, S. Dosen, M. Strbac, M. Valle, and D. Farina, “A System for Electrotactile Feedback Using Electronic Skin and Flexible Matrix Electrodes: Experimental Evaluation,” *IEEE Trans. Haptics*, vol. 10, no. 2, pp. 162–172, 2017, doi: 10.1109/TOH.2016.2618377.

[36] E. Farella, A. Pieracci, D. Brunelli, L. Benini, B. Riccó, and A. Acquaviva, “Design and implementation of WiMoCA node for a body area wireless sensor network,” *Proc. - 2005 Syst. Commun. ICW 2005, Wirel. - ICHSN 2005, High Speed Networks - ICMCS 2005, Multimed. Commun. Syst. - SENET 2005, Sens. Networks*, vol. 2005, pp. 342–347, 2005, doi: 10.1109/ICW.2005.39.

[37] D. Brunelli, E. Farella, L. Rocchi, M. Dozza, L. Chiari, and L. Benini, “Bio-feedback system for rehabilitation based on a wireless body area network,” *Proc. - Fourth Annu. IEEE Int. Conf. Pervasive Comput. Commun. Work. PerCom Work. 2006*, vol. 2006, pp. 527–531, 2006, doi: 10.1109/PERCOMW.2006.27.

[38] A. Drimus, M. Borlum Petersen, and A. Bilberg, “Object texture recognition by dynamic tactile sensing using active exploration,” *Proc. - IEEE Int. Work. Robot Hum. Interact. Commun.*, pp. 277–283, 2012, doi: 10.1109/ROMAN.2012.6343766.

[39] L. Pinna, G. Carlini, L. Seminara, and M. Valle, “Interface electronics for tactile sensing arrays,” *2011 18th IEEE Int. Conf. Electron. Circuits, Syst. ICECS 2011*, pp. 468–471, 2011, doi: 10.1109/ICECS.2011.6122314.

[40] S. Kim, H. Shin, K. Song, and Y. Cha, “Flexible piezoelectric sensor array for touch sensing of robot hand,” *2019 16th Int. Conf. Ubiquitous Robot. UR 2019*, pp. 21–25, 2019, doi: 10.1109/URAI.2019.8768644.

[41] M. D’Alonzo, S. Dosen, C. Cipriani, and D. Farina, “HyVE: Hybrid Vibro-Electrotactile Stimulation for Sensory Feedback and Substitution in Rehabilitation,” *IEEE Trans. Neural Syst. Rehabil. Eng.*, vol. 22, no. 2, pp. 290–301, Mar. 2014, doi: 10.1109/TNSRE.2013.2266482.

[42] D. Pamungkas and K. Ward, “Electro-tactile feedback system for a prosthetic hand,” *22nd Annu. Int. Conf. Mechatronics Mach. Vis. Pract. M2VIP 2015*, pp. 27–38, 2015.

[43] C. Hartmann *et al.*, “Towards prosthetic systems providing comprehensive tactile feedback for utility and embodiment,” *IEEE 2014 Biomed. Circuits Syst. Conf. BioCAS 2014 - Proc.*, pp. 620–623, 2014, doi: 10.1109/BioCAS.2014.6981802.

[44] S. C. Gandevia and G. Macefield, “Projection of low-threshold afferents from human intercostal muscles to the cerebral cortex,” *Respir. Physiol.*, vol. 77, no. 2, pp. 203–214, 1989, doi: 10.1016/0034-5687(89)90007-8.

[45] H. Huang *et al.*, “Multi-modal Sensory Feedback System for Upper Limb Amputees,” in *2017 New Generation of CAS (NGCAS)*, Sep. 2017, pp. 193–196, doi: 10.1109/NGCAS.2017.62.

[46] K. R. Schoepp, M. R. Dawson, J. S. Schofield, J. P. Carey, and J. S. Hebert, “Design and Integration of an Inexpensive Wearable Mechanotactile Feedback System for Myoelectric Prostheses,” *IEEE J. Transl. Eng. Heal. Med.*, vol. 6, no. April, pp. 1–11, 2018, doi: 10.1109/JTEHM.2018.2866105.

[47] D. Goger, N. Gorges, and H. Worn, “Tactile sensing for an anthropomorphic robotic hand: Hardware and signal processing,” in *2009 IEEE International Conference on Robotics and Automation*, May 2009, pp. 895–901, doi: 10.1109/ROBOT.2009.5152650.

[48] P. Gastaldo, L. Pinna, L. Seminara, M. Valle, and R. Zunino, “Computational intelligence techniques for tactile sensing systems,” *Sensors (Switzerland)*, vol. 14, no. 6, pp. 10952–10976, 2014, doi: 10.3390/s140610952.

[49] U. Martinez-Hernandez, T. J. Dodd, and T. J. Prescott, “Feeling the Shape: Active Exploration Behaviors for Object Recognition with a Robotic Hand,” *IEEE Trans. Syst. Man, Cybern. Syst.*, vol. 48, no. 12, pp. 2339–2348, 2018, doi: 10.1109/TSMC.2017.2732952.

[50] “Bayesian exploration for intelligent identification of textures _ Enhanced Reader.”

[51] M. Madry, L. Bo, D. Kragic, and D. Fox, “ST-HMP: Unsupervised Spatio-Temporal feature learning for tactile data,” *Proc. - IEEE Int. Conf. Robot. Autom.*, pp. 2262–2269, 2014, doi: 10.1109/ICRA.2014.6907172.

[52] T. Bhattacharjee, J. M. Rehg, and C. C. Kemp, “Haptic classification and recognition of objects using a tactile sensing forearm,” *IEEE Int. Conf. Intell. Robot. Syst.*, pp. 4090–4097, 2012, doi: 10.1109/IROS.2012.6386142.

[53] J. M. Gandarias, J. M. Gomez-De-Gabriel, and A. Garcia-Cerezo, “Human and object recognition with a high-resolution tactile sensor,” *Proc. IEEE Sensors*, vol. 2017-Decem, no. June 2020, pp. 1–3, 2017, doi: 10.1109/ICSENS.2017.8234203.

[54] M. Alameh, Y. Abbass, A. Ibrahim, and M. Valle, “Smart Tactile Sensing Systems Based on Embedded CNN Implementations,” *Micromachines*, vol. 11, no. 1, p. 103, Jan. 2020, doi: 10.3390/mi11010103.

[55] M. Osta *et al.*, “An energy efficient system for touch modality classification in electronic skin applications,” *Proc. - IEEE Int. Symp. Circuits Syst.*, vol. 2019-May, pp. 6–9, 2019, doi: 10.1109/ISCAS.2019.8702113.

[56] A. Ibrahim and M. Valle, “Real-Time Embedded Machine Learning for Tensorial Tactile Data Processing,” *IEEE Trans. Circuits Syst. I Regul. Pap.*, vol. 65, no. 11, pp. 3897–3906, Nov. 2018, doi: 10.1109/TCSI.2018.2852260.

[57] M. Bianchi, R. Haschke, G. Büscher, S. Ciotti, N. Carbonaro, and A. Tognetti, “A Multi-Modal Sensing Glove for Human Manual-Interaction Studies,” *Electronics*, vol. 5, no. 4, p. 42, Jul. 2016, doi: 10.3390/electronics5030042.

[58] F. Vidal-Verdú *et al.*, “A large area tactile sensor patch based on commercial force sensors,” *Sensors*, vol. 11, no. 5, pp. 5489–5507, 2011, doi: 10.3390/s110505489.

[59] K. Ward and D. Pamungkas, “Multi-channel Electro-tactile Feedback System for a Prosthetic Hand,” in *Mechatronics and Machine Vision in Practice 3*, vol. 3, Cham: Springer International Publishing, 2018, pp. 181–193.

[60] B. Choi, S. Kang, and H. Choi, “Development of Fingertip Tactile Sensor for Detecting Normal Force and Slip,” 2005, [Online]. Available: http://2005.iccas.org/submission/paper/upload/ICCAS_Tactile_Sensor.pdf.

[61] R. S. Dahiya *et al.*, “Towards Tactile Sensing System on Chip for Robotic Applications,” *IEEE Sens. J.*, vol. 11, no. 12, pp. 3216–3226, Dec. 2011, doi: 10.1109/JSEN.2011.2159835.

[62] J. A. Schmitz, J. M. Sherman, S. Hansen, S. J. Murray, S. Balkir, and M. W. Hoffman, “A Low-Power, Single-Chip Electronic Skin Interface for Prosthetic Applications,” *IEEE Trans. Biomed. Circuits Syst.*, vol. 13, no. 6, pp. 1186–1200, Dec. 2019, doi: 10.1109/TBCAS.2019.2948006.

[63] H. Fares *et al.*, “Screen Printed Tactile Sensing Arrays for Prosthetic Applications,” *Proc. - IEEE Int. Symp. Circuits Syst.*, vol. 2018-May, no. c, pp. 1–4, 2018, doi: 10.1109/ISCAS.2018.8351892.

[64] R. S. Dahiya, A. Adami, C. Collini, M. Valle, and L. Lorenzelli, “POSFET Tactile Sensing Chips Using CMOS Technology,” no. November, pp. 2–6, 2013, doi: 10.1109/ICSENS.2013.6688149.

[65] L. Seminara, M. Capurro, P. Cirillo, G. Cannata, and M. Valle, “Electromechanical characterization of piezoelectric PVDF polymer films for tactile sensors in robotics applications,” *Sensors Actuators A Phys.*, vol. 169, no. 1, pp. 49–58, Sep. 2011, doi: 10.1016/j.sna.2011.05.004.

[66] R. S. Dahiya, G. Metta, M. Valle, and G. Sandini, “Tactile Sensing — From Humans to Humanoids,” vol. 26, no. 1, pp. 1–20, 2010.

[67] M. Zirkl *et al.*, “An All-Printed Ferroelectric Active Matrix Sensor Network Based on Only Five Functional Materials Forming a Touchless Control Interface,” *Adv. Mater.*, vol. 23, no. 18, pp. 2069–2074, May 2011, doi: 10.1002/adma.201100054.

[68] A. L. At *et al.*, “Europäische patentanmeldung (51),” vol. 1, no. 19, pp. 1–12, 2012.

[69] M. P. Macedo, “A Tactile Sensing System Based on Arrays of Piezoelectric Polymer Transducers.”

[70] “Highly Sensitive Flexible Pressure Sensors with Micro-structured Rubber Dielectric Layers.” Accessed: Jun. 20, 2019. [Online]. Available: http://news.stanford.edu/news/2010/september/sensitive-artificial-skin-091210.html.

[71] “DDC232, 32-Channel, Current-Input Analog-to-Digital Converter,” 2004. Accessed: May 02, 2019. [Online]. Available: www.ti.com.

[72] W. Generation Measurement, A. Technical Committee of the IEEE Instrumentation, and M. Society, “IEEE Standard for Terminology and Test Methods for Analog-to-Digital Converters Sponsored by the Waveform Generation Measurement and Analysis Technical Committee IEEE Instrumentation & Measurement Society,” 2011. Accessed: Jun. 21, 2019. [Online]. Available: http://class.ece.iastate.edu/djchen/ee509/2018/IEEE1241-2011.pdf.

[73] “Available online: http://www.analog.com/media/en/training-seminars/tutorials/MT-003.pdf (accessed on 1 November 2020).” .

[74] S. W. Smith, “Digital Signal Processing, Chapter 15,” *Calif. Tech. Publ.*, pp. 277–284, 1999.

[75] “Available online: http://www.dsdtech-global.com/2017/08/hc-05-datasheet-and-how-to-enter-at.html (accessed on 1 November 2020).” .

[76] “Available online: http://infocenter.nordicsemi.com/pdf/nRF51822_PS_v3.1.pdf (accessed on 1 November 2020).” .

[77] “Tecnalia. Inspiring Business.” .

[78] “OT Bioelettronica - Home.” .

[79] G. Gescheider, “Psychophysics: The fundamentals, 3rd ed. - PsycNET,” in *Psychophysics: The fundamentals, 3rd ed.*, Lawrence Erlbaum Associates, 1997.

[80] H. Cao, J. Zhang, X. Cao, R. Li, and Y. Wang, “Optimized SVM-Driven Multi-Class Approach by Improved ABC to Estimating Ship Systems State,” *IEEE Access*, pp. 1–1, 2020, doi: 10.1109/ACCESS.2020.3037251.

[81] L. Demidova and I. Klyueva, “SVM classification: Optimization with the SMOTE algorithm for the class imbalance problem,” in *2017 6th Mediterranean Conference on Embedded Computing (MECO)*, Jun. 2017, pp. 1–4, doi: 10.1109/MECO.2017.7977136.

[82] S. Ben Chaabane, S. Kharbech, A. Belazi, and A. Bouallegue, “Improved Whale optimization Algorithm for SVM Model Selection: Application in Medical Diagnosis,” in *2020 International Conference on Software, Telecommunications and Computer Networks (SoftCOM)*, Sep. 2020, pp. 1–6, doi: 10.23919/SoftCOM50211.2020.9238265.

[83] C. E. Santos, L. dos S. Coelho, R. C. Sampaio, R. Jacobi, H. Ayala, and C. H. Llanos, “A SVM optimization tool and FPGA system architecture applied to NMPC,” in *Proceedings of*

the 30th Symposium on Integrated Circuits and Systems Design Chip on the Sands - SBCCI '17, 2017, pp. 96–102, doi: 10.1145/3109984.3110007.

[84] J. Masood, S. Javaid, S. Ahmed, S. Ullah, and N. Javaid, "An Optimized Linear-Kernel Support Vector Machine for Electricity Load and Price Forecasting in Smart Grids," in *2019 International Conference on Advances in the Emerging Computing Technologies (AECT)*, Feb. 2020, pp. 1–6, doi: 10.1109/AECT47998.2020.9194152.

[85] O. Chapelle and O. Bousquet, "Choosing Multiple Parameters for Support Vector Machines," 2002.

[86] A. De Marcellis, E. Palange, L. Nubile, M. Faccio, G. Di Patrizio Stanchieri, and T. Constandinou, "A Pulsed Coding Technique Based on Optical UWB Modulation for High Data Rate Low Power Wireless Implantable Biotelemetry," *Electronics*, vol. 5, no. 4, p. 69, Oct. 2016, doi: 10.3390/electronics5040069.

[87] A. De Marcellis, G. Di Patrizio Stanchieri, E. Palange, M. Faccio, and T. G. Constandinou, "An Ultra-Wideband-Inspired System-on-Chip for an Optical Bidirectional Transcutaneous Biotelemetry," *2018 IEEE Biomed. Circuits Syst. Conf. BioCAS 2018 - Proc.*, 2018, doi: 10.1109/BIOCAS.2018.8584822.

[88] P. Bulić, G. Kojek, and A. Biasizzo, "Data Transmission Efficiency in Bluetooth Low Energy Versions," *Sensors*, vol. 19, no. 17, p. 3746, Aug. 2019, doi: 10.3390/s19173746.

[89] K. Mikhaylov and J. Tervonen, "Evaluation of Power Efficiency for Digital Serial Interfaces of Microcontrollers."

[90] H. Fares, Y. Abbass, M. Valle, and L. Seminara, "Validation of Screen-Printed Electronic Skin Based on Piezoelectric Polymer Sensors," *Sensors*, vol. 20, no. 4, p. 1160, Feb. 2020, doi: 10.3390/s20041160.